Performance Load Testing and Structural Adequacy Evaluation of Road Bridge Decks

by

Lungten Jamtsho

Submitted in fulfilment of the requirements for the degree of

Master of Engineering (Research)

Faculty of Built Environment and Engineering

Queensland University of Technology

2011

Abstract

Many ageing road bridges, particularly timber bridges, require urgent improvement due to the demand imposed by the recent version of the Australian bridge loading code, AS 5100. As traffic volume plays a key role in the decision of budget allocations for bridge refurbishment/ replacement, many bridges in low volume traffic network remain in poor condition with axle load and/ or speed restrictions, thus disadvantaging many rural communities. This thesis examines an economical and environmentally sensible option of incorporating disused flat rail wagons (FRW) in the construction of bridges in low volume, high axle load road network. The constructability, economy and structural adequacy of the FRW road bridge is reported in the thesis with particular focus of a demonstration bridge commissioned in regional Queensland. The demonstration bridge comprises of a reinforced concrete slab (RCS) pavement resting on two FRWs with custom designed connection brackets at regular intervals along the span of the bridge. The FRW-RC bridge deck assembly is supported on elastomeric rubber pads resting on the abutment.

As this type of bridge replacement technology is new and its structural design is not covered in the design standards, the in-service structural performance of the FRW bridge subjected to the high axle loadings prescribed in AS 5100 is examined through performance load testing. Both the static and the moving load tests are carried out using a fully laden commonly available three-axle tandem truck. The bridge deck is extensively strain gauged and displacement at several key locations is measured using linear variable displacement transducers (LVDTs). A high speed camera is used in the performance test and the digital image data are analysed using proprietary software to capture the locations of the wheel positions on the bridge span accurately. The wheel

location is thus synchronised with the displacement and strain time series to infer the structural response of the FRW bridge.

Field test data are used to calibrate a grillage model, developed for further analysis of the FRW bridge to various sets of high axle loads stipulated in the bridge design standard. Bridge behaviour predicted by the grillage model has exemplified that the live load stresses of the FRW bridge is significantly lower than the yield strength of steel and the deflections are well below the serviceability limit state set out in AS 5100. Based on the results reported in this thesis, it is concluded that the disused FRWs are competent to resist high axle loading prescribed in AS 5100 and are a viable alternative structural solution of bridge deck in the context of the low volume road networks.

Keywords

Disused flat rail wagons, low volume traffic bridges, bridge decks, performance load testing, grillage method, composite action, serviceability limit states, ultimate limit state high axle loads, structural adequacy.

Publications

Conference Papers

L.Jamtsho, M.Dhanasekar, N.Palliyaguru and W.Bayissa (2010). "Effects of opening in the cross girders of the flat bottom rail wagons to the load transferring mechanisms when used as road bridge deck." *Proceedings of the 21st Australian Conference on the Mechanics of Structures and Materials*, CRC Press (Taylor and Francis Group), Victoria University, Melbourne, Australia,

N.Palliyaguru, L.Jamtsho, M.Dhanasekar and W.Bayissa (2010). "Alternate structural system of incorporating flat rail wagons as low volume road bridge deck." *Proceedings of the 5th Civil Engineering Conference in the Asian Region and Australasian Structural Engineering Conference* 2010, Engineers Australia, Sydney convention and Exhibition Centre, Sydney,

TABLE OF CONTENT

List of Figures

List of Tables

List of Symbols

The following symbols are used in this thesis:

A_w	Gross sectional area of the web
b_f	Flange width
b_w	Web depth
d_p	Depth of the deepest web panel
E	Young's modulus of elasticity
E_l	Effects of the loads
f_y	Yield stress of steel
f_{uw}	Nominal tensile strength of weld metal
G	Modulus of rigidity
I_y	Second moment of area of the section about the minor principal y-axis
J	Torsion constant for a cross section
L	Length of segment
L_e	Effective length
k_L	Load height factor
k_{rl}	Lateral rotation factor
k_r	Reduction factor
k_1	Twist restraint
M_b	Nominal member moment capacity
M_o	Elastic buckling moment
M_{oa}	Elastic buckling moment for a member subject to bending
M_s	Nominal section moment capacity for bending about the major principal x-axis
M_x^*	Design bending moment about the major principal x-axis
R	Resistance
R_u	Design action effect
r_y	Radius of gyration about the minor principal y-axis

S^*	Design capacity
t_t	Design throat thickness
t_w	Thickness of web
V_b	Shear buckling capacity of the web
V_u	Nominal shear capacity of the web
V_v	Nominal shear capacity of the web
V_w	Nominal shear capacity of the web
V^*	Design shear force
V_w^*	Design force per unit length
Z_e	Effective section modulus
Z_{en}	Effective section modulus of the non compact section
α	Dynamic load allowance
α_m	Moment modification factor
α_s	Slenderness reduction factor
β_m	Ration of the smaller to the larger end moments in the length L
ϕ	Capacity reduction factor

List of Abbreviations

3D	Three Dimensional
AADT	Average Annual Daily Traffic
AASHTO	American Association of State Highway and Transportation Officials
ADT	Average Daily Traffic
AS	Australian Standard
BCB	Buchanan County Bridge
BM	Bending Moment
BMD	Bending Moment Diagram
CRE	Centre for Railway Engineering
DAQ	Data Acquisition
DLA	Dynamic Load Allowance
FEM	Finite Element Model
FRW	Flat Rail Wagon
GFRP	Granular Fibre Reinforced Polymer
GVW	Gross Vehicle Weight
ISU	Iowa State of University
LVDT	Linear Variable Displacement Transducer
NAASRA	National Association of Australia State Road Authorities
NDT	Non Destructive Testing
QLD	Queensland
QRN	Queensland Rail National
QUT	Queensland University of Technology
RCC	Reinforced Concrete Beam
RCS	Reinforced concrete slab
RHS	Rectangular Hollow Section
RRC	Rockhampton Regional Council
SF	Shear Force
SFD	Shear Force Diagram
UDL	Uniformly Distributed Load
UK	United Kingdom
US	United States
WCB	Winnebago County Bridge

Statement of Original Authorship

The work contained in this thesis has not been previously submitted to meet requirements for an award at this or any other higher education institution. To the best of my knowledge and belief, the thesis contains no material previously published or written by another person except where due reference is made.

Signature: _____

Date: _____

Acknowledgments

Firstly I would like to express my deep and sincere gratitude to my principal supervisor, Professor Manicka Dhanasekar for his supervision, guidance, continued support and advice as well as providing never-ending encouragement and constructive suggestions throughout the research work. His professional and energetic support helped me in writing this thesis; a task which I could not have accomplished alone. Moreover, his wide knowledge, logical way of thinking, detailed and constructive comments have been of great value for me. In addition, I would like to express my sincere appreciation for giving me opportunity to work as the tutor. I once again thank you for everything you have contributed towards this research. I would also like to extend my sincere appreciation to my associate supervisor, Wirtu L. Bayissa for his moral support, advice and constructive comments throughout this work. During this work I have collaborated with many people for whom I have great regard and I wish to extend my warmest thanks to all those who have helped me in my experimental field testing; they are Paul Byod and Josh McDonald (CRE, CQU) and Janaraj Thangarajah (PhD student, QUT). I would like to express my appreciation to my colleagues Nish Palliyaguru and Christopher McDonald in the research team, for their friendship and fruitful discussions we have had. The Royal Government of Bhutan is highly appreciated for awarding scholarship and continued support during the course of research; without your financial assistance, the possibility of upgrading knowledge and skill is almost impossible. Last but not the least, I am very grateful to my parents for their love, moral support and patience during the study period. I sincerely thank my wife and son for being with me in Australia and for their unwavering love, support, patience and encouragement and finally understanding me during my difficult days in writing the thesis.

Chapter 1: Introduction

Bridges are an important and integral part of modern transportation systems and play a vital role in the lives of communities and therefore should be maintained at service level at all time. However, it has challenged the local councils/governments in maintaining the bridge assets to their maximum service level due to the difficulties associated with gaining funding to replace or rehabilitate the ageing bridges on low volume roads network. In addition, the Australia national bridge design standard AS 5100 (2004) demands quite stringent design processes with the prescribed axle loads considered futuristic (i.e, not an existing vehicle construct) and quite heavy, thus compounding the bridge replacement techniques within the limited annual budget.

Rural local roads account 71.6% of the total roads in Australia; local government bodies in Australia are responsible for maintenance and operations of over 20,000 timber bridges (Crews et al., 2004). The majority of these bridges are in excess of 50 years old with many of them having degraded or structurally weak to resist high axle wheel loads. Rehabilitating or replacement of these ageing bridges, especially the old timber bridges on low volume roads network is a daunting challenge within the limited fund in light of the available technological solutions that are expensive. Therefore, it is against this background that this research study is carried out to develop a cost-effective bridge replacement solution using decommissioned flat rail wagons (FRW) as the bridge superstructure.

Aim, objective and scope

The main aim of this research is to evaluate the structural adequacy of disused FRW as the low cost bridge superstructure in low volume traffic roads network through performance load testing using three-axle tandem truck loading and 3D grillage modelling.

Research Problem

There are many ageing road bridges, particularly those timber bridges in the rural low volume roads network which require urgent improvement due to the high axle load demand imposed by the recent version of the Australian bridge loading code, AS 5100.2 (2004). As traffic volume plays a key role in the decision of budget allocations for bridge improvement or replacement, many bridges in low volume traffic roads network remain in poor condition with axle load and/ or speed restrictions, thus disadvantaging many rural communities.

Significance of this research

The significance of this research lies in addressing a viable solution of FRW as the road bridge superstructure in low volume traffic roads network, which will not only facilitates replacing old aging bridges, particularly those timber bridges which have outlived the design life in the rural places but also can increase the load carrying capacity thereby able to enhance the economic activities. As this type of bridge can be constructed on the existing or new abutments with minimum skilled personnel and

within short period of time, it is regarded as cost effective when compared to other available bridge replacement alternatives.

Relationship of this research to the project

The research reported in this thesis forms part of a project that incorporates three master theses.

- The first thesis deals with laboratory experimental investigation of the flat rail wagon (FRW). This thesis has recently been successfully examined.
- The current thesis primarily deals with the design, construction and performance testing of a demonstation road bridge containing FRW.
- The final thesis deals with design of alternate pavements for the FRW bridge. This thesis is under preparation.

Outline of the thesis

The thesis is organised into 8 chapters as follows:

Chapter 1: Introduction

This chapter presents the background and introduction to the topic, defines the research problem, states the aim, objective and scope, significant of the study and outlines the method of investigation adopted in the research project.

Chapter 2: Literature Review

This chapter presents an overview of previously published literature in the field of disused rail wagons as a low cost bridge structures based on case studies in the USA. It also reviews the type of bridge systems adopted in low volume road network, bridge design standards of AS 5100, which need to be adhered for all new bridge construction in Australia and the type of field load tests adopted in the evaluation of bridge structures, with emphasis on the performance load testing. Finally, a summary of the literature review findings related to the FRW Bridge and performance field load testings are presented.

Chapter 3: FRW structural system and its adoption as the road bridge superstructure

This chapter presents overview of Flat Rail Wagons (FRW) available with Queensland Rail National (QRN) and their structural system to resist high axle wheel loads in line with the structural adequacy as the bridge superstructure. The member capacity of the main load bearing members were compared with the maximum load effects under high axle loads of AS 51000.

Chapter 4: Modelling and analysis

This chapter presents the development of 3D grillage model of FRW, in SPACEGASS structural engineering software. Single and double bare frame FRW models are calibrated with the results from the laboratory testing. Finally the updated models are analysed for

different sets of SM 1600 loadings and the results compared with the member capacities.

Chapter 5: Bridge design and construction

This chapter presents the design of FRW bridge, with the emphasis on the longitudinal connection design between two FRWs, reinforced concrete slab as the driving surface to the traffic and modification process required therein to resist design loads prescribed in AS 5100.2 (2004). This chapter also presents the selection criteria of FRW required for successful and viable solution of bridge replacement techniques and the construction sequence for the construction of a demonstration bridge in rural place on low volume road and the cost associated with it.

Chapter 6: Performance load testing

This chapter outlines the procedure adopted for performance load testing using normal three-axle tandem truck loaded with crushed rocks. Use of high speed camera to video record the load testing program to exactly locate the wheel position to accurately correlate the load position with the sensor measurement at a later stage is introduced. The field load test results are linearly increased to M1600 load equivalent and compared with the code serviceability limit to evaluate the structural adequacy of FRW as the low cost bridge superstructure in low volume roads. The chapter concludes with the field load test results and the performance of FRW as the low cost bridge in low volume roads.

Chapter 7: Structural adequacy of the FRW Bridge

This chapter presents the comparison of results between the 3D grillage model presented in chapter 4 and field load test results from chapter 6. The calibrated model is further analysed for higher loads of SM1600 in line with the serviceability and ultimate limits criteria of the standard AS 5100.2 (2004) in assessing the structural adequacy of FRW Bridge on low volume roads.

Chapter 8: Conclusion

This final chapter highlights the main contributions and outcomes of this research. Recommendations for further research are also provided.

Chapter 2: Literature review

2.1 Introduction

This chapter presents literature review in the context of the low volume road bridges in Australia and around the world. The review begins by describing the characteristics of the bridges in the low volume road network and their intended functional requirements. Some case studies from the Iowa State of the United States of America are reviewed and their advantages in the bridge rehabilitation in comparison to other structurally adequate available solutions are presented. Bridges, particularly in the rural and remote areas of many countries around the world are the least upgraded or replaced due to limited maintenance budget and also owing to its low average annual daily traffic (AADT) data. However, it is quite evident that many bridges in the US, Canada, Europe, Australia and elsewhere is ageing (Faber et al., 2000) and deteriorating at an increasing rate. One of the reasons for the accelerated deterioration might be that these old bridges, designed and built based on the old loading configurations and design codes, are now subjected to higher axle loads imposed by the current heavy truck.

Despite many old bridges that have been designed according to old design standards, due to conservative design, they may possess reserve capacities to resist higher axle loads. Load testings have demonstrated such phenomenon (Faber et al., 2000). Therefore, prior to replacement or strengthening of the structure, it is imperative to

carry out non-destructive load testings that would provide an insight into the bridge response to the applied load, thereby saving cost from unnecessary replacement.

This chapter also provides an overview of the Australian Bridge Design Standard AS 5100 (2004) that is considered mandatory in the design of bridges both on the national highways and as well on the local roads in most state highway departments and regional councils respectively. The traffic is often quite different for the bridges on the highways and local roads; therefore the bridges designed on the local road in accordance to the national standard, can be regarded over-designed causing budgetary pressures. The design requirement for the local road bridge will, therefore, be reviewed and its structural response demand highlighted in this Chapter.

2.2 Review of low volume Road Bridges

A bridge is a structure built to span physical obstacles like a body of water, gorge, valley, or road, to provide passage over the obstacle. Designs of bridges vary depending on the function of the bridge, the nature of the terrain where the bridge is intended to be constructed, the material used and the funds available to build it.

According to Roadfacts (Austroads, 2005), there are approximately 37,078 bridges in Australia. Of these, over two thirds are located on local or rural roads under the local government administration. Many of these bridges are either single lane or double lane bridges and built with timber, which are currently impaired over the time. A typical timber bridge constructed in Australia is shown in Figure 2.1.

Figure 2.1 Timber bridge on low volume road (Champion et al. 2002)

Concrete culvert spanning up to 15m is another commonly adopted bridge construction methodology on the low volume road; however they are more expensive relative to the annual maintenance budget allotted to the regional councils. Steel girder and precast concrete decks are also used on the low volume road as this type of bridges require less time to construct and result in a comparatively better quality than the concrete panels.

2.2.1 Low volume traffic network

According to AASHTO (2001) a road is considered as "low volume" if the average daily traffic (ADT) is less than 400 vehicles and design speed typically less than 80km/h. Most roads in the rural areas are therefore can be considered as low volume roads. In the Australian context, ADT is less than 500 vehicles for low volume roads with two lane (AS 5100, 2004). For single lane access roads, traffic can be less than 150 vehicles per day (clause 9.4 of AS 5100, 2004). They are built to provide access to farmers and their produce. A low volume road can be either metalled or un-metalled as shown in the Figure 2.2 (a) and (b). A general road hierarchy in Australia

was first published by National Association of Australia State Road Authorities (NAASRA). Austroad, replacing NAASRA in 1991 classified the road as follows:

(i) National Highway

(ii) Rural arterial

(iii) Urban arterial

(iv) Rural local

(v) Urban local

Table 2.1 shows the type of roads in Australia and their total length in km. The information presented in the table below is based on data contained in the RoadFacts (2005 p. 14)

Table 2.1 Road length by road type and travel comparisons

Road type	Length (km)	% length	Travel (million veh-km)	% travel
National highway	18,773	2.3	25,679	13.3
Rural arterial	109,031	13.4	40,270	20.9
Urban arterial	13,051	1.6	80,892	41.9
Rural local	**581,903**	**71.6**	**13,826**	**7.2**
Urban local	90,215	11.1	32,147	16.7

As it can be seen from above table that the rural local road has the greatest length of road, however on average they carry the least amount of traffic.

(a) Metalled rural road (b) Un-metalled rural road

Figure 2.2 Typical low volume rural roads (Factsheet, 2010)

2.2.2 Low volume road bridges: characteristics

Bridges in the low volume road, particularly those in remote areas, demand a different approach to bridge engineering. Standards commonly used for high volume road bridges are excessive for low volume applications, especially in fatigue design limits. Roadway width, sidewalk provision, barrier details and approach flares are other factors that need to be addressed for the specific application.

Though AS 5100, as the national standard, requires to be stringently referenced for all road bridge designs and construction in Australia, the same code via clause no. 9.4 AS 5100.1.2004 allows the relevant authority or owner of a bridge to make changes as deem necessary. For single lane access roads with traffic volumes less than 150 vehicles per day (clause 9.4 AS 5100.1, 2004), a bridge width to be adopted between the barriers is 4.2 to 4.5 m (whilst for high volume bridges the minimum clear width is width of traffic lanes + 2.4m). If a walkway is provided on road bridges, then the clear width of walkway available for use by pedestrians shall be 1.8 m minimum. For bridge without walkway, the edge clearance from the edge of the traffic lane to the face of the safety barriers on each side of a bridge is 600 mm for low volume, two lane roads, whilst the edge clearance for high volume roads ($\geq$ 5000 vehicles per day) is 1200mm. Traffic barriers are not essential for traffic volume less than 150 vehicles per day.

2.3 Bridge rehabilitation/replacement technologies

Like any other structures, bridges too are susceptible to degradation and deterioration over time, thus further evaluation of the structure will be required after initial design. In addition, bridges will require evaluations due to increased heavy vehicle mass limits, changing design standards, and changing bridge usage and lane configurations.

An important part of the bridge rehabilitation is the proper inspection of bridge structures and depending on the condition of the structure and its geometric features, a bridge may be classified as *adequate*, *structurally deficient* or *functionally obsolete*. Structurally deficient bridges are then repaired/or strengthened to carry higher load in line with the current code while functionally obsolete structures are completely replaced with new structure systems. Several bridge rehabilitation/repair options are available for example concrete overlay on the timber decking to distribute the load, supplementing timber girder with steel beam, timber girder concrete decking system or other. Alampalli and Kunnin (2002) used light weight FRP deck on the truss bridge replacing completely the deteriorated concrete deck as a rehabilitation measure to increase the load carrying capacity. Obsolete bridges on low volume road can be replaced with similar structures but with higher load carrying like TransiSpan (BlueScope, 2009) bridge system, engineered wood products, concrete culvert, hume deck unit (Holcim, 2010), steel girder and concrete deck and disused rail wagons.

2.4 Bridge superstructure overview

Bridge superstructures are those structures above the bearing and consist of girders and deck. Even the classification of bridge is done based on the superstructure as girder, truss, cable and arch bridges. Girder Bridge is a common form of bridge construction on low volume roads. The common forms of girder bridges are:

- Solid Slabs (span 4m – 12m)
- Voided Slabs (span 8m – 16m)
- T-Girder and slab (span 12m – 25m)
- Box Girder (Single or Multi span) (span 25m – 60m)

2.5 Australian Bridge Codes of Practice AS 5100

AS 5100 (2004) is the current standard that is stringently adhered to for the design of new bridges, both on the highways as well as the low volume roads across Australia. However, clause 9.4 of AS 5100 allows adoption of widely accepted local standards especially for the geometry requirements. AS 5100 (2004) has replaced earlier bridge design codes/standards commonly followed in Australia, eg., Austroads-1992, HB 77.2-(1996) and NAASRA (1985).

For complete design of a bridge, starting from the substructure to the superstructure, the following sub categories of the standard are referenced:

- AS 5100.1 Part 1: Scope and general principles
- AS 5100.2 Part 2: Design loads
- AS 5100.3 Part 3: Foundations and soil-supporting structures
- AS 5100.4 Part 4: Bearings and deck Joints

- AS 5100.5 Part 5: Concrete
- AS 5100.6 Part 6: Steel and composite construction
- AS 5100.7 Part 7: Rating of existing bridges

However in this thesis only a selected few sections that are pertinent to the design, construction and load testing are reviewed as given below:

- AS 5100.1 Part 1: Scope and general principles
- AS 5100.2 Part 2: Design loads
- AS 5100.6 Part 6: Steel and composite construction
- AS 5200.7 Part 7: Rating of existing bridges

2.5.1 AS 5100.1 – Scope and general principles

Under this section only the geometric requirements like bridge carriageway width and clear edge distance that are of concern to the FRW bridge will be reviewed. Clause 9.4 of AS 5100.1 (2004) states that the bridge carriageway width shall be specified by the relevant authority based on the consistent level of service whilst taking into account the road geometry, traffic volume and the bridge locality. In the absence of relevant applicable guidelines of the bridge with the owner or authority, clause 9.4(i) of AS 5100.1 (2004) specifies that for single lane road with traffic volume less than 150 vehicles per day; the minimum carriageway width between the barriers will be 4.2 m. The edge clearance of 600 mm from the edge of the traffic lane needs to be maintained in case of bridges without walkways.

2.5.2 AS 5100.2 – Design loads

Trafficable bridge loading is primarily due to the vehicular traffic that crosses the bridge. The loading configuration that need to be employed to analyse the effects of the traffic movements can be regrouped into three categories namely (i) individual loads, (ii) stationary loads and (iii) moving loads. Individual load consists of W80 and A160 axle loads which are to be placed anywhere on the bridge members so as to cause the most adverse effect.

2.5.2.1 W80 wheel load

It consists of single individual heavy load of 80kN uniformly distributed over the contact area of 400 mm × 250 mm. The W80 wheel load shall be applied anywhere on the roadway surface and to all structural elements for which the critical load is a single wheel load.

2.5.2.2 A160 wheel load

A160 wheel load consists of single individual heavy axle load of 80kN each per wheel as shown in the Figure 2.3.

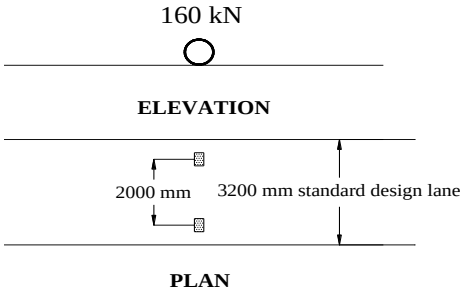

Figure 2.3 A160 axle loading plan

2.5.2.3 S1600 stationary traffic load

The S1600 stationary traffic load models a queue of stationary loads on the bridge together with uniformly distributed load over the standard design width of 3.2 m. In order to produce the most adverse effects due to S1600 loading (in plan), the variable spacing of the tri-axle groups may be adjusted and the uniformly distributed load placed to any length deemed necessary. The S1600 loading in plan is shown in the Figure 2.4.

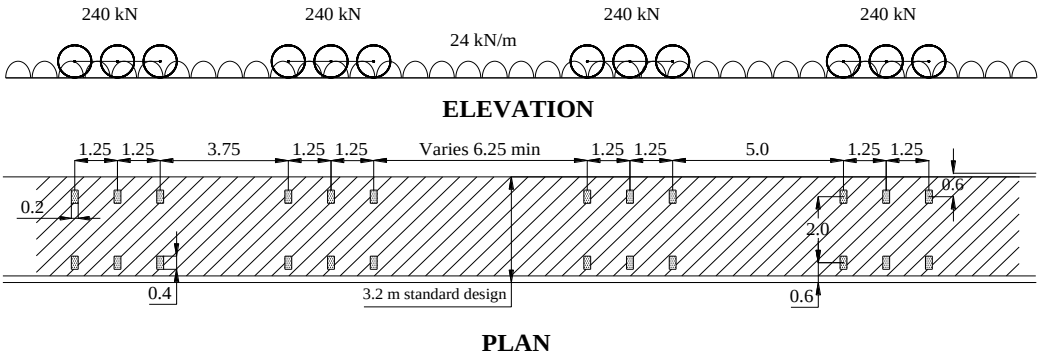

Figure 2.4 S1600 stationary traffic loading plan from AS 5100.2

2.5.2.4 M1600 moving traffic load

The last group of SM1600 load is the M1600 moving load as shown in the Figure 2.5. The M1600 load train models a moving stream of traffic along the bridge. It consists of tri-axle set of wheels, each wheel having a magnitude of 60 kN at varying spacing and uniformly distributed load (UDL) of 6 kN/m distributed over the entire standard design width of 3.2 m. The UDL component of the M1600 can be placed to any length as deemed necessary together with the tri-axle group of loads to produce the most adverse effects.

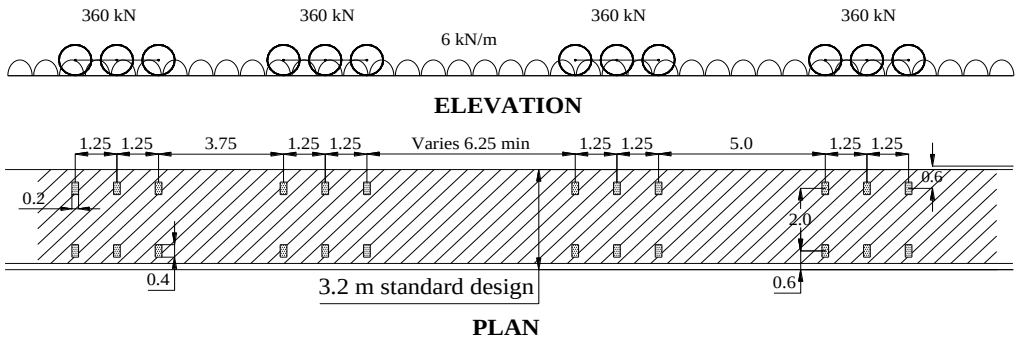

Figure 2.5 M1600 moving traffic loading plan from AS 5100.2

2.5.2.5 Dynamic load allowance (DLA)

When a bridge is loaded with moving load an increase in the internal forces is observed when compared to an equivalent static applied load. This increase in the forces is due to dynamic amplification of the static load and need to be incorporated in the design. Clause 6.7 of AS 5100.2 (2004) recommends the dynamic load allowance (α) to be included in the design action for both the serviceability and the

ultimate limit states. The DLA for appropriate loading is specified in the standard in the Table 6.7.2 (AS 5100.2 (2004)) and is reproduced in Table 2.2.

Table 2.2 Dynamic load allowance for the traffic loads (AS 5100.2 (2004))

DYNAMIC LOAD ALLOWANCE (α)	
Loading	**Dynamic load allowance (α)**
W80 wheel load	0.4
A160 axle load	0.4
M1600 tri-axle group (see Note 2)	0.35
M1600 load (see Note 2)	0.30
S1600 load (see Note 2)	0
HLP loading	0.1
Notes: 1 Dynamic load allowance is not required for centrifugal forces, braking forces or pedestrian load. 2 Including the UDL component of the traffic load.	

The magnitude of the design action is therefore determined as follows:

$$Design\ action = (1+\alpha)\times(the\ load\ \ factor)\times(applied\ action) \qquad 2.1$$

where;

α = dynamic load allowance

The load factor is given in clause 6.10 of AS 5100.2, which is taken from the standard and reproduced in Table 2.3.

Table 2.3 Load factors for the traffic loads (AS 5100.2 (2004))

LOAD FACTORS FOR DESIGN ROAD TRAFFIC LOADS		
Traffic load	**Limit state**	
	Ultimate	**Serviceability**
W80 wheel load	1.8	1.0
A160 axle load	1.8	1.0
M1600 moving traffic load	1.8	1.0
S1600 stationary traffic load	1.8	1.0
Heavy load platform load	1.5	1.0

2.5.3 AS 5100.6 – Steel and composite construction

AS 5100 sets out the minimum requirements for the design of the structural steel work in bridges including design of steel piles, steel railings and sign structures. In addition, the standard outlines the design of composite steel and concrete members, the general requirements of the design of concrete and fatigue design of steel structures.

2.5.4 AS 5100.7 – Rating of existing bridges

AS 5100 specifies procedures for rating the safe load capacity of a bridge for defining its remaining life. The rating concept is based on the limit states design principle wherein the minimum strength capacity of the bridge shall be greater than the assessed maximum load applied. Both the serviceability and the ultimate limit state capacities need to be considered. The general rating equation according to this standard is defined as:

$$RF = \frac{Available\ bridge\ capacity\ \ for\ live\ load\ effects}{Live\ load\ effects\ of\ \ nominated\ rating\ vehicle} \qquad 2.2$$

where;

RF = Rating factor

Also the standard outlines the load testing procedure for both non-destructive testing (static proof load testing and static performance load testing) and destructive testing.

2.6 Use of Rail Wagons in Road Bridges: The US experience

Iowa State University (ISU) in the United States (US) has carried out extensive research on the usage of disused rail wagons as the bridge superstructure. A feasibility study conducted by ISU (Wipf et al. 1999) focused on the use of rail wagons as low cost bridge replacement alternatives on low volume county roads. The study concluded that the construction of such bridges can cost up to sixty percent less than constructing an equivalent structural steel or RC slab bridge and the rail wagon bridges therefore, represent a viable and economical bridge replacement alternative for the low volume roads. In order to demonstrate the constructability, economy and adequacy of this type of bridge, several demonstration bridges were designed, constructed and load tested in 2003 (Doornink et al. 2003). Figure 2.6 shows one typical single span bridge constructed using rail wagons in Buchanan county whilst Figure 2.7 show multi-span bridge built using disused rail wagons in Winnebago county.

Figure 2.6 Demonstration bridge in Buchanan County (Klaiber et al. 2003)

Figure 2.7 Demonstration bridge in Winnebago County (Massa, 2008)

A brief description of the bridges and their research findings are discussed in the section following, and their rail wagon structural components compared with the FRW of Queensland.

2.6.1 US FRW Bridges

A single and multi-span bridges constructed using disused rail wagons were reviewed. The single span bridge was built in Buchanan county located five miles southwest of Independence, Iowa whilst multi-span FRW bridge was constructed in Winnebago county, located three miles southeast of Buffulo centre on Buffulo creek, Iowa. An overview of both single and multi-span bridges constructed in the low volume roads were shown in Figure 2.8 and Figure 2.9.

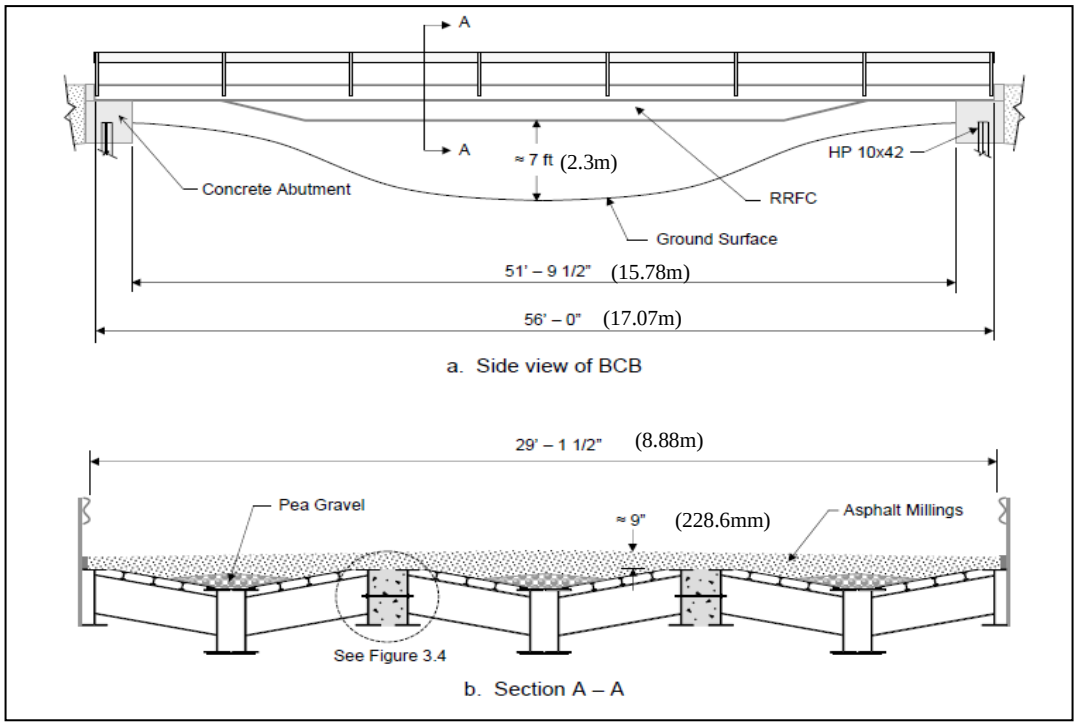

Figure 2.8 Single Span Bridge layouts (Taken from Doornink et al. 2003)

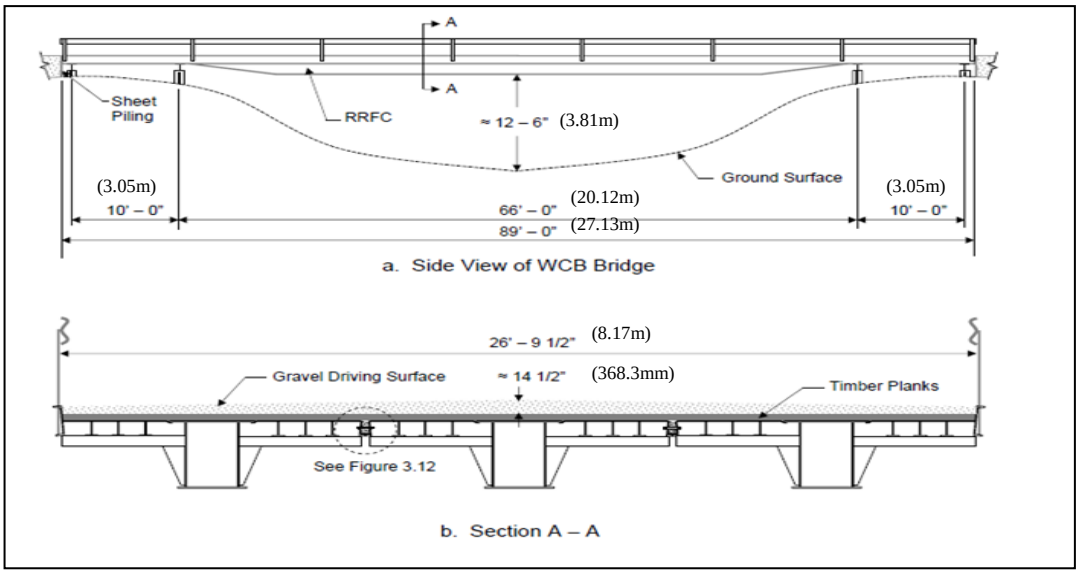

Figure 2.9 Multi-span bridge layout (Massa, 2008)

In both the bridges constructed in the low volume roads in Iowa state of US, two or more wagons were used as the bridge decks arranged side-by-side and connected at one of their edges with reinforced concrete beam as shown in Figure 2.10.

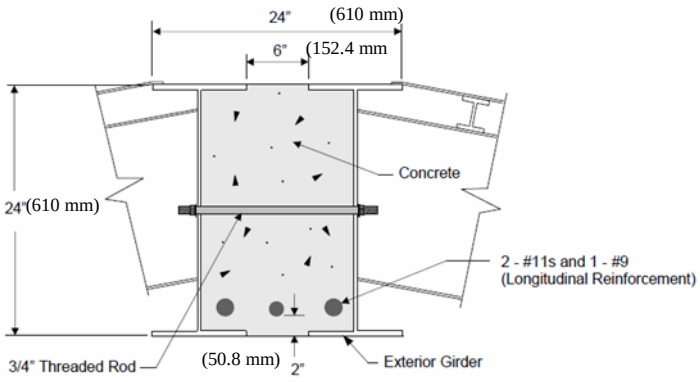

Figure 2.10 Longitudinal connection beam at the centre connecting two wagons (Taken from Doornink et al. 2003)

Doornink et al. (2003) and Massa, (2008) carried out three load tests. Instrumentations were placed across the wagons on the pre-determined critical locations. The first load test occurred after installation of the wagons but before the construction of the longitudinal wagon connection. The second load test was carried out following the construction of the longitudinal connection and the third test approximately after one year of service. In each test the bridges were subject to a loaded tandem truck carrying Iowa legal loads of approximately 22 tonnes. A grillage models were also constructed by the authors to compare theoretical results with the experimental results.

All the stresses and deflections were below the allowable limit of AASTHO (2003). Strain and deflection measured in the second test were found to be smaller than the first test, indicating adequacy of the longitudinal connection to provide lateral load transfer. The results from the final test were similar to the second test, indicating no change in the structural behaviour of the bridge even after one year of the bridge was put under service. Finally the study concluded that rail wagon bridge represents viable and economical bridge replacement alternatives on low volume road.

Several rail wagon bridges were designed, built and load tested by ISU and California in the US and in the Canada; all of them have demonstrated the structural adequacy of the rail wagons as the bridge superstructures in low volume road. Some of them were built in 1999 and still after a decade, the bridge is in perfect condition, serving the county. In all the studies carried out so far, fatigue was considered less significant and the major design was for static loading.

Similar project of using disused FRW from QRN is undertaken by the Queensland University of Technology (QUT) to examine if a low cost alternative could be developed for the replacement of ageing bridges in the rural low volume roads network, where usually the rehabilitation and maintenance fund is limited. However, the FRW in comparison to US rail wagon differ significantly and thus detailed independent studies are carried out. The structural difference between the US rail wagon and the Queensland FRW are as follows:

1. The dimensions of the central box girders of the US rail wagons (705 mm deep × 578 mm wide) are significantly larger than the FRW (660 mm deep × 400 m wide) of.
2. The US rail wagons have larger longitudinal edge beams (610 mm deep) (particularly the BCB rail wagon) while the FRW has an edge beam of approximately 200 mm deep.
3. The decking system of the US rail wagons consists of transverse members with continuous secondary beams topped with steel decking while the FRW consists of folded plates running in both the longitudinal or transverse directions without steel decking.

4. The decking members of the FRW are inconsistent in their connection to the main box girder and other members of the wagon, and several of these beams are heavily corroded thereby limiting the load bearing capacity.
5. The US used RC beam at the centre connecting two wagons together while FRWs were connected together at their edged Z beams with custom made brackets (discussed in detail Chapter 5).

Figure 2.11 shows the overall overview of the FRW available with QRN, Australia.

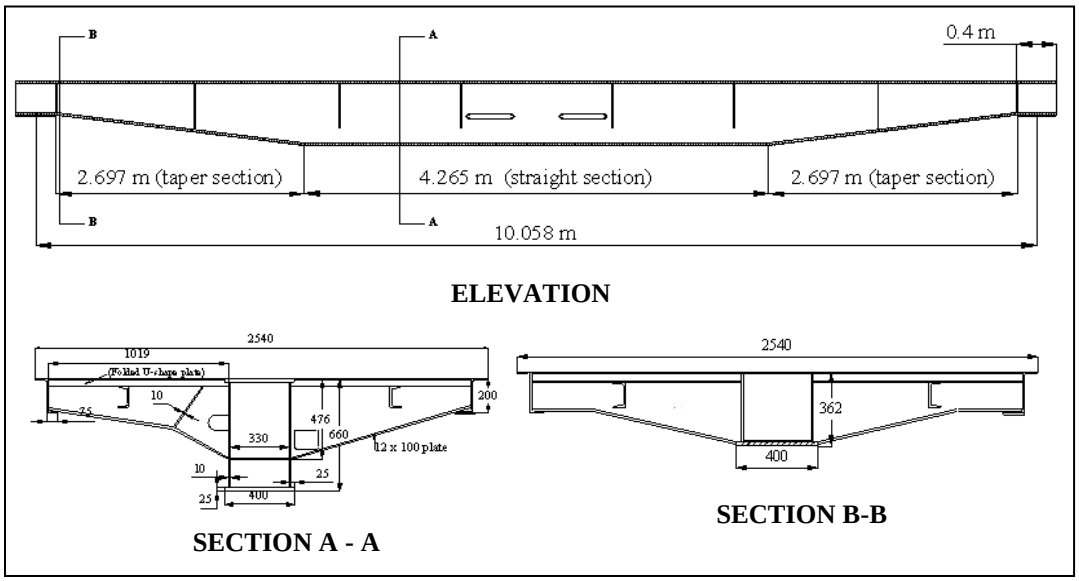

Figure 2.11 Overall overview of FRW from QRN

Limited similarities also exist between the two wagon systems; for instance, the longitudinal profiles of the primary load carrying box girders are tapered at both ends. These observations indicate that the FRW available from QRN, Australian rail industry has fewer primary load carrying members than that of rail wagons in the US and detail investigation and certain degree of modifications, for example replacement of decking members with stronger similar members when they are to be used as the bridge superstructure in the low volume road are required.

McDonald (2010) and Dhanasekar and Bayissa (2011) have studied the structural adequacy of FRW as the bridge superstructure in low volume road through full scale laboratory testing. SM 1600 loadings of AS 5100 (2004) was applied at the critical locations to the FRW and displacement and strains were measured. All the test results remained well below the serviceability limits prescribed in AS5100 (2004). The finite element model (FEM) was updated with the experimental results and further ultimate analysis was carried out. The structural adequacy of FRW as the bridge superstructure in low volume road was demonstrated based from the lab tests data and a calibrated FEM analysis. The FRW tested in the lab was not provided with driving surface/ pavement for enabling vehicle movement; only the bare FRW structure was examined.

2.7 In-service performance evaluation of bridges through non-destructive load testings

Non-destructive load testing is an effective method of evaluating the performance and structural capacity of bridges; this method helps to establish the serviceability limit prescribed in the standards using the deformations and strains measured at the critical locations of the bridge deck structure under the influence of the static and moving loads. The principle of load testing is to compare the field response, for instance, load versus deflection or load versus strain, of critical members of a bridge with their characteristic performance as predicted in theoretical analyses, in order to assess the actual capacity of the bridge to resist live loads (AS 5100.7, 2004). Although the assessment of the bridge can be carried out by means of analytical and theoretical analyses alone, it has been determined through extensive load testing in

Ontario, Canada that the bridges often show significantly higher capacity than predicted by above theoretical methods (Bakht et al. 1981). Experimental load testing have demonstrated that it is rather inaccurate to determine the live load carrying capacity of a bridge theoretically because of various assumptions taken in the theoretical modelling and analysis, which do not accurately reflect the actual behaviour as narrated in many literatures (Bakht et al. (1990); Ghosn et al. (1986) and Nowak and Tharmabala (1988)).

Load testing helps removing some of the assumptions made during design of the bridge such as the load distribution, composite action, material properties, unexpected continuity, and end restraint effects (Nowak and Tharmabala (1998); Ghosn and Moses (1992) and Heywood and Ransom (1997)). Load testing is used to both evaluate the load bearing capacity of existing bridges (Bakht (1988); Saraf, V., and Nowak (1998); Liu et al. (2009) and Barker (1999)) and to validate the design of new constructions before they are opened to traffic (Cho et al. 1998).

Testings (both static and moving) are carried out on existing bridges that have failed their analytical assessments; such bridges are left to be in service because the load testings have revealed that their load carrying capacity is larger than the calculated capacity (Ryall, 2010, p. 178). Field load tests are also widely carried out on newly constructed bridges to provide information whenever novel construction methods or materials are engaged and to give assurance of the performance of these bridges ((Stone et al. (2001); Stiller et al. (2006); Mehrkar-Asl and Bolton (1999); Beben (2005) and Ji et al. (2007)). Stone et al. (2001) and Stiller et al. (2006) have examined the performance of GFRP deck laid on steel girders through field load

testing. It is a common practice in France and Switzerland to carry out the load test of all new bridges with a static load (Favre et al. 1992).

Various methods of bridge testing are used to determine different aspects of bridge behaviour. These tests differ in both their purposes and the loads used. Ryall, (2010 p. 178) described three types of load tests for the bridge superstructure:

- Performance load testing
- Proof load testing and
- Collapse load testing

Since the main aim of this thesis is the performance load testing and structural adequacy evaluation of road bridge superstructure using disused FRW, the literature review will focus more on the performance bridge testing with minor reference to proof load test and collapse load tests.

2.7.1 Performance Load Test

Performance (also known as supplementary loads tests) are carried out using predetermined loads that are normally not greater than the existing traffic load and therefore will not pose a significant risk of permanent structural damages to the bridge. This type of load testing is a serviceability limit state test and normally employed to evaluate the in-service performance of bridge structure (Harris et al. 2008). The aim of the performance load testing is not to test the bridge at its ultimate load but to establish that it has sufficient capacity to resist the serviceability loads; therefore, this test examines only the elastic response of the bridges. The

performance load test data are normally used to calibrate mathematical models of the bridge so that they reflect more closely the behaviour of the real bridge (Mehrkar-Asl and Bolton, 1999).

Performance load tests can provide invaluable information on how transverse load are distributed through the bridge and also in determining the actual measured stiffness parameters as opposed to the theoretical values (Allison and Woodward 2005, p.175). In addition performance load testing is often used for determining factors that provide an extra amount of hidden strengths in a bridge deck; for instance higher material properties, degree of composite action, support conditions, non-conforming details and other co-existing support systems i.e. membrane action and end-restraint effects that are not obvious and usually omitted in the analytical models (Ryall (2010, p.182); Bahkt and Jaeger (1990)). The calibrated analytical models closely reflect the observed responses. Therefore, bridges can be re-analysed for the ultimate limit state load (Richard et al. 2010). Alternatively the ultimate load capacity can be deduced by extrapolating the results of the performance load test (Ryall 2010, p. 179). However Allison and Woodward (2005) note that care should be taken due to the relatively low level of load applied during the testing compared to the ultimate load level.

Switzerland has a long history of load testing of new bridges prior to opening to the traffic. According to Moses et al. (1994) the Federal and Cantonal Administration requires a load test of every major bridge in Switzerland before they are opened to traffic; basically to validate the assumptions made during the design stage and to determine the response of any special features which may not have been predicted by

theoretical analysis and modelling. As a result of this requirement, over 200 bridges have been load tested in Switzerland to date. The load applied is normally 80% of the code recommended maximum live load for a simply supported span, which gives a target load of 250kN per vehicle. This load is normally very small when compared to ultimate load applied in other countries.

In the United Kingdom (UK), performance load testing of bridges is usually employed to calibrate analytical models. As mentioned above the loads applied to the bridge during a performance test must be sufficient enough to provide a measurable response whilst not high enough to cause irreversible damage to the structure. A safe level of loading for the test can be determined from the finite element model or grillage model (Mehrkar-Asl and Bolton 1999). Applied loads generally should not exceed the level of normal traffic loads experienced or expected to be experienced by the bridge (Allison et al. 2005). Loads can be applied to a bridge through a number of methods, including; pillow or mattress water tanks, flexible water tanks, or water bags hung from a structure. The most preferred and commonly used method of loading for performance load tests is the use of loaded trucks (Ryall 2010, p.191). Loaded trucks filled with aggregate, weighing in the range of between 30-35 tonnes are commonly used as they can be filled to the approximate load required and weighed at weighbridges or on site using portable scales. One of the main advantages of using loaded trucks is the flexibility they provide in being able to move the load easily to difference positions on the bridge.

Guidelines for load testing are normally provided by the relevant authority (AS 5110.7, 2004 in case of Australia). The guidelines note that using the correct type of

test, amount and location of instruments is crucial in achieving a satisfactory outcome. Generally instrumentations used in the performance load testing are displacement transducers and strain gauges to measure deflections and strains (Mehrkar-Asl and Brookes 1997). A carefully planned major performance testing of a demonstration FRW bridge constructed in a low volume high axle load roads network is the major outcome of this thesis.

2.7.2 Proof load test

Proof load testing is a non-destructive test that involves loading the bridge incrementally and loads are often higher than the maximum legal loads and closer to the loads factored for the ultimate limit state design (Heywood et al. (1997) and Boully et al. (1997)). Proof load tests are carried out on a bridge as a self-supporting alternative to theoretical assessments (Allison et al. 2005). However proof load tests are often considered high risk and can lead to structural damage of the bridge, leading to rapid deterioration and collapse (Mehrkar-Asl and Brookes 1997). In the UK, proof load tests are not considered acceptable methods of bridge assessment by the Department of Transport (Heywood et al. 1997). However Ryall (2010, p.189) notes that the London Bridge Engineering Group are of the opinion that it may be preferable to accept a small risk of damage to the structure during proof load testing to establish conclusively that a bridge has sufficient strength at ultimate loads.

Although proof load testing is relatively new to Australia, several bridges have been proof load tested to evaluate the actual load carrying capacity of old bridges, predominantly in New South Wales and Victoria (Heywood et al. 1996).

2.7.3 Collapse load test

Collapse load test is a destructive test that is used to measure the bridge response to failure under loading. They are project specific and normally carried out on older bridges that are marked for replacement. This type of test is either used for design validation, establishing common methodologies for assessing the safe carrying capacity of bridges or for examining the remaining strength of deteriorated bridges (usually carried out on bridges marked for demolition). Collapse load test is conducted to collect information on the bridge response to the live loads that can then, be applied to the assessment of other similar bridges (Ryall, 2010, p.190). Richard et al. (2010) have carried out a collapse load test in Sweden, where a vertical point load was applied at the mid span and experimental arrangements were designed to study the failure from the combination of shear and bending.

2.8 Summary

This chapter has presented characteristics of low volume road, the currently available bridge replacement technologies using rail wagons in the United States and the way the field load tests are conducted in the bridge projects. The Australian national bridge standard AS 5100 (2004) with the prescribed axle loads regarded quite heavy on the international scale is reviewed, discussed and presented. Types of load testing of bridges to evaluate and rate the structure to the applied load have also been discussed.

Important literature findings related to the low volume bridge alternatives using rail wagons and performance load testings for evaluation of structural adequacy of FRW bridge are summarised as follows:

- Iowa State of University (ISU) in the US has designed, built and load tested single and multi span road bridges containing rail wagons; both. The field test results have demonstrated that such bridges are a viable economic alternative for low volume road bridges. However, the rail wagons of QRN have fewer main load bearing members with smaller sectional dimensions compare to US wagons and thus separate independent study was required.
- The success of the road bridges containing rail wagons can be directly linked to the careful selection of rail wagons, careful overall design and construction practices as the design is not straightforward and is generally not guided by national standards.
- Road bridges containing rail wagons are reported to be relatively less expensive and can be constructed in a short period with limited skilled labour.
- The full scale laboratory testing of the FRW obtained from QRN (without running surface) has demonstrated adequate structural capacity to resist high axle loads prescribed in AS 5100 (2004).
- Performance load testing is a relatively low risk method for assessing field load response of bridges and is widely implemented internationally. The test results are generally used to validate the theoretical models for further analysis.

Chapter 3: FRW structural system and its adoption as a road bridge

3.1 Introduction

This chapter presents an overview of the FRW available in QRN including its structural components layout and their applicability as the road bridge superstructure. Capacity calculations of each member are determined using the guidelines provided in AS 5100.6 (2004). The theoretical analysis of the FRW components is conducted in line with the adaptability of their members as the bridge structural element, for example the main box beam of the wagon is realised as the main load bearing girder of the bridge. Desktop study is essential because the FRW has been initially designed for rail freights subjected to complex imposed and traffic related dynamic loading from above and below respectively which will be different to that when they are to be placed as part of a bridge superstructure.

3.2 Structural overview of FRW

The structural system of a single FRW is shown in Figure 3.1 through Figure 3.3. In the longitudinal direction, there exists a single central box girder (designated as the primary structural member), two secondary edge Z-beams and two bracing channels located in the vicinity of the two end supports. In the transverse direction the FRW consists of two main box girders – one at each ends and one each at bolster supports, six ‘inverted’ T-section cross beams welded to the primary longitudinal box girder

on both sides and eight bracing channels welded to the cross beams. The primary box girder and the inverted cross beams are generally tapered as shown in Figure 3.3(b). The FRW decking system is made up of a series of folded plate sections welded to the primary box girder, edge Z-beams and the cross beams, at an average spacing of 160mm in both the longitudinal and the transverse orientations. Figure 3.2 shows the components of FRW when one of the wagons used in the demonstration bridge was positioned upside down while preparing for the full scale laboratory testing in the lab.

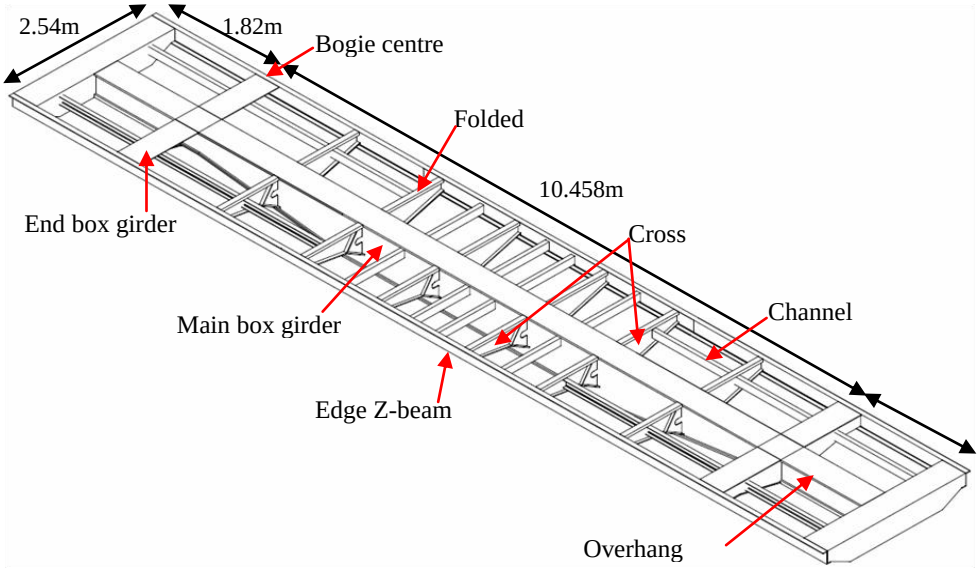

Figure 3.1 Isometric view of the main structural components of FRW

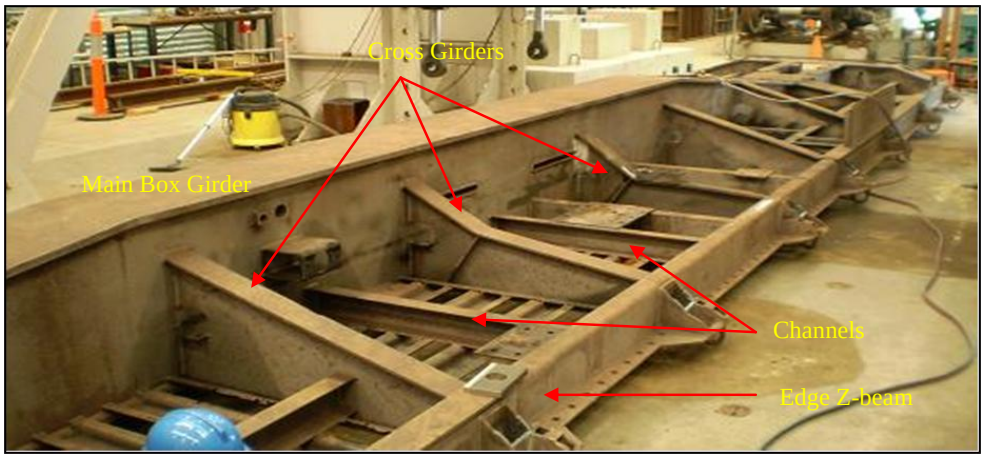

Figure 3.2 Inverted view of FRW

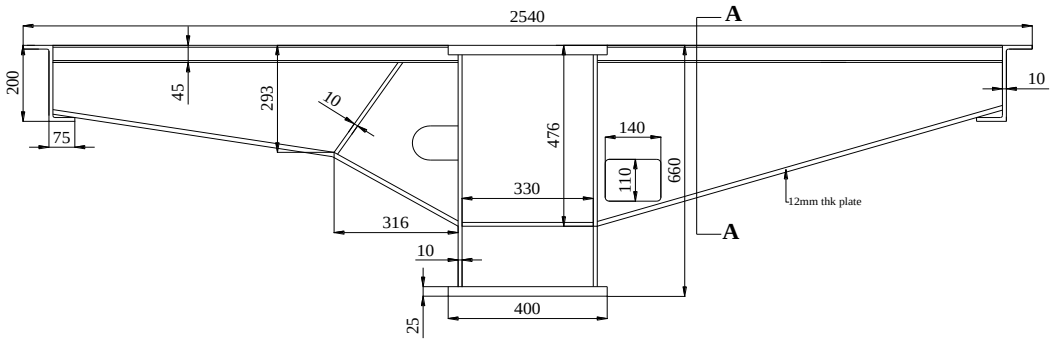

(a) Cross section of FRW at the mid span

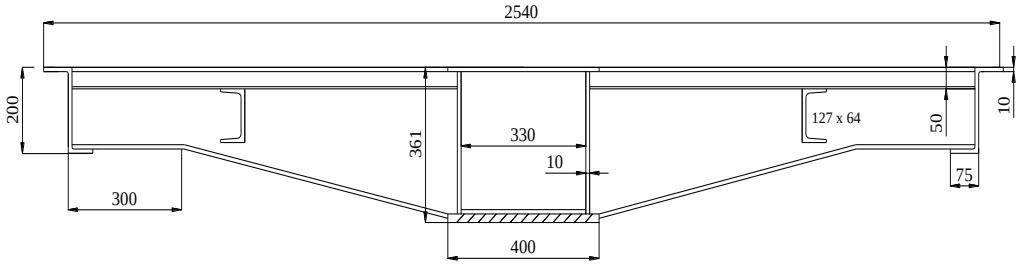

(b) End box girder (support location)

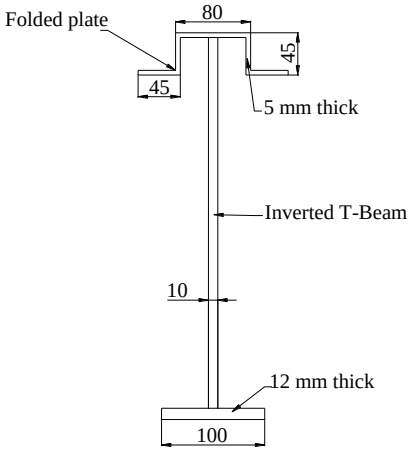

(c) Section A-A

Figure 3.3 Transverse member details of the FRW

3.2.1 Primary member: main girder

The FRW considered for use as the bridge superstructure is 14.10 m long and approximately 2.54 m wide as shown in Figure 3.1. The overhang parts in Figure 3.1 constitute thin members that are unsuitable for bridge superstructure; therefore, these members were removed and the FRW modified as shown in Figure 3.4. The length of the wagon after removing of the overhang members is 10.458 m.

General overview of the main longitudinal girder of the FRW is presented in Figure 3.1. The main box girder is 660 mm deep and 400 mm wide and tapers to 341 mm deep at the bogie centres at either end of the wagons as shown in the Figure 3.5. The upper and lower flanges are 25 mm thick steel plate welded to 10 mm steel webs forming hollow box beam. Ultrasonic test was conducted on the girders to check any loss of metal due to corrosion. The test result showed that there was no significant loss of steel and the steel thickness were almost constant throughout the girder, with slight (5%) loss of thickness near the bolster region. The ultrasonic test result is summarised in the Appendix A.

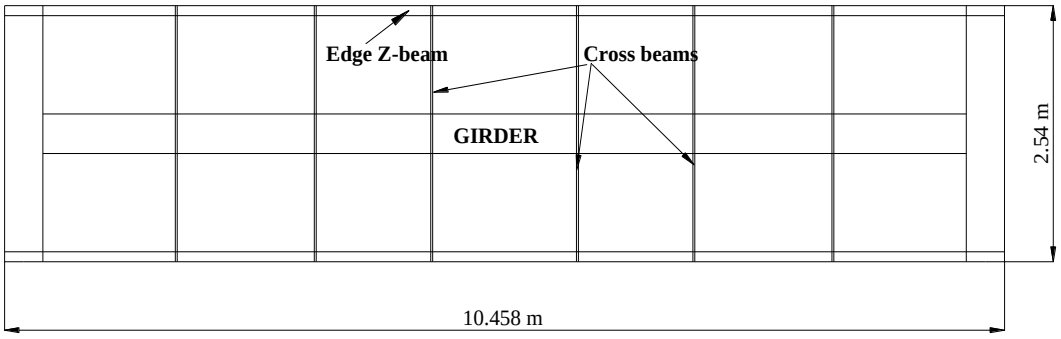

Figure 3.4 Plan view of FRW after cutting off the overhang parts for bridge construction

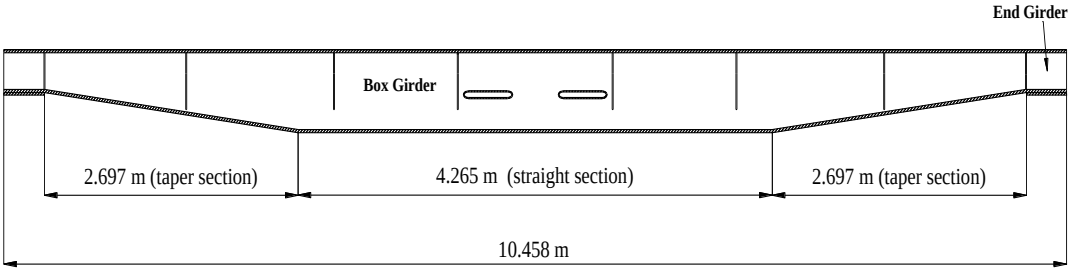

Figure 3.5 Elevation of FRW; showing profile of main box girder

3.2.2 Secondary members: end box girders and intermediate inverted T- beams (cross girders)

The secondary members spans in the transverse direction and comprises of two small box girders (Figure 3.2 (b)) at the bogie centre at the end of the wagons and twelve (six on each side) built-up inverted T- section beams welded to the main box girder (Figure 3.2 (a)). The end cross girder is 341 mm deep at the centre and tapers to 200 mm on both sides and they are welded to edge Z-beams. The intermediate cross girders details are shown in Figure 3.2. The lower flange of the inverted T-beam is 12 mm × 100 mm plate, fillet welded to the web of 10 mm thick steel. The beam depth varies from 476 mm at the main box girder to 152 mm at the edge Z-beam with circular and rectangular holes near the main girder as shown in the Figure 3.2 (a) and Figure 3.3 respectively. No significant metal loss was observed in the results of the ultrasonic test.

3.2.3 Decking grillages

The FRW decking system is made up of series of folded plate beams welded to the primary box girder and the edge Z-beams as well as the cross beams and channels, at

an approximate spacing of 160mm in either the longitudinal or the transverse orientation. Figure 3.6 (a) shows typical cross section of the folded plate beam. In the rail transport system, the gap between the two folded plates was filled with hard timber as shown in the Figure 3.7.

Although the suitability of the FRW as the bridge superstructure was realised initially during the desktop study and in the full scale laboratory testing (McDonald, 2010), the member stiffness of the folded plate was found to be insufficient to resist the high axle load in bearing as well as flexure and shear. Therefore, they were replaced with 100mm × 50mm × 4 mm rolled hollow section (RHS) in the actual bridge construction (Figure 3.6 (b)).

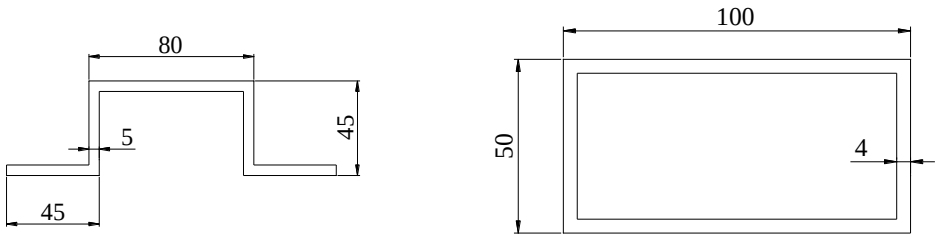

(a) Folded plate beam (b) RHS beam

Figure 3.6 Typical cross section of decking members

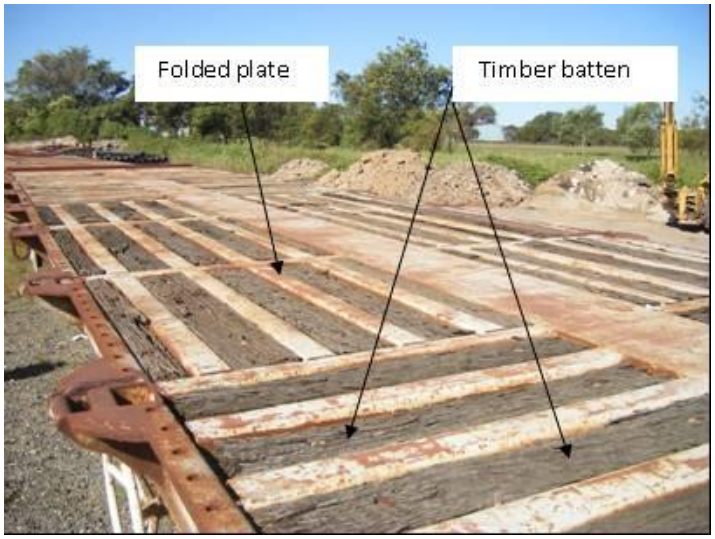

Figure 3.7 Top view of FRW before removal of the timbers and folded plates

3.3 Capacity Calculations

A general principle in the engineering design is that the resistance of the materials and the cross sections supplied exceed the demands put on them by applied loads.

$$R \geq E_l \qquad 3.1$$

where;

R = Resistance

E = Effects of the loads

Capacity design method, a simplified form of the limit state design method is used in AS5100 (2004) wherein it requires that the structure is durable, serviceable, and adequately strong while serving its intended function.

The bridge and its components were designed as per AS 5100.1 (2004) and AS 5100.6 (2004) respectively. According to clause 3.2 (c) of AS 5100.6 (2004), '*all members and components are to be proportioned so that the design capacity is not less than the design action effect'* as shown in Equation. 3.2:

$$S^* \leq \phi R_u \qquad 3.2$$

where;

S^* = the design capacity

ϕ = capacity reduction factor (normally less than 1.0) and

R_u = the design action effect

In the capacity computations in the following sections, the yield stress of the steel was taken as 90% of the original 250 MPa (225 MPa) mentioned in the rail drawings obtained from QRN; considering 10% degradation of materials over time the rail wagons were put into service. However, it was assumed there is no change in the stiffness (E = 200 GPa) of the structure.

3.3.1 Primary members: main girder

They are the main load bearing structural members of the FRW bridge and laterally supported with inverted T beam at regular intervals.

3.3.1.1 Flexural Capacity

The flexural capacity of the rectangular box beam is computed in accordance with AS 5100.6 (2004). The box girder is laterally supported with cross girders at regular intervals. Clause 5.1.6 states that a member with compact cross-section bent about the section major principal x-axis shall satisfy Equation 3.3:

$$M_x^* \le \phi M_s \qquad 3.3$$

where:

M_x^* = design bending moment about the major principal x-axis

ϕ = capacity reduction factor (0.9 for structural steel in bending)

M_s = nominal section moment capacity for bending about the major principal x-axis

Prior to computing the nominal member moment capacity of the critical segments of box girder, the section capacities of the main box girder (taper section) at various depths were determined as follows:

For compact section, the nominal section capacity is determined by Equation 3.4:

$$M_s = f_y Z_e \qquad 3.4$$

where:

f_y = yield stress of steel

Z_e = effective section modulus

For non compact section, the nominal section moment capacity is determined as follows:

$$M_s = f_y Z_{en} \qquad 3.5$$

where:

Z_{en} = effective section modulus of the non compact

The section capacity of main box girder (taper section) at different depths is computed and presented in Table 3.1.

Table 3.1 Section moment capacity of main box girder for bending

Girder depth (mm)	Section moment capacity (ϕM_s) kNm
341	675
380	779
418	882
456	989
495	1101
533	1214
571	1329
610	1452
660	1612

Next the nominal member moment capacity (M_b) of a critical segment with full or partial restraints at both ends was computed as follows:

Firstly the critical segments (constant cross section at the centre and tapering section at ends) were checked for their full lateral restraint according to the clause 5.3.2.4 of AS 5100.6 (2004) using Equation 3.6:

$$\frac{L}{r_y} = (1800 + 1500\beta_m)\left(\frac{b_f}{b_w}\right)\left(\frac{250}{f_y}\right) \qquad 3.6$$

where;

L = length of segment

r_y = radius of gyration about the minor principal y-axis

β_m = ratio of the smaller to the larger end moments in the length L

Conservatively taken as -1.0

b_f = flange width

b_w = web depth

f_y = yield stress use in design

For straight section;	For tapering section
L = 1545mm	L = 1454mm
r_y = 115mm	r_y = 115mm
b_f = 400mm	b_f = 400mm
b_w = 610mm	b_w = 440mm
f_y = 250MPa	f_y = 250MPa

Both the segments satisfy the Equation 3.6 and shall be considered to have full lateral restraint.

For segments fully restrained, the nominal member moment capacity (M_b) is given by Equation 3.7;

$$M_b = \alpha_m \alpha_s M_s \leq M_s \qquad 3.7$$

where;

α_m = moment modification factor

= 1.0

α_s = slenderness reduction factor given by Equation 3.8

$$\alpha_s = 0.6\left[\sqrt{\left(\frac{M_s}{M_{oa}}\right)^2 + 3} - \left(\frac{M_s}{M_{oa}}\right)\right] \qquad 3.8$$

where;

$M_{oa} = M_o$ where M_o is the reference elastic buckling moment given by Equation 3.9

$$M_o = \sqrt{\left(\frac{\pi^2 E I_y}{L_e^2}\right) GJ} \qquad 3.9$$

where;

E, G = elastic moduli

I_y, J = section constants

L_e = effective length determined by Equation 3.10

$$L_e = k_1 k_L k_{rl} L \qquad 3.10$$

where;

k_1 = twist restraint

= 1.0

k_L = load height factor

= 1.0

k_{rl} = lateral rotation factor

= 0.85

$L_e = 1.0 \times 1.0 \times 0.85 \times 1454 = 1236mm$ for taper section

$L_e = 1.0 \times 1.0 \times 0.85 \times 1524 = 1295mm$ for straight section

From Equation 3.7, the nominal member moment capacity is less than or equal to the nominal section moment capacity, and therefore for conservative design the nominal member capacity is taken as the section capacity. The member capacity is thus compared with the design bending moment under M1600 critical loading discussed in Chapter 4 in Table 3.2.

Table 3.2 Comparison of design moment under M1600 loading and member capacity

Girder depth (mm)	Length from the bolster end (mm)	ϕM_b (kNm)	M^* (kNm)
341	0	675	0
380	300	779	219
418	600	882	302
456	900	989	451
495	1200	1101	523
533	1500	1214	557
571	1800	1329	602
610	2100	1452	620
660	2690	1612	732

It can be seen from Table 3.2 that the main box girders has sufficient member capacity to resist high axle load even under the bare frame (without driving surface on top of decking members).

3.3.1.2 Shear Capacity

Clause 5.10.1 of AS 5100.6 (2004) states that a web subjected to a design shear force shall satisfy Equation 3.11:

$$V^* = \phi V_v \qquad 3.11$$

where;

V^* = design shear force

ϕ = capacity reduction factor (0.9 for structural steel)

For uniform shear stress distribution,

$$V_v = V_u \qquad 3.12$$

where,

V_u = is the nominal shear capacity of a web

when the maximum web panel depth to thickness ratio satisfies the Equation 3.13:

$$\frac{d_p}{t_w} \leq \frac{82}{\sqrt{\frac{f_y}{250}}} \qquad 3.13$$

then the nominal shear capacity is of the web is taken as;

$$V_v = V_w \qquad 3.14$$

Where;

V_w = is the nominal shear yield capacity of the web, which is given by the Equation 3.15:

$$V_w = 0.6 f_y A_w \qquad 3.15$$

where;

f_y = yield stress of steel

A_w = gross sectional area of the web

For web panel depth to thickness ratio $\left(\frac{d_p}{t_w}\right)$ satisfying Equation 3.16:

$$\frac{d_p}{t_w} \leq \frac{82}{\sqrt{\frac{f_y}{250}}} \qquad 3.16$$

The nominal shear capacity of the web given as follows:

$$V_u = V_b \qquad 3.17$$

where;

V_b = shear buckling capacity of the web.

Using the steps above, the shear capacity of the main box girder was computed and presented in Table 3.3 and compared with the design shear under M1600 loading analysed in Chapter 4.

Table 3.3 Comparison of design shear under M1600 loading and shear capacity

Length from the bolster end (mm)	Girder depth (mm)	(ϕV_v) kN	V^* (kN)
0	341	707	473
300	380	802	473
600	418	894	339
900	456	986	339
1200	495	1081	339
1500	533	1174	189
1800	571	1266	189
2100	610	1361	15
2690	660	1482	5

It is seen from Table 3.3 that the main box girder has sufficient shear capacity to resist high axle load loads even when the FRW bridge is without driving surface (bare frame only).

3.3.2 Secondary members: inverted T-beams (cross girder)

These members are assumed to prop the main box girders and share the applied loading where such load directly rests on top.

3.3.2.1 Flexural capacity

The bending capacity of the inverted T-beam (cross girder) is determined using equations described in Section 3.3.1.1. The FRW contains two sets of cross girders (Figure 3.3); single tapered section aligned on side of the main box girder and double tapered section on the other side of the main girder. Therefore, bending member capacities of each cross girder at different locations were computed at approximately 200 mm length interval from the connection end of cross girder to the main box beam (Figure 3.8) and presented in Table 3.4. The table also shows the design bending moments determined from the modelling described in Chapter 4. For the cross girder W80 is the most critical load and hence other (for example, M1600) was not considered. The details of the determination of the BM are presented in Section 4.3.1 of Chapter 4.

Table 3.4 Comparison of member capacity against design moment under W80 load

Girder distance (x*) from end of main box beam (mm)	Member capacities (kNm)		Design Bending (kNm)	
	Single taper section	Double tapered section	Single taper section	Double tapered section
	ϕM_b	ϕM_b	M^*	M^*
0	73	73	50.0	50.0
200	68	64	31.0	22.0
400	64	59	23.0	10.0
600	59	57	10.0	6.0
800	57	56	3.5	3.6
1000	56	55	1.0	0.5

: For definition refer to Figure 3.8

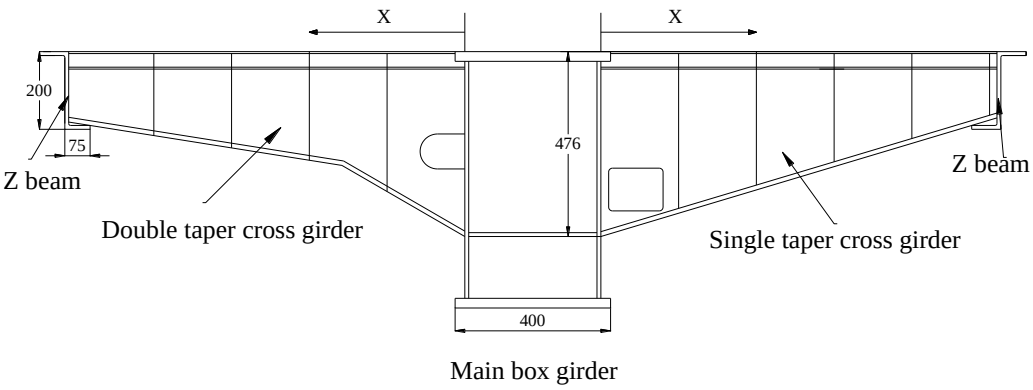

Figure 3.8 Details of cross girder idealisation for computing member capacities

3.3.2.2 Shear yield capacity

The shear yield capacity of the inverted T-beam is determined using equations described in Section 3.2.1.2. The shear capacity was computed at the same locations as adopted for the bending capacity in Section 3.3.2.1 and presented in Table 3.5. The design shear force corresponding to W80 ultimate load (determined from the grillage modelling presented in Chapter 4) is also shown in the table.

Table 3.5 Comparison of shear capacity of cross girder against the design shear

Beam length from the main box girder (x*) (mm)	Shear capacity (kN)		Design shear (kN)	
	Single taper section	Double tapered section	Single taper section	Double tapered section
	ϕV_v	ϕV_v	V^*	V^*
0	579	579	177	177
200	484	414	175	174
400	412	319	164	163
600	339	281	19	17
800	266	242	14	14
1000	185	199	10	10

: For definition refer to Figure 3.8

It can be seen from Table 3.5 that the shear capacity of the cross girders is sufficient to resist the W80 ultimate load.

3.4 Weld capacity

The cross girders are welded to the main box girder at their greatest depth, resisting both flexure and shear due to the applied live load. Therefore, weld (fillet weld as shown in the original QRN drawing - Appendix B) should be of high strength to resist the forces of SM1600 loads. Dye penetration and ultra-sonic tests carried out in the laboratory have revealed that the welds were free of defects. However, since the applied loads are of very high magnitude that may take any position along the span, the capacity of the weld was deemed necessary to be checked. Therefore, the strength of the fillet weld with the weld detail provided in the QRN drawings was theoretically assessed as per the clause 12.6.7.2 of AS 5100.6 (2004).

A fillet weld group subjected to a design force per unit length of weld $\left(V_w^*\right)$ at the ultimate limit state shall satisfy Equation 3.18:

$$V_w^* < \phi V_w \qquad 3.18$$

where,

ϕ = capacity factor (0.8 for structural purpose)

V_w^* = design force per unit length i.e the vectorial sum of the design forces per unit length on the effective area of the weld

V_w = nominal capacity of a fillet weld per unit length calculated as follows:

$$V_w = 0.6 f_{uw} t_t k_r \qquad 3.19$$

where;

f_{uw} = nominal tensile strength of weld metal

t_t = design throat thickness

k_r = reduction factor to account for the length of a welded lap connection $\left(k_r = 1\right)$

The strength of the fillet weld was assessed with Equations 3.18 and 3.19, and presented in Table 3.6. It is seen that the weld is very strong.

Table 3.6 Comparison of fillet weld capacity and design force per unit length

V_w^* (N/mm)	ϕV_w (N/mm)
261	708

3.5 Summary

This chapter presented the general overview of FRW obtained from QRN, Australia. Member details, especially those members that are able to support the applied loads were provided. Since the FRW as the bridge superstructure will be subjected to AS 5100 loadings, their main load bearing members were checked for member capacities in line with the standard AS 5100.6 (2004). This chapter concludes that the bare frame double FRW have sufficient member capacities to resist high axle loads. Despite having not found any defects in the weld quality from the non-destructive tests like dye penetration test and ultrasonic test, the theoretical capacity of the weld was also computed and checked. The theoretical computations have shown that the main load bearing members are capable enough to resist high axle loads and there is sufficient strength in the fillet weld. However, the computations incorporated assumptions on the strength of the materials including the weld. The following chapters present investigations, data and analyses to verify the validity of these assumptions.

Chapter 4: Modelling and Analysis

4.1 Introduction

The potential of the FRW as a low cost bridge superstructure deck has been realised by Dhanasekar and Bayissa (2011) and McDonald (2010). They have concluded through extensive full scale laboratory testing that the FRW (bare frame without driving surface) possess high potential as low cost bridge replacement alternatives in the low volume roads (traffic count between 25-150 (RCC, (2010)) where fatigue is less prominence.

Three dimensional grillage models of the bridge were developed. The theory and application of grillage analysis is well established and has been discussed by many authors (West (1973); Keogh and O'Brien (1996); O'Brien and Keogh, (1998) and Battaglia and Malerba (2003)). Results have been compared to models and full-size bridges and the method has been found to be reasonably accurate for many shapes of structure, loading conditions and support arrangements. The accuracy, speed and simplicity of the grillage method make it the most suitable model for bridge analysis (Jaegar et al. 1982 and Zeng et al. 2000).

A single bare frame FRW model was first developed and validated with the experimental test data (McDonald, 2010) corresponding to W80 mid span load position. Several static load analyses for various possible load positions were

performed and the results compared with the experimental tests for calibration of single and double FRW bare frame.

Since the single FRW of 2.54 m cannot form a single lane bridge as at least 4.2 m width between the kerbs is required, two FRWs connected along their length has been used. The connections were achieved at their longitudinal edge Z-beams with custom made brackets. Reinforced concrete slab (RCS) pavement was added on top of FRW to provide driving surface and the RCS tied to the box girder of the FRW though shear connectors. The single lane FRW Bridge was modelled and calibrated with the field load test results using deflections measured on the main box girder at the mid span in Chapter 7.

4.2 Grillage model

A 3D grillage model of the FRW was created using beam elements with six degrees of freedom at each node in the SPACE GASS computer program, commercially available in Australia. The reasons for selecting grillage structural analysis and design program compared to other sophisticated widely available finite element software are:

- It is simple, easy to comprehend and use and quick in accomplishing the model of any complicated structural arrangements
- It requires normal desktop and laptop to work and requires less computational time

- The library function of the program contains AS 5100 design loads which eases the analysis procedure.
- The moving load analysis component aids is an added attraction.

First the structural components of the FRW was studied in detail, grouped into two categories; (i) straight members and (ii) taper members and idealised and modelled mathematically. The most popular mathematical model uses the concept of nodes connected by elements.

Straight members were modelled as single beam element at their geometric centroid while the tapered members (cross girders and main box girder towards the ends in Figure 3.2 and Figure 3.3 in Chapter 3) were divided into many sub-members. The sub-members are then modelled individually at their centroid and connected to the adjacent members with rigid link connection which is achieved with master-slave constraint method available in the program. A rigid connection was assumed in the model – a design check of the welded connections has proved that the weld sizes were quite conservative, thus alleviating any fear of early relative rotation of members during serviceability/ultimate loading. Also the ultrasonic test conducted in the laboratory testing has confirmed no suspected areas of cracking in the welds. Figure 4.1 shows the master-slave constraint approach to connect two nodes of the elements/members having different neutral axis depth in order to maintain the structural compatibility.

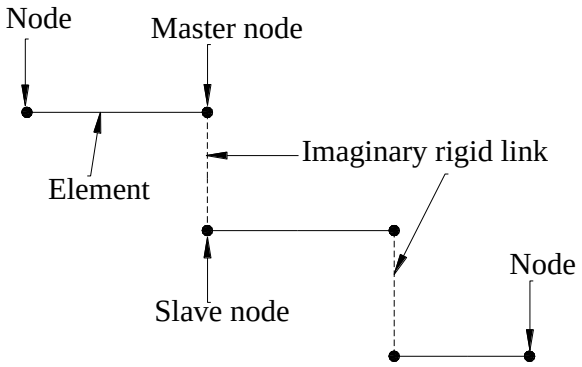

Figure 4.1 Typical connections of two nodes through master-slave constraint

Every single member of the FRW was modeled and connected with master-slave constraints (rigid link connection) as described in Figure 4.1 between the two member elements. The structural elements modeled included the main primary longitudinal built-up box section, secondary transverse built-up box section at the supports, inverted T-section cross girders, channels and decking folded plate sections. Figure 4.2 illustrates modelling of individual members of the FRW.

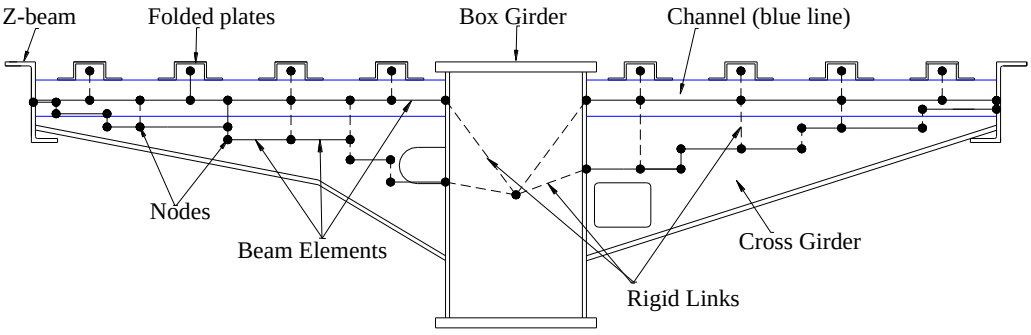

Figure 4.2 Typical single FRW model idealizations: cross girder modeling

To cater for the effective traffic path for a single traffic lane, in accordance with the requirements of AS 5100 (2004), two single FRWs were connected at edge Z-beams by custom made box bracket through incorporating Z-beam at the edges and it was modeled as beam element at their centriod. Figure 4.3 shows the top view plan of the grillage model of the fully assembled single lane FRW bridge.

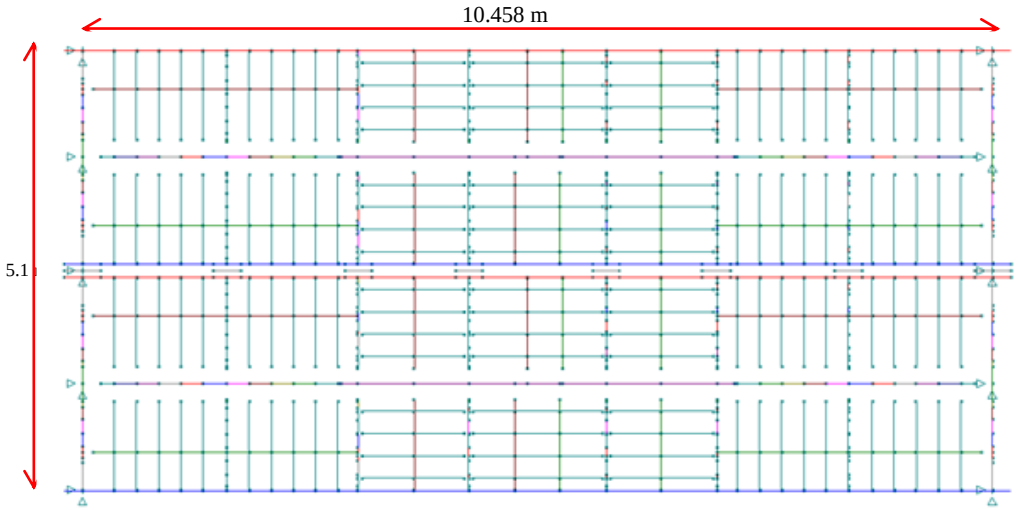

Figure 4.3 Grillage model of FRW Bridge (top view)

Single and double FRW models developed in SPACE GASS Program are shown in Figure 4.4 and 4.5 respectively.

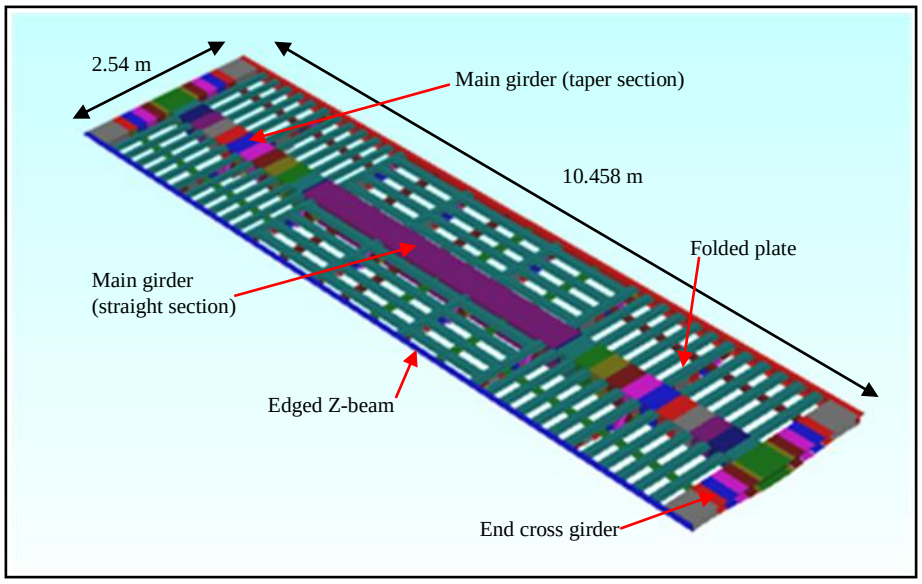

Figure 4.4 Single FRW model (rendered 3D top view)

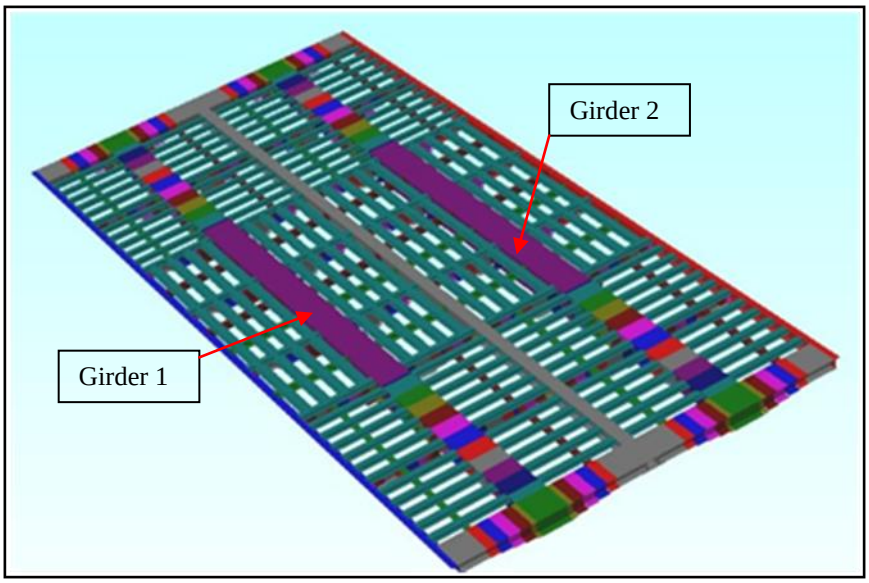

Figure 4.5 Double FRW model connected at Z-beam (rendered 3D top view)

4.2.1 Material and section properties

The SPACE GASS structural analysis program automatically computes the section properties based on the member dimensions provided. The material properties adopted for the model are summarised in Table 4.1 while the section properties of straight and taper sections of the main box girder are computed separately as shown in Figure 4.6 and are summarised in Table 4.2. For cross girders, only one single average section property is provided as there is minimum variation in the cross section.

Table 4.1 Summary of material properties used in the bridge model

Material Type	Properties	
Steel	E = 200,000 MPa	Modulus of Elasticity
	v = 0.30	Poisson's ratio
	ρ = 7850 kg/m^3	Mass density
Concrete	E = 31,000 MPa	Modulus of Elasticity
	v = 0.20	Poisson's ratio
	ρ = 2500 kg/m^3	Mass density

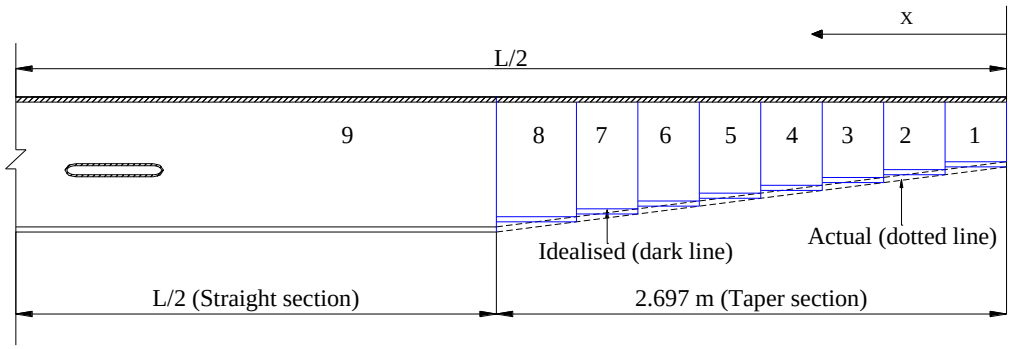

Figure 4.6 Idealisation of taper section (box girder) in the grillage model

Table 4.2 Summary of section properties employed in the model

Beam type		Section Properties			
		Area (mm^2)	I_z (mm^4)	I_y (mm^4)	J (mm^4)
Box Girder (straight section)		32200	2.395E+09	6.194E+08	1.209E+09
Box Girder (tapered section)	Section 1	26180	6.079E+08	4.453E+08	5.488E+08
	Section 2	26760	7.242E+08	4.621E+08	6.105E+08
	Section 3	27340	8.517E+08	4.788E+08	6.728E+08
	Section 4	29740	9.908E+08	4.956E+08	7.357E+08
	Section 5	28500	1.142E+09	5.124E+08	7.989E+08
	Section 6	29700	1.492E+09	5.471E+08	9.309E+08
	Section 7	30860	1.881E+09	5.806E+08	1.059E+09
	Section 8	32020	2.322E+09	6.142E+08	1.189E+09
Cross Girder (typical)		5220	9.375E+07	1.033E+006	1.862E+05
Concrete Slab		112500	4.746E+08	2.344E+09	1.362E+09

4.2.2 Boundary conditions

Proper identification and application of boundary conditions is essential to the accuracy of the model. Boundary conditions are especially important when results of the analyses are compared with the known test results. Improper selection of boundary conditions can lead to either an under or over constrained model and will provide incorrect results. Bakht and Jaeger (1988) and Schulz et al. (1995) have reported that small differences in boundary conditions can have significant effects on

the analysis results. Bakht and Jaeger also demonstrated that girder restraint can reduce live loads by up to 20%.

In both the laboratory and field load testing programs, the FRW was simply supported on the elastomeric rubber pads; however their layout and placement differed due to conditions at the site. Therefore it is imperative to include this support (boundary) conditions exactly and with correct accuracy in the model to avoid incorrect/ inaccurate results. In the FRW model developed, flexible restraint was assigned to the support node to simulate the elastomeric rubber pads through implementation of spring support function of the program. The technical detail and the standard stiffness material properties of the elastomeric pad provided by the supplier with the materials (confirming to AS 5100.4 (2004)) were incorporated in the flexible restraint. The FRW bridge is supported at five points on each abutment as shown in Figure 4.7. At the support below the main box girder location, two such elastomeric pads were installed while a pad each was placed under the external supports, below the Z-beams.

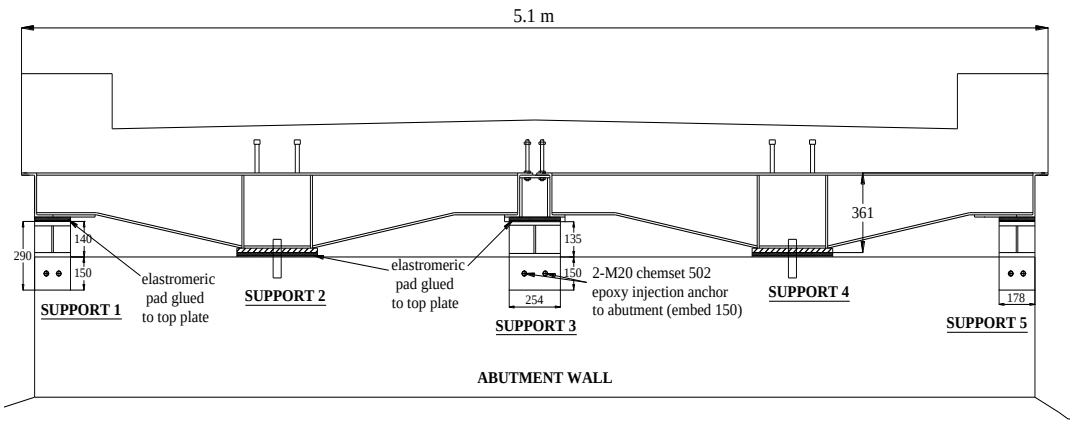

Figure 4.7 Support arrangements on the abutments

The spring stiffness values adopted in the model are shown in the Table 4.3

Table 4.3 Spring stiffness values used in the model

Support Location	Spring stiffness (kN/mm)
Below main box girder	192.5 $\times$2
Below Edged Z-bam	192.50
Centre connection beam	192.50

4.3 Static analysis

Like any other finite element modelling and analysis thereon, prior to carrying out the detail analysis and in order to represent the near-exact model of the bridge, the 3D grillage model of the single FRW (bare frame) generated was also validated by comparing deflection output of the model with the deflection results from the laboratory test. Both W80 and M1600 loadings were considered for this purpose. The calibrated grillage model was then further used for the analysis of bridge design loads as per AS 5100.2 (2004), which is discussed later in the Chapter. The load application locations and the experimental results are used and referred consistently in validating the grillage model.

4.3.1 W80 wheel load

As described in chapter 3, W80 is the heaviest single wheel load that can be applied anywhere on the structure and to all structural elements for which the critical load is a single wheel load. For single bare frame FRW model validation, initially W80 was applied on the main box girder as illustrated in the Figure 4.8. This was the same

load position adopted in the laboratory testing. The magnitude of W80 loading was 112kN for serviceability limit state and 201.6kN for ultimate limit state. The magnitude of the load is determined as per the clause 6.7.2 of AS 5100.2 (2004) and presented in Table 4.4.

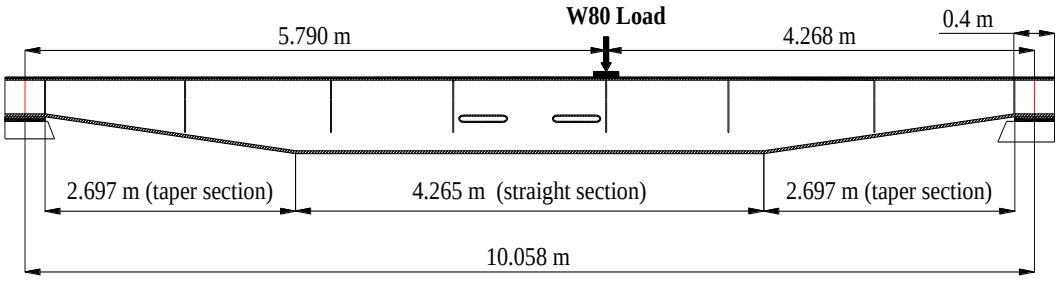

Figure 4.8 W80 load applied to main box girder in the laboratory testing

Table 4.4 Summary of design action under W80 loading configuration

Wheel load	Load (kN)	Dynamic load (kN)		Serviceability load (kN)		Ultimate load (kN)	
		Factor	Load	Factor	Load	Factor	Load
W80	80	0.4	32.0	1.0	112.0	1.8	201.6

The displacement output from the grillage model was then compared with the actual experimental testing results considering pristine condition of the structure without incorporating the degradation of the FRW members. Figure 4.9 illustrate the initial deflection plot between the model and experimental test results.

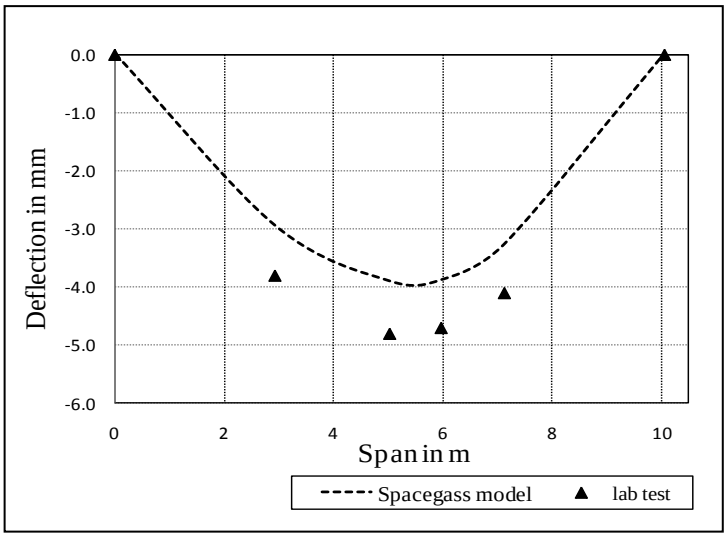

Figure 4.9 Initial centreline displacement measured underneath the main box girder of FRW for single wagon condition under W80 load applied at the mid span

It can be seen from Figure 4.9 that for pristine structural condition without considering the degradation of steel; although the deterioration of the wagons were apparent in the extensive visual observations and through non-destructive test, the experimental deflection under the W80 serviceability load showed higher value than that of displacement generated by the grillage model. This difference can be attributed to: the FRW at the lab would have been subjected to unknown number of cyclic loading in its commissioned life which would have resulted in loss of strength.

The non destructive ultrasonic testings conducted on the wagon structural elements have indicated small amount of metal loss which had demonstrated the occurrence of some loss of structural stiffness. On the other hand, the section and metal loss of the decking frame, especially the folded plates were apparent from the visual inspection itself as shown in the Figure 4.10.

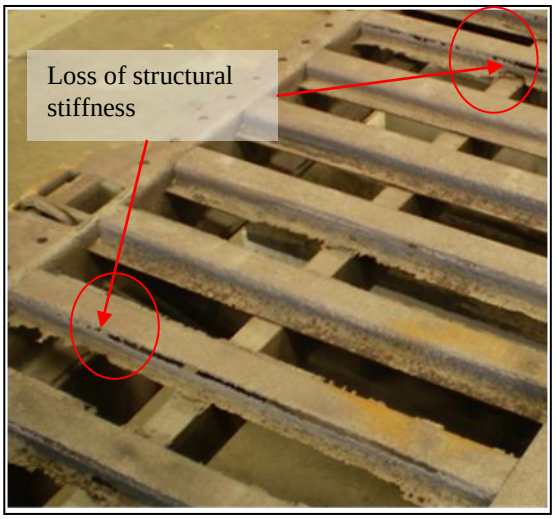

Figure 4.10 Image of decking frames on top of FRW

Dhanasekar and Bayissa (2011) in their study on the structural adequacy assessment of a disused FRW as the road bridge deck through novel half of full scale laboratory testing have calibrated the Finite Element Model of FRW developed in ABAQUS using static, vibration and ultrasonic testing and have resulted in Young's modulus of 180GPa for the main structural members and 80GPa for the folded plate decking member. The same stiffness values are used in updating and refining the 3D grillage model because the same laboratory test wagon was later used as one of the two wagons connected together at their centre in the demonstration bridge construction project. The displacement obtained from the refined model is plotted in the Figure 4.11. It can be noted from Figure 4.11 that a better correlation in the displacement was obtained incorporating degradation of material in terms of loss of stiffness. The percentage difference in the mid span deflection between the experimental and model is approximately about 3.5%.

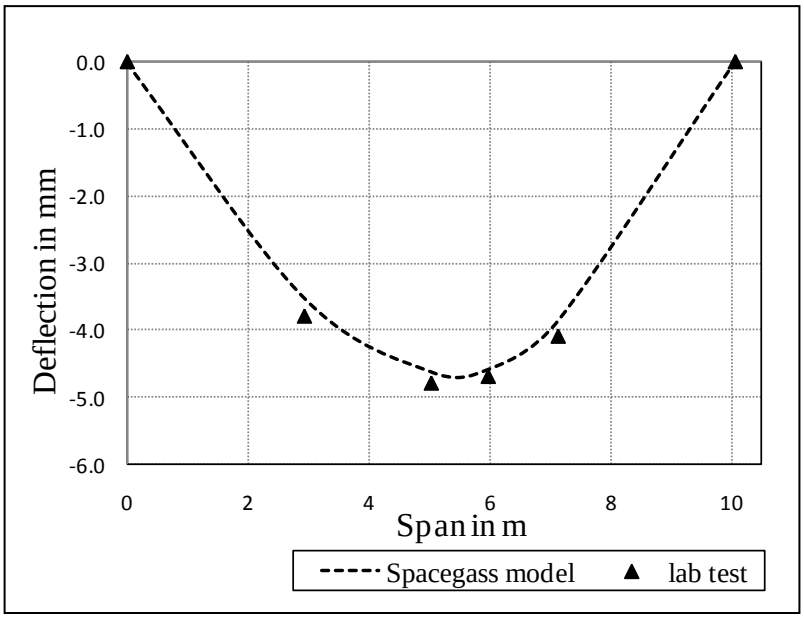

Figure 4.11 Comparison of deflection between the test and the updated model

The updated single FRW model was used to further analyse the effect of W80 loading (ultimate) to the secondary cross girders at two different locations as shown in Figure 4.12 and Figure 4.13.

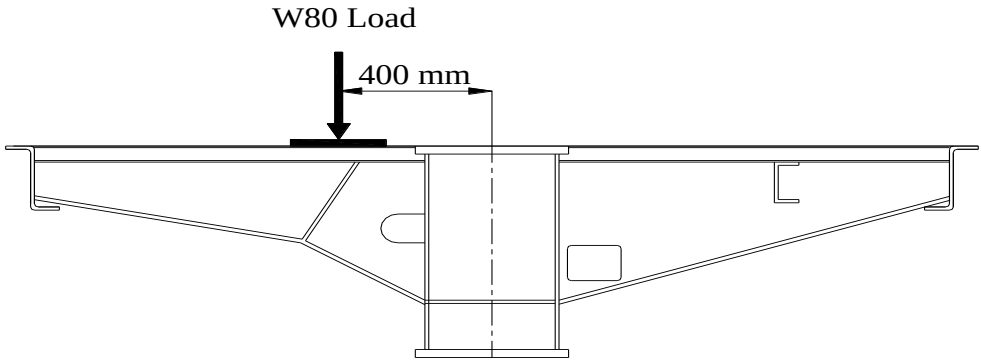

Figure 4.12 W80 load; offset to check shear capacity of cross girder

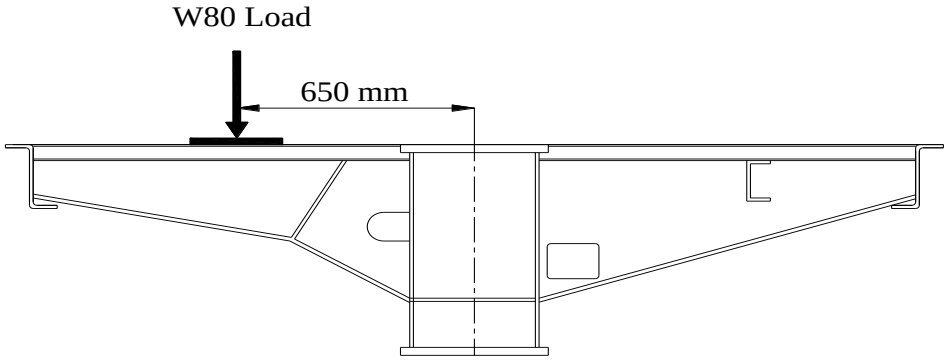

Figure 4.13 W80 load; offset to check bending capacity of cross girder

The maximum bending moment (BM) and shear force (SF) of the cross girder generated under the W80 ultimate load and their comparison with the member capacities determined in Chapter 3 are presented in Table 4.5. It can be seen from Table 4.5 that the cross girders have sufficient member capacities to resist high single wheel load of W80.

Table 4.5 Maximum BM and SF against the member capacities of the cross girder

Loading type	Offset distance (mm)	Maximum		Member capacities	
		M^* (kNm)	V^* (kN)	M_b (kNm)	V_b (kN)
W80	400	27	190	71	412
W80	625	49	177	63	266

Once the single FRW grillage model was updated and tuned to represent the true wagon, next step was to connect two wagons together to form a single lane bridge deck of 4.2 lane width as per the standard AS 5100.1 (2004). It was decided to use the wagon tested in the laboratory as one of the two FRWs required for the construction of the demonstration bridge as the wagon has shown sufficient strength to resist high axle loads. The second wagon therefore required similar configuration and type and was obtained from Bindha Railway Yard, Brisbane. Two FRWs were connected together at the cross girder location along the edge Z-beams with custom made connection brackets. The details of this custom made connection bracket and its connection procedures are explained in Chapter 5.

4.3.2 A160 axle load

The A160 load models an individual heavy axle and can take any position on the bridge. For adverse effect, A160 was placed at mid span on top of the cross girder

from one end of the FRW as shown in Figure 4.14. The maximum net deflection measured under A160 service load at the mid span of the main girder is 5.4mm, whilst the maximum BM and SF of main box girder under the ultimate load are 445 kNm and 130 kN respectively. They are below the member capacities of the main box girder.

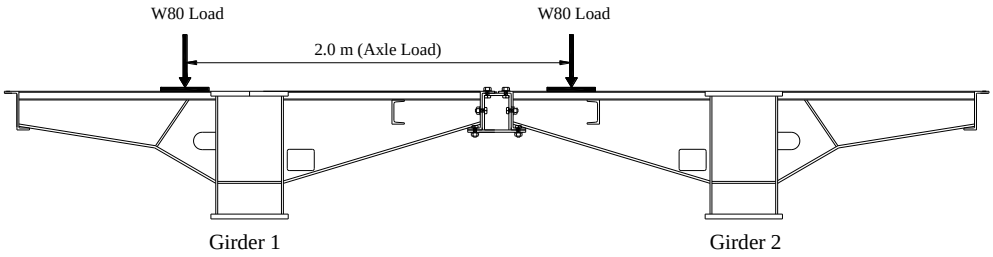

Figure 4.14 A160 load applied on the double FRW at mid span

M1600 sets of loads are more critical than A160 load for single lane bridge and is discussed in the section following.

4.3.3 M1600 traffic load

The 3D grillage model of the single lane bridge was calibrated by comparing deflection at the mid span between the model and the lab test under M1600 static load. The M1600 load configuration is detailed in Chapter 2. For the FRW bridge considered, only the portion shown in Figure 4.15 forms the critical M1600 loading.

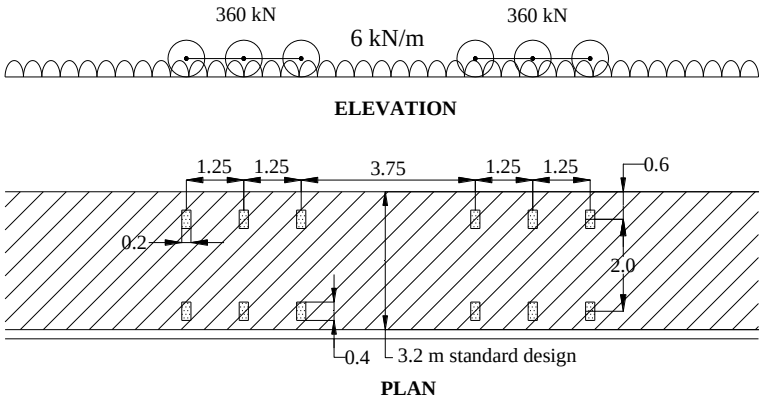

Figure 4.15 M1600 traffic load applied in the lab test

The 6kN/m UDL component of M1600 traffic load is spread over a 3.2 m design lane and assumed continuing along the length of the bridge for adverse effect. In absence of running surface on the top of the FRW, the UDL was applied as an equivalent wheel load together with the tri-axle group of wheels as follows:

$$\frac{6kN/m}{3.2m}\times 10.5m = 19.69kN/m \qquad 4.1$$

As there are twelve sets of wheels in 8.75 m length of load model considered in the analysis, the equivalent UDL wheel load on each wheel is computed as below:

$$\frac{19.69}{12} = 1.64 \cong 2.0kN(conservative) \qquad 4.2$$

Table 4.6 Summary of M1600 static traffic load applied in the model

Wheel load	Load (kN)	Dynamic load (kN)		Serviceability load (kN)		Ultimate load (kN)	
		Factor	Load	Factor	Load	Factor	Load
Truck	60	0.35	21.0	1.0	81.0	1.8	140.4
UDL	2	0.30	0.6	1.0	2.6	1.8	4.6
Total load per wheel (kN)					83.6		145.0

In order to exactly space the distance between the wheels in the model, dummy member were created and wheel loads applied as the point load. For comparison of displacement along the main box girder, M1600 serviceability load as shown in the Table 4.6 was applied in the grillage model at a distance of 295 mm from the centre of the main box girder. In the laboratory testing double FRWs was simulated by applying boundary condition constraints along one of the longitudinal edges as shown in Figure 4.16.

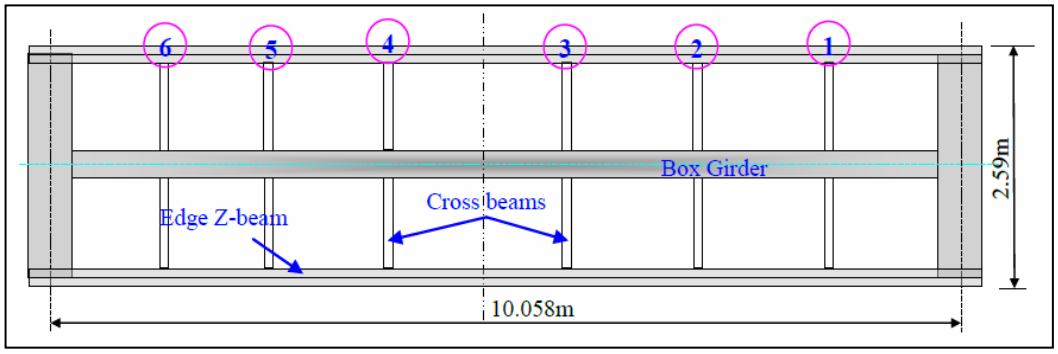

Figure 4.16 Boundary constraints setups used for lab testing of 'equivalent single lane double FRW bridge system' (Dhanasekar and Bayissa, 2011)

Figure 4.17 shows the displacement profiles along the main box girder under M1600 serviceability load.

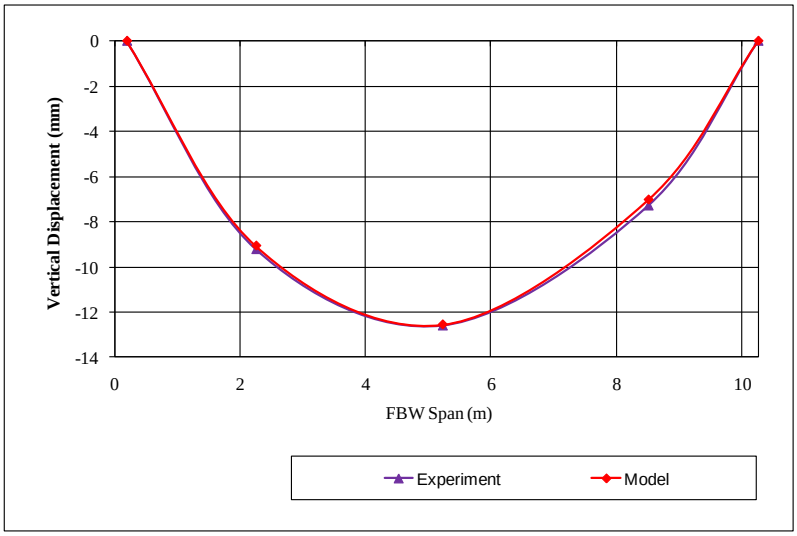

Figure 4.17 Vertical displacement profiles along the main box girder (Girder 1 in Figure 4.6)

It can be seen from the Figure 4.17 that the vertical displacement profiles along the girder 1 under M1600 serviceability loading is in good agreement; only small variation is observed. The updated model was then further analysed for M1600 ultimate loads at the critical locations and the maximum bending moment diagram (BMD) and shear force diagram (SFD) are presented in Figure 4.18 and Figure 4.19. The maximum bending moment and shear force outputs from the grillage were compared with the member capacities in Chapter 3 and have shown that the main load bearing members have sufficient capacities to resist high axle loads.

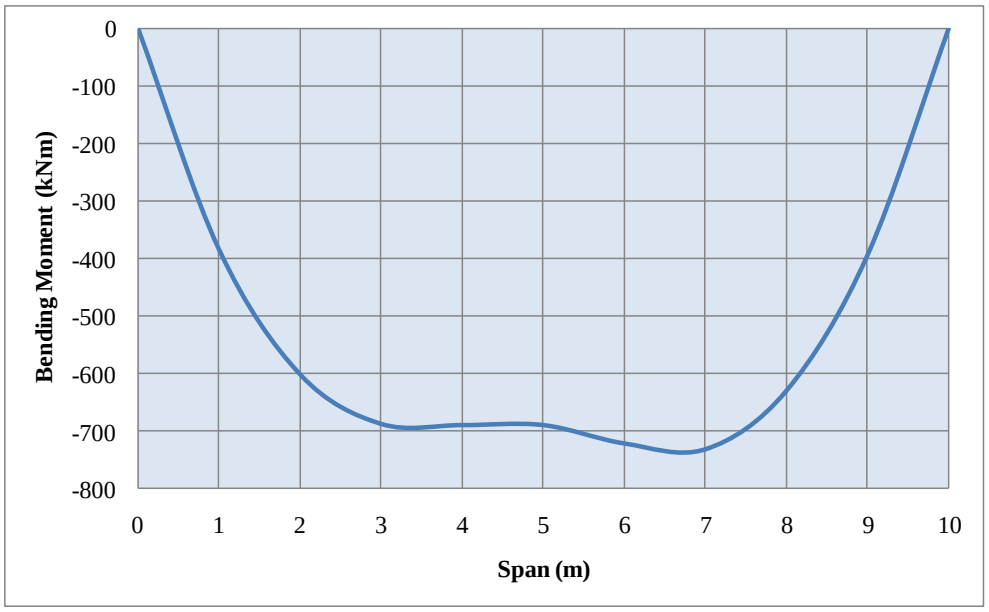

Figure 4.18 M1600 ultimate load BMD. Maximum ordinate (732kNm)

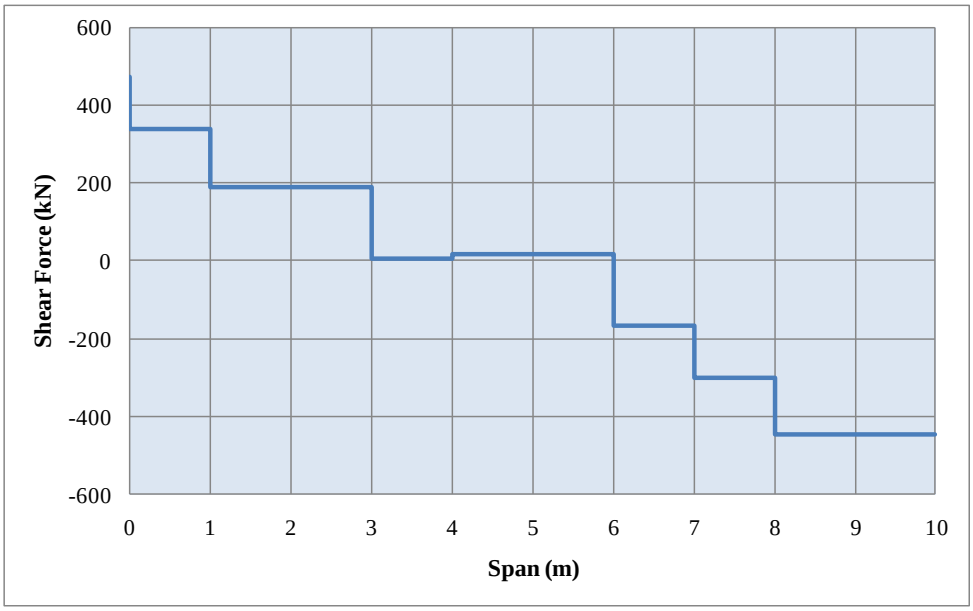

Figure 4.19 M1600 ultimate load SFD. Maximum ordinate (473kN)

4.4 Summary

Three dimensional grillage model of FRW was calibrated using the laboratory experimental data. The calibrated grillage model (bare frame only) was used for analysis of SM1600 design loads and the results were compared with the member capacities. It was found that the FRW (bare frame) had sufficient strength to resist high axle design loads. The calibrated model is later used in Chapter 7 and reinforced concrete slab is added on its top as the driving surface.

Chapter 5: Bridge design and construction

5.1 Introduction

This chapter presents an outline of the design of abutment, reinforced concrete slab pavement and the construction sequence of FRW bridge. Construction of FRW bridge involve selecting suitable disused wagon from the available stock at QRN in line with the wagon already selected for the experimental specimen (McDonald, (2010)). For effective low cost bridge replacement using FRW as the bridge superstructure, proper selection of disused wagon is very essential and is highlighted in this chapter.

The width of the wagons servicing in the Queensland's narrow gauge rail (1067mm gauge) was only 2.54m, which falls short of the minimum lane width of a road bridge specified in AS 5100.1 (2004), which is 4.20m. Therefore, it was required to connect two FBWs along their longitudinal edged Z-beams for single lane bridge. The integrity of the two FRWs as one unit in resisting the high axle loads was necessary in transferring the load to the sub-structures and the lateral distribution of loads. Therefore, suitable design of connection of two FRWs is discussed in this chapter.

The single lane demonstration bridge was constructed within the Rockhampton Regional Council (RRC) jurisdiction, Queensland. The procedure employed in the bridge construction and modification of FRW was carried out to meet the design requirements and is discussed in detail in this chapter.

5.2 Design of Abutments

The RRC as a research partner has designed and constructed the abutments and the reinforced concrete slab pavement whilst QUT provided appropriately certified FRW bridge superstructure deck design suitable for erection. .

The design of abutment and concrete slab pavement was carried out by the RRC through the design consultant, VDM Consulting Pvt. Ltd., and therefore, the design detail and its calculations are beyond the scope of this thesis. Only a brief outline of the design is described in this section.

Topographical survey

The site selection and topographical survey were conducted by RRC and made available to the design consultant. Normally the bridge length is determined after studying the site condition (survey drawing); however, in this case as the bridge span was governed by the available span of the FRW (10.458m), the abutments were suitably located to safely accommodate the FRW.

Geotechnical Investigation

RRC conducted geotechnical study and its report was made available to the design consultant for safe design of the bridge substructure. Based on the borehole test data, the pile dimensions were determined and the abutments were designed.

The abutment designed consisted of two 6.5m piles driven into hard rock on each bank and cap beam of 1130mm high by 1100mm wide casted on top as shown in Figure 5.1. The detail design drawing of abutment is enclosed in Appendix B.

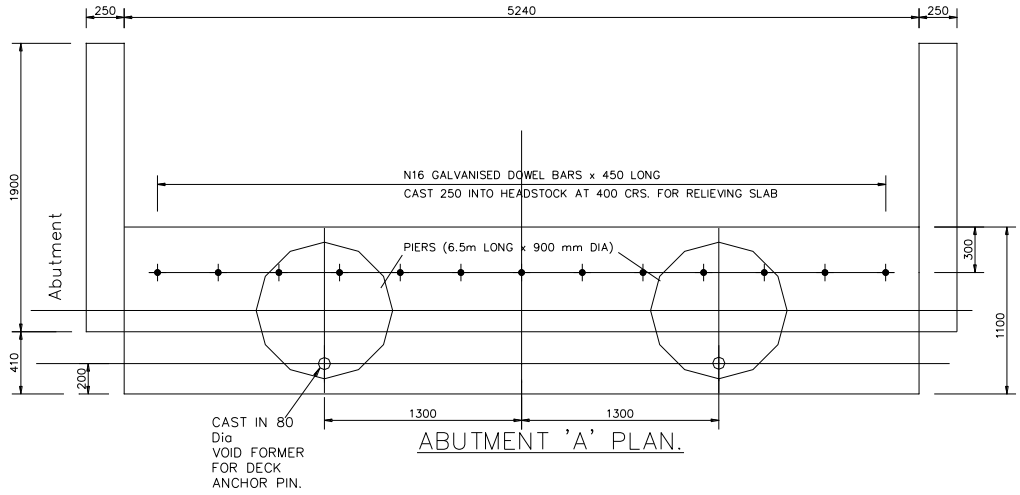

Figure 5.1 Detail of abutments (plan view)

5.3 Selection & Design of FRW

Success of FRW bridge is directly linked to the proper selection of FRW and its design of RCS pavement and the connection system to connect two FRWs together.

5.3.1 Selection of FRW

The feasibility studies carried out in 2009 have found out that QRN wagons do possess the potential as the bridge replacement alternatives in the low volume road. The decommissioning of wagons by QRN was for business reasons and not for technical reasons such as the end of design life or damage due to involvement in accident. These rail stocks are made available routinely at the scrap value of the

metal, which makes the idea of using it as the bridge superstructure as quite economical and environmentally sensible as a good structural system (FRW) is wastefully furnace as scrap metal in the current practice.

Although the wagons are considered fit to service rail transport at the time of stacking at the yard, it is essential to thoroughly examine the FRWs in the yard through a rigorous selection process as the wagons will be used as a bridge superstructure, the loading to which . The wagon selected for the experimental lab testing was of the open goods wagon class 'PHOB' from the railway yards in Queensland. The results from the lab testing on the wagons have shown sufficient strength to resist high axle load, therefore it was decided to limit the selection to similar class of PHOB type as selection of appropriate FRW is critical to the success of low cost FRW bridge decks. Therefore, a selection criterion was developed to assist in the wagon identification process:

(i) Structural element size

The main central box girder was considered as the main load bearing structure and therefore, the structural element size was limited to this member only. The following points were considered:

- The member should be free from corrosion and weld cracks.
- The girder will be supported at the abutment/pier at the bolster end and therefore the end transverse box girder should be in sound condition; free from major weld defects and corrosion.

(ii) Member straightness/damages

The QRN wagons are decommissioned purely for business reasons; however, at storage yard they could get damaged/ deformed due to inappropriate stacking. Deformed members are weak in transferring the load. The edge Z-beam need must be as straight as possible to facilitate connection between FRWs. Visual inspection complemented with string line and portable metal thickness detector were adopted in the selection process. Figure 5.2 shows a typical FRW discarded during the physical visual inspection as there was some damage on the top flange of the main girder (perhaps due to cutting of a welded straight).

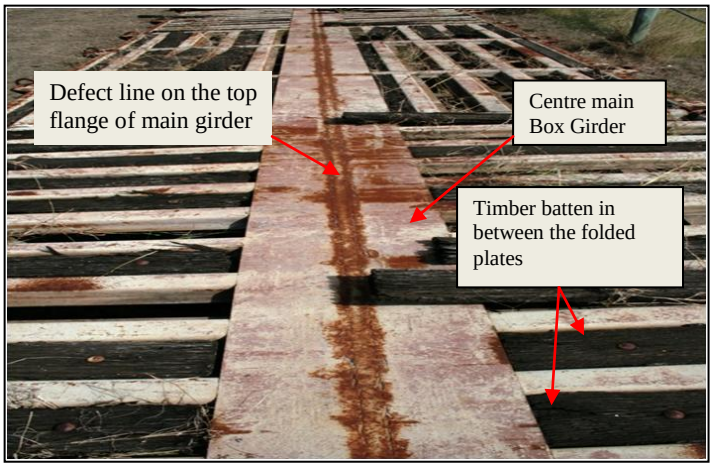

Figure 5.2 Discarded wagon during the selection process: This wagon had continuous defect on the top flange of the main box girder

(iii) Weld connection

Observations have shown that all the members of QRN wagons are connected by welds. The welds were checked for cracks. Non destrutive testing (NDT) is

recommended to be performed on the main girder, particularly if the weld quality could not be acertained through visual inspection.

(iv) Availability of FRW

Although QRN mainly stocks 'PHO' class of wagons, other type of wagons are also available from the narrow gauge rails. For single lane bridge of 4.2 m carriage way width between the kerbs as per the standard AS 5100.1 (2004), two FRWs are required to be connected. Therefore, to avoid unwarranted differential displacement between the FRWs due to eccentric loading, the wagons must be of same type and class; in our case PHOB class (Figure 5.3)

Figure 5.3 PHOB type wagon with identification plate (PHOB 38159) containing wagon type and information on the load carrying capacity

In this reseacrh work, wagons were selected from the QRN railway yards in Bindha site.

5.3.2 Design of FRW

The members of the selected FRW were accurately measured and the measurements were compared to the specification in the QRN design drawing (Appendix – B). Only the width of Z beam was found smaller than the dimension specified in the drawing by 25mm (100mm design against 75mm actual). This discrepancy was incorporated in the design of the connection beam for the two FRWs.

5.3.2.1 Centre connection beam

The two wagons were connected together along their longitudinal edge Z-beams. Two connection options were studied initially as below:

(a) Cutting off the part of the Z-beam and bolting together, and
(b) Single small box section running parallel to the length of the Z-section. The box section could be either welded or bolted to the existing Z-beams.

The second option was considered more stable and capable of providing sufficient integrity in terms of continuity along the lateral direction of the FRWs by forming a small box beam as shown in Figure 5.4. These brackets were bolted to the existing Z-beams at the cross girder locations as shown in Figure 5.5.

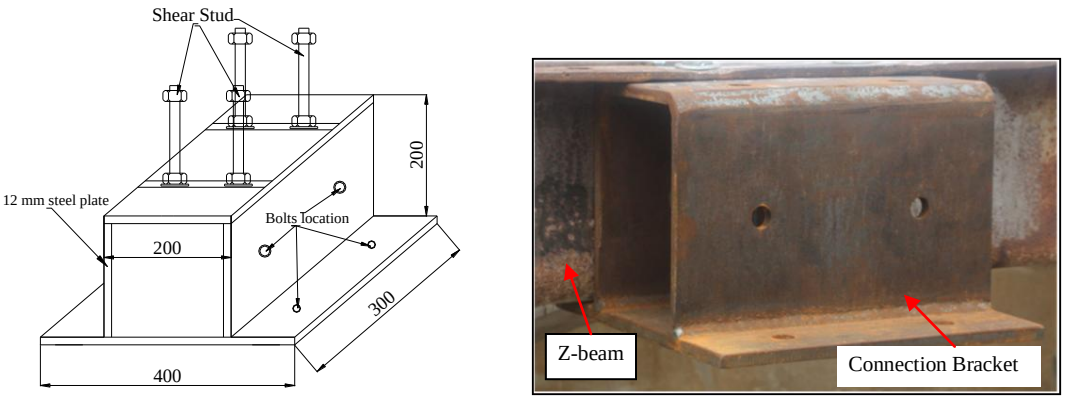

(a) A beam-Bracket Connection Details (b) Trail fitting at the fabrication yard

Figure 5.4 Central connection brackets to connect two FRWs

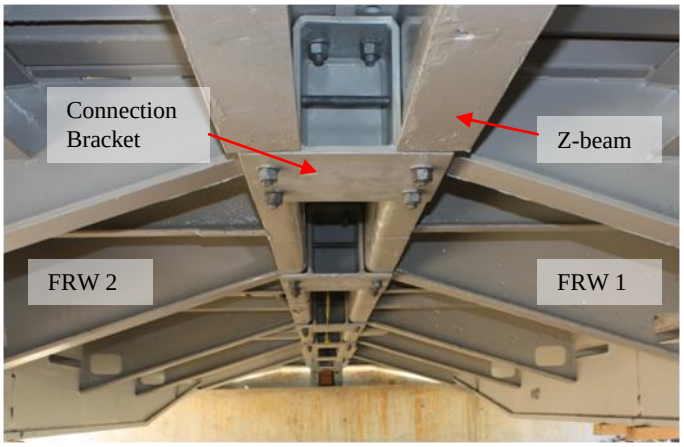

Figure 5.5 Two FRWs connected with brackets at the centre

5.3.2.2 Reinforced concrete slab pavement

Initially two options of driving surface on top of the FRW members were considered: (1) hard wood timber decking and (2) reinforced concrete slab (RCS). The timber solution required all FRW members, including the folded plate section to be load bearing; in some instances the risk of local failure of these minor elements due to timber decking solution was considered high. The reinforced concrete solution, on the other hand, has relied on load transfer to only the main box girder element, thereby minimising the risk of local failure of minor members, such as the folded

plates. Overall the RCS solution was considered more economical and faster to construct compared to the timber deck solution. At the time of writing this thesis the timber decking solution is being pursued by another master research student under the same research project group.

The reinforced concrete slab was designed as a simply supported one way slab resting on two supports provided by the box girder (S1 and S2 in Figure 5.6). The contributions from other members of FRW to resist the applied load were disregarded in the design. The M1600 load consists of wheel loads and UDL, which have been applied as specified in AS 5100.2 (2004). The cantilever portion of the RCS paving was checked with W80 load as W80 load is the heaviest single load that can take any position on the structure for adverse effect.

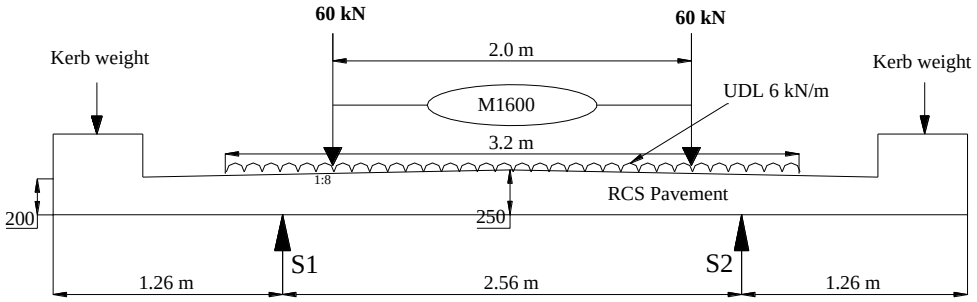

Figure 5.6 M1600 load centrally placed in the design of RCS pavement

The final design has resulted in a reinforced concrete slab whose central thickness was 250 mm at the centre cambering to a thickness of 200 mm at both ends as shown in Figure 5.6. Road kerbs of 450 mm high and 500 mm wide RC blocks were constructed at both sides of the slab. The grillage configuration of the FRW minimised the need for scaffolds during concreting.

5.4 Construction

The RRC has significantly contributed to the FRW bridge concept because of its high potential as economic bridge replacement alternatives in low volume roads network. The demonstration bridge was therefore constructed on T-Ramm road in Raglan within the jurisdiction of the RRC low volume roads network (Factsheet 2010).

5.4.1 Modification of FRW

Before the FRW was transported to the bridge site and installed to the abutments, rail furniture was removed, corroded layers sandblasted and steel members painted. Figures 5.7 to 5.11 shows the modification process both carried out in the lab and fabrication yard in Rockhampton.

The modification works included the following:

- Cutting of extra length of FRW from the bogie centre as the members away from the bogie centre.
- Cutting of extra members from the edge Z-beam and grinding for receiving connection brackets.
- Attaching plate on the face of end box girder to prevent entering of surface water (Figure 5.10)
- Major modification work was concentrated on replacing the corroded folded plates with stronger RHS on the decking frame (Figure 5.9). This was required to support the weight of the wet concrete and construction live load.

- Sandblasting and aluminium painting as per the standard AS 1580 (2004). Two coats of paint were applied on all the members of FRW.
- Shear studs were welded on the upper flange of the main box girder. The shear studs were spaced at 120mm in the longitudinal direction along the span of the bridge to form composite action between the RCS and FRW.
- Instrumentation such as strain gauge installation was carried out in the yard after completion of modification work and painting. Further details on location and types of strain gauges used are provided in Chapter 6.
- The FRWs were carefully packed with timber battens to avoid damages to the strain gauges and the associated wires and transported to the site.

Figure 5.7 Rail furniture removed from FRW

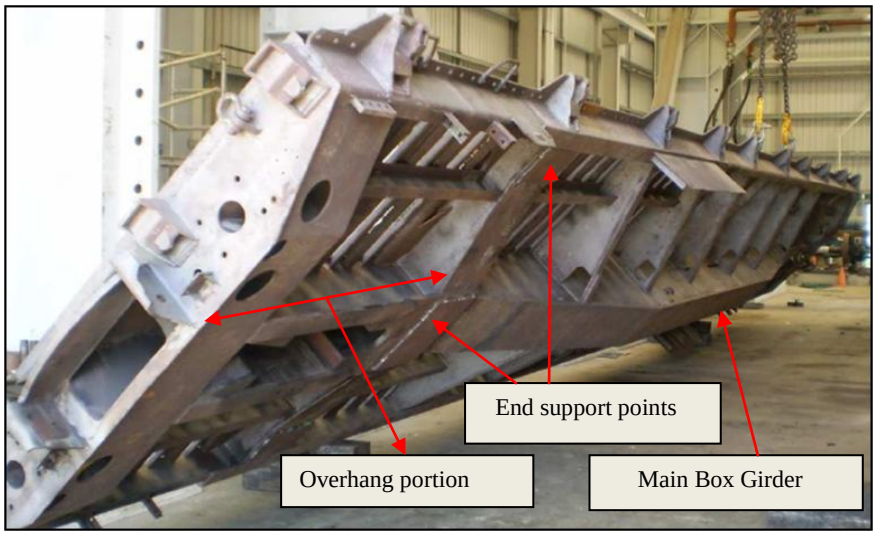

Figure 5.8 FRW after removal of rail furniture and lifted up before setting up in the lab; this FRW was used as one of the two FRWs required in the bridge construction

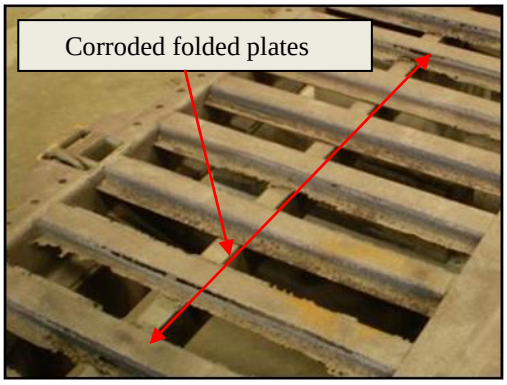

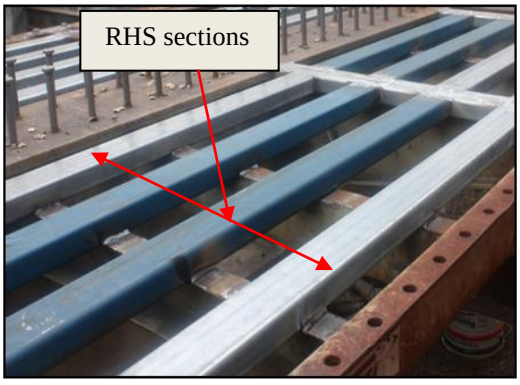

(a) Corroded folded plates (b) RHS section replacing folded plates

Figure 5.9 Replacement of corroded decking members; folded plates were completely replaced with RHS

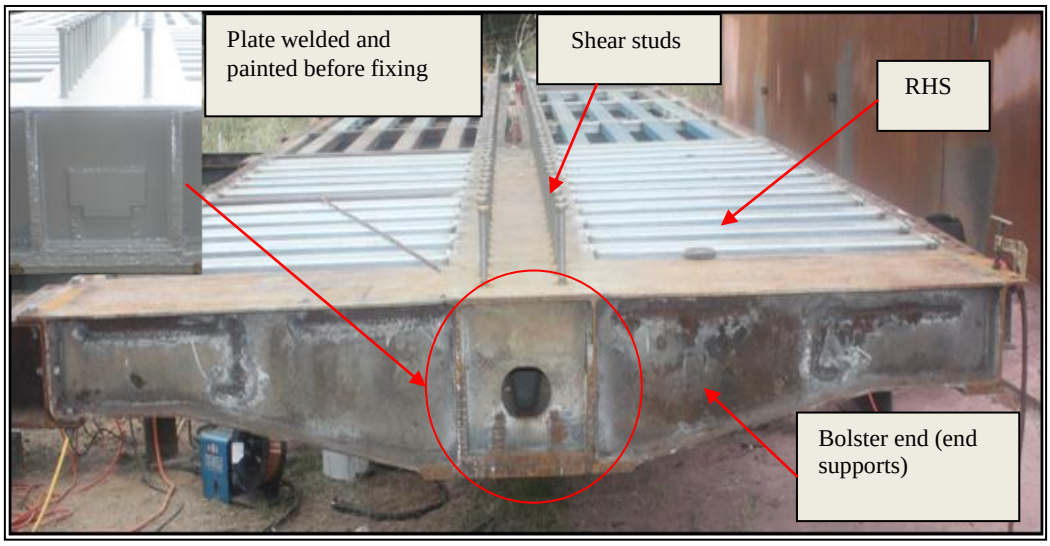

Figure 5.10 Modification in the fabrication yard. Overhang parts of the FRW were cut and the circular opening seen in the image was later sealed with steel plate

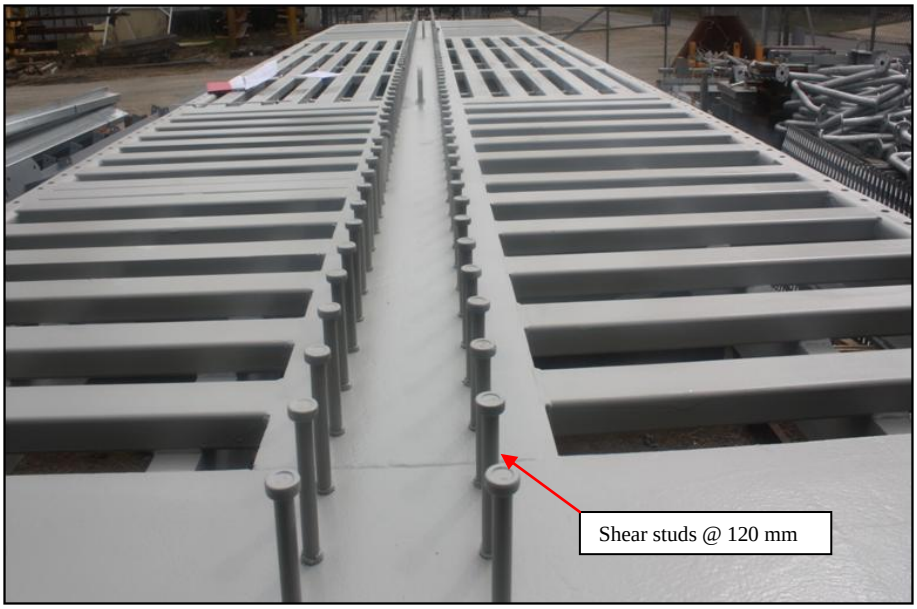

Figure 5.11 FRW ready for installation after sand blasting and corrosion paint applied; shear studs were welded on the main box girder in the fabrication yard

5.4.2 Abutment

Abutment consisted of two bored piles of 900 mm diameter on each bank, driven to the bedrock approximately 6.5 m length, the concrete cap beams on top and back

walls as shown in Figure 5.12. This type of substructure is commonly designed and constructed in bridge structures. The dimensions and reinforcement details of the substructure design are presented in Appendix - B.

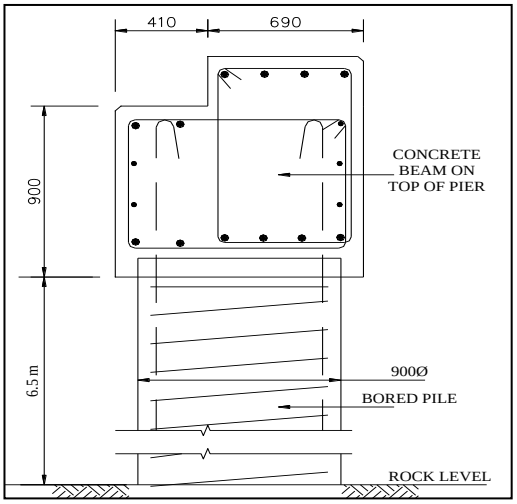

(a) Details of abutment

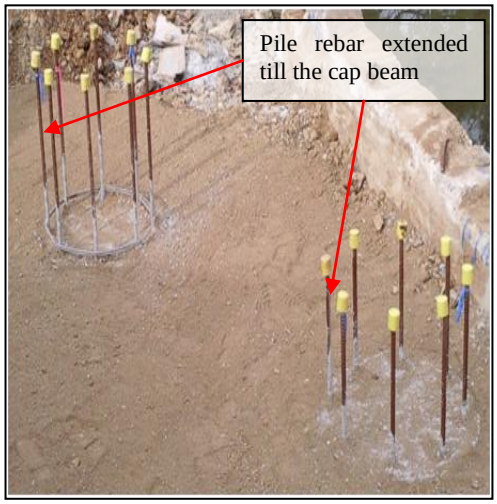

(b) Extended rebar from the pile

(c) Formwork for abutment

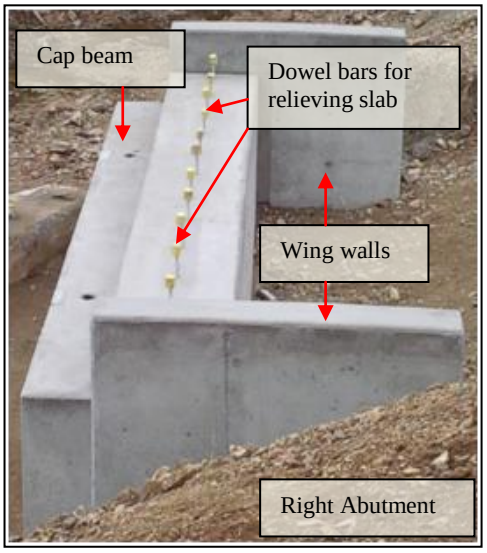

(d) Completed right abutment

Figure 5.12 Side views of bridge abutment

The abutment was designed to support the only the main box girders of the two FRWs through a shear pin of 40 mm diameter as shown in Figure 5.13. This pin restraints the movement of FRW in both the longitudinal and the transverse

directions but do not prevents the structure from uplift. To prevent possible uplift of the structure from the flood buoyancy, end brackets connecting the two FRWs were bolted with 20mm bolts to the abutment.

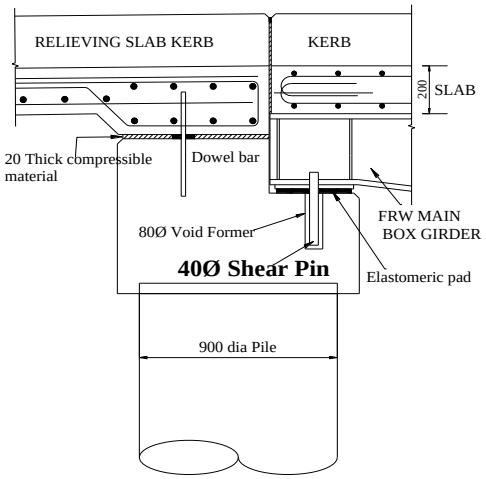

Figure 5.13 Shear pin connection detail at the abutment

Due to lack of perfect leveling of the cap beam of the abutment, the FRW could not be seated firmly as was assumed in the design stage. Furthermore, as the bottom flange of the two main box girders was 181 mm lower than the edge Z-beams, the edge Z beams were designed to be hanging in the air as shown in Figure 5.14. Compounding the overhang with the imperfect seating of the bottom flange of the box girders has caused lateral imbalance of the FRWs making it difficult to align them for bolting of brackets as envisaged. The designers assumed the concrete slab would provide enough rigidity to the overhanging Z beams due to composite action thereby minimising the risk of lateral instability due to potential extreme eccentric traffic load. It was also checked that the concrete slab will suffer crack widths less than 0.1mm for the heaviest W80 with the worst eccentricity. In spite of these calculations, the research team at QUT and the author of the thesis in consultation

with the RRC construction crew have designed six additional custom made supports as shown in Figure 5.15 – one under each of the Z beam overhang – on both abutments. Elastomeric rubber pads were arranged on top of the supports before casting of slab.

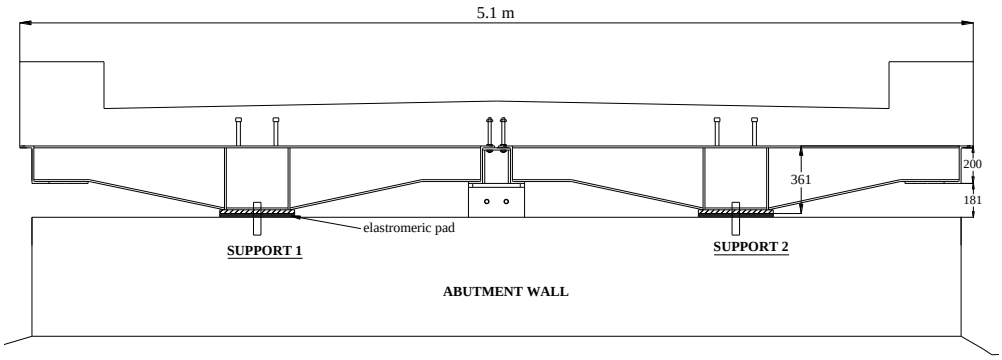

Figure 5.14 Initial support arrangements at the abutment cap wall

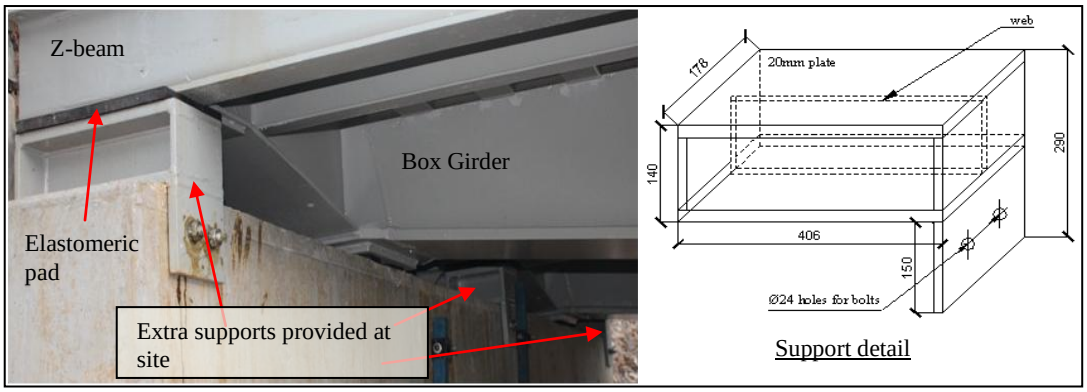

Figure 5.15 Extra supports supporting edged Z-beams and central connection bracket

In the January 2011 during the Queensland flooding, the bridge was totally submerged but was found undamaged withstanding buoyancy, thus validating the assumptions in the design calculations of the bolts and support system. The supports also remained in place without slight dislodgement.

5.4.3 Installation of FRW

The FRWs completed in all aspects were transported to the bridge site on semi trailer. To minimise the transportation cost and to cause less disruption to the normal traffic movement on the busy Bruce Highway, FRWs were placed on top of each other and transported. Heavy duty crane was used for loading, unloading and installing FRW on the abutments at site as shown in Figures 5.16 to 5.17.

Figure 5.16 Transportation and handling of FRWs

Figure 5.17 Installation of FRWs on the abutment

Before the FRW was placed on the abutment, elastomeric rubber pads were laid accurately on the cap beam. Shear pin was installed on the abutment and the FRW was lowered slowly and exactly fitting the pin into the hole of main box girder on both sides of the wagon. Connection brackets were then bolted along the longitudinal edge Z-beam of the wagon as per the design drawings to connect two FRWs together.

5.4.4 Reinforced concrete slab pavement

The driving surface of the FRW bridge was achieved with RCS. Figure 5.18 illustrates the RCS pavement on top of FRW - detail construction drawing of concrete slab is presented in Appendix - B.

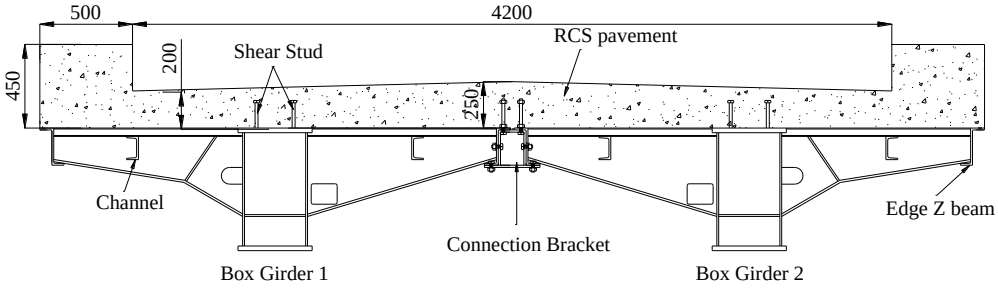

Figure 5.18 RCS pavement on top of FRW. Slab is connected to the main box girders by shear studs at 120 mm spacing in the longitudinal direction

Prior to placing reinforcing bars and pouring of concrete, fibre cement sheeting was placed on top of RHS as a self supporting formwork. This type of construction arrangement has eliminated the need for expensive formworks and scaffolds, thus minimising the cost of construction. Other activities of the construction of RCS pavement was carried out as follows:

- Placing of reinforcement bars as per the issued construction drawings.
- Erection of formwork for side bridge kerbs.
- Cleaning of dust and foreign bodies prior to pouring of concrete
- Pouring of concrete from one end of the bridge and compacting.
- Surface finish of fresh concrete as per the specification.
- Curing of concrete as per the standard specification.

The completed bridge is shown in Figure 5.19 whilst the construction sequence of RCS pavement and approach slabs are illustrated in Figure 5.20.

Figure 5.19 Completed FRW Bridge before field load testing

(a) Placing of reinforcement

(b) Erection of site formwork for kerb

(c) Pouring of concrete from one end

(d) Finishing work on the fresh concrete

(e) Approach road reinforcement

(f) Finished FRW Bridge with RCS deck

Figure 5.20 Construction sequence of RCS pavement

5.5 Construction schedule and cost

The demonstration bridge was constructed over a period of five months with lots of interruptions in between due to unseasonal wet weather in the Rockhampton region. The abutments were completed in four weeks and reinforced concrete slab was done in two weeks. The fabrication work which required complete replacement of decking members of FRW, cutting overhang parts, sandblasting and corrosion painting etc took eight weeks to complete. However, it is envisioned that FRW bridge can be constructed in approximately eight weeks if there are no other interruptions during the construction. This relatively short construction time can reduce the time the road is out of service, and thus, providing less inconvenience time to the local residents.

For this research studies, QRN has generously donated two FRWs and the necessary technical information required. However, the disused wagons can be purchased from QRN at a scrap price of the metal - approximately the cost of one FRW is $ 5000. The cost of constructing FRW bridge is estimated to be approximately $ 3,800 per m^2 which compares favourably against the cost of, for example RC bridges with the bidding cost of approximately $ 9000 - $ 1000 per m^2 and RC box culverts in the order of $ 5500 per m^2. Therefore, FRW bridge is cheaper and can also be erected within a very short period of time.

5.6 Summary

This chapter outlined the design and construction of the FRW demonstration bridge at T.Ramm road within the jurisdiction of the RRC. The traffic in the road was less than 150 vehicles per day making it a low volume road network bridge for which fatigue consideration was of less important. Compared to other available bridge replacement solutions, FRW bridge was relatively found cheaper as its construction duration was very short.

Although the FRWs were decommissioned for business reasons and not really due to technical incompetency to resist applied static freight loads, they still should possess sufficient strength and must remain free from serious damages such as the plate buckling, deformations, weld defects etc when using as the bridge superstructure. Therefore, an appropriate selection criterion was detailed in this chapter.

Chapter 6: Performance load testing

6.1 Introduction

The major component of this research thesis is the performance load testing of the demonstration bridge, the construction of which is described in Chapter 5.

This chapter presents performance load testing carried out using a 22.5-tonne normal traffic three- axle tandem truck on the demonstration bridge. The primary aim of the performance load testing was to assess the serviceability limit state behaviour of the bridge. In particular actual deformation and strains of the FRW caused by the loading truck running at varying operational speeds have been measured and checked whether or not they remain within the serviceability limit state in line with the standards.

6.2 Theory & Standard

Non-destructive load testing can provide insight into the bridge response to the applied loads and is an effective method of evaluating the performance of bridges (Chajes et al. 2000; Ryall, 2001). The data may also be used to assess the ultimate load behaviour using calibrated analytical/ numerical models (Richard et al. 2010; Ransom, 2000, p.3-14). As trucks capable of carrying much smaller load levels can be used in performance tests (Stone et al. 2001), these tests are cheaper and possess low risk relative to the proof load test that requires trucks carrying full design load.

Load tests are performed on the ageing bridges that are in service (Saraf et al. 1998); tests are also carried out on newly constructed bridges that incorporate novel construction materials or design. Stone et al. (2001) and Stiller et al. (2006) have examined the performance of GFRP deck laid on steel girders through field load testing and field investigation of an innovative sandwich plate system bridge deck was studied by Harris et al. (2008).

Despite various methods of load application, the most preferred and commonly used method of loading for performance load tests is the use of trucks loaded with aggregate/sand. One of the main advantages of using loaded trucks is the flexibility they provide in being able to move the load easily to different positions on the bridge deck.

6.3 Field testing procedure

A detour that was constructed during the construction of FRW bridge was maintained to operate till the field load tests were completed, thereby complete independent excess to the bridge site facilitated to carry on the test accurately. The detail of each component of load testing is presented in the following sections.

6.3.1 Loading truck

The FRW bridge was loaded with a three-axle tandem tipper truck with gross vehicle weight of 225.25 kN. The truck was fully loaded with crushed rocks and its gross weight was determined using a weigh-bridge scale. Each wheel load was also

carefully measured at site, prior to each test, using a portable weighing scale as shown in Figure 6.1 to an accuracy of 0.5kN. The sum of the wheel loads measured at site correlated well with the weigh-bridge gross weight of 225.25kN.

Figure 6.1 Portable weighing scale used to measure the wheel load

Wheel load measurement at site

Since only four sets of portable scales could be sourced in QLD and the test truck consisted of six wheels (considering two wheels each in front, middle and rear), the wheel loads were measured carefully and accurately as described in steps below:

(i) The scales were positioned accurately underneath the front and middle wheels of the truck on the completed bridge and readings were recorded.
(ii) The scales from the front wheel were moved to the rear wheel and readings were recorded. The middle wheels were left undisturbed.

The measurements were repeated twice and average values were taken as the final wheel load as shown in the Table 6.1. Figure 6.2 illustrates the wheel load measurements at site.

Table 6.1 Average wheel load measurement recorded at site

Wheel location	Average Load Left (kN)	Average Load Right (kN)
Front wheel	23.00	26.50
Middle wheel (right)	44.50	47.50
Rear wheel (right)	40.25	43.50

Figure 6.2 Measurement of wheel load at site

The measured wheel load distribution and layout of the wheel are shown in Figure 6.3. It can be seen from the Figure 6.3 and Table 6.1 that the truck wheels were consistently loaded heavier on the driver side for its full length; the passenger side was approximately 4.37% under loaded relative to the driver side.

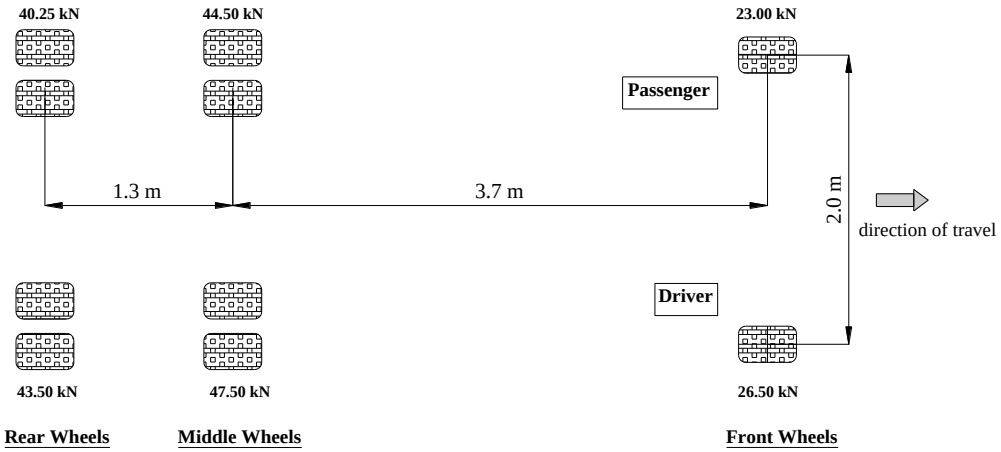

Figure 6.3 Wheel load configuration of the test truck

The test truck was driven within the clear markings of ‘lanes’ on the bridge deck (Figure 6.4). Two load positions were used for the bridge testing; centric loading and eccentric loading. Centric loading was symmetrical to the longitudinal centre line of the bridge whilst eccentric loading was 700 mm eccentric to the centre line as shown in the Figure 6.5. This is in accordance with the recommendation of Mehrkar-Asl and Brookes (2004), which helps in gaining comprehensive understanding of the behaviour of the bridge deck.

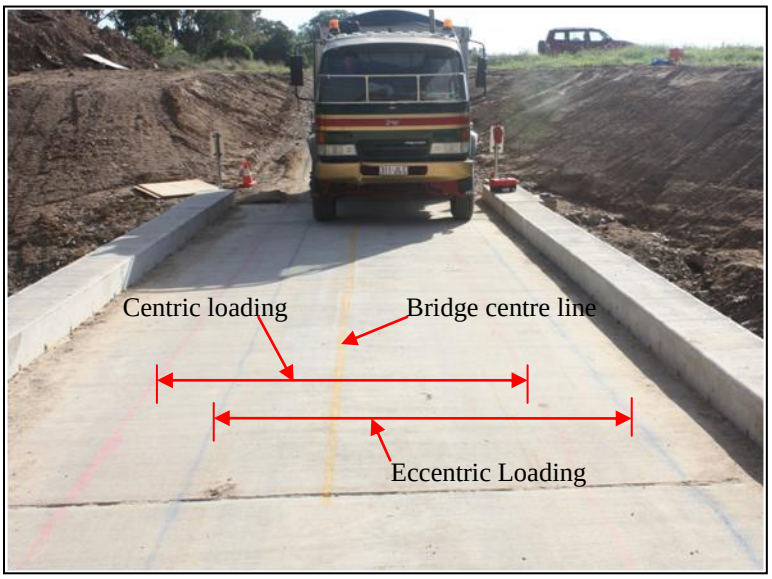

Figure 6.4 Test truck and markings on the slab to assist the driver to position the truck for different load tests

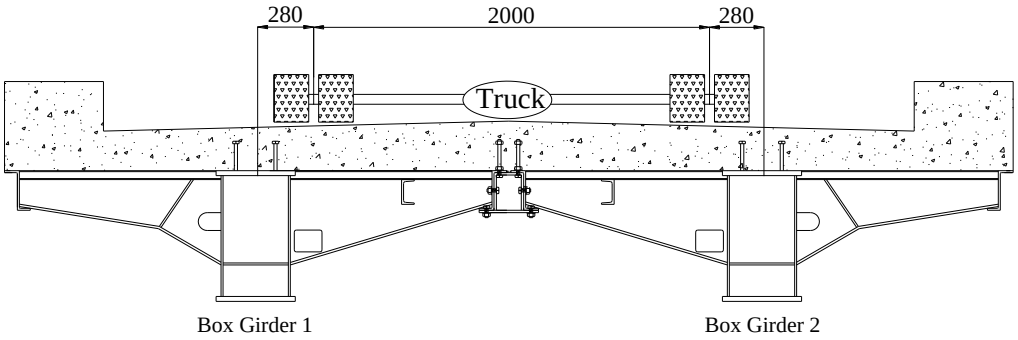

(a) Centric Loading

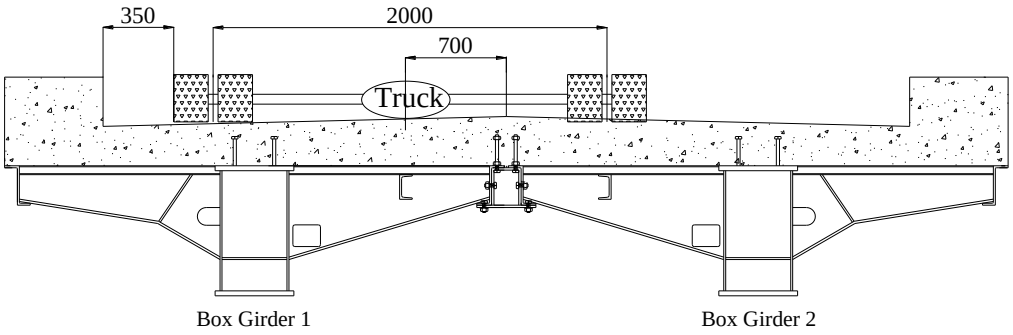

(b) Eccentric loading

Figure 6.5 Load positions adopted for the performance test

Accurate wheel positions are vital to make conclusions on the structural adequacy of the FRW in road bridges; therefore, to capture the wheel locations, a high speed camera was used, which is described in the following section. For clear and distinct identification of truck wheel along the bridge in the recorded video for motion analysis at a later stage, several target points were pasted on the tandem truck body (Figure 6.6) by plumbing and measuring the distance between the centres of axles.

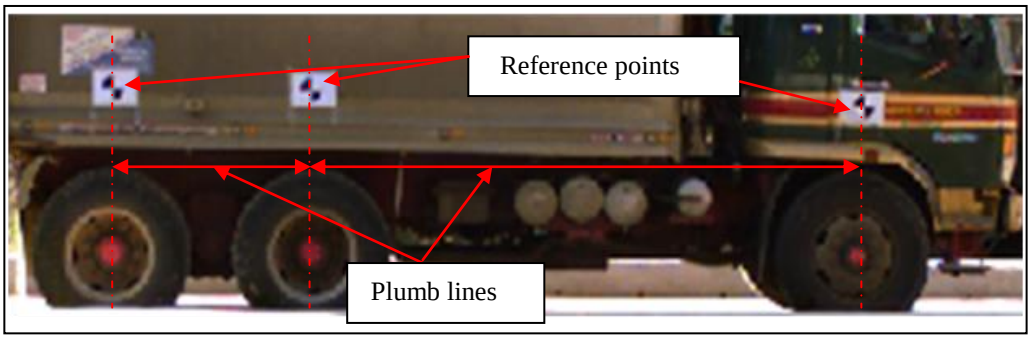

Figure 6.6 Reference points (targets) on the body of the truck to identify the position of wheels in the video analysis

For the determination of maximum bending strains and deflections, the middle axle of the truck was positioned exactly at the centre of the span of the bridge (Figure 6.7 (a)). For maximum shear, the truck wheels were positioned as shown in Figure 6.7 (b).

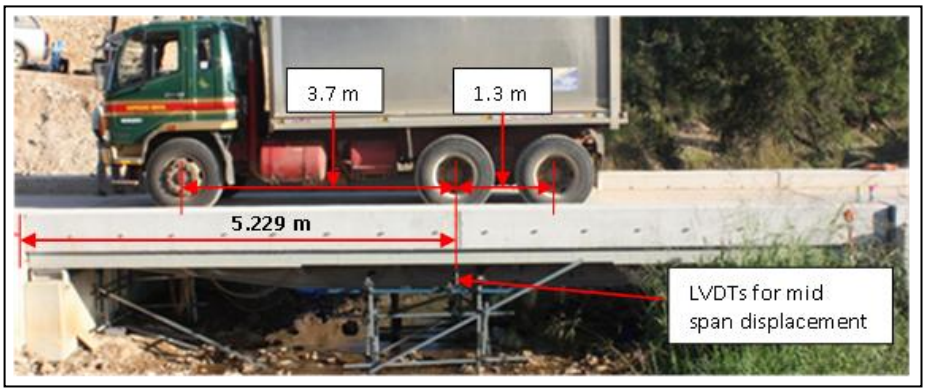

(a) Wheel locations for maximum bending and deflection

(b) Wheel locations for maximum shear

Figure 6.7 Location of truck during the static test

6.3.2 Sensors

Sensor system comprised of strain and displacement sensors. Displacements and strains were measured as the response of the bridge deck to the wheel loads. Linear variable displacement transducer (LVDT) and two types of strain gauges: uniaxial gauge and rectangular rosette are employed in the test instrumentations as shown in the Figure 6.8 below. Uniaxial gauge was used for bending strain while rosettes were employed for shear near the supports.

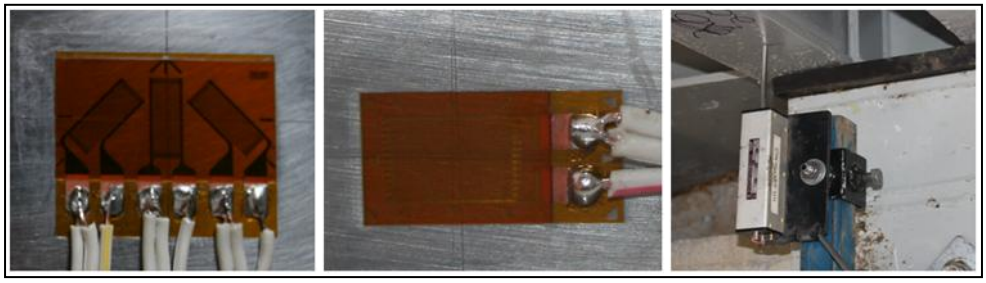

(a) Rosette (b) Uniaxial gauge (c) LVDT (spring type)

Figure 6.8 Sensors used in the performance load testing

6.3.2.1 LVDTs and mounting frames

Displacement instrumentation plan is shown in Figure 6.9. As seen in Figure 6.9, eight LVDTs (shown as D1-D8) were placed, mainly at the mid span locations. Displacement was measured along the span and across the width of the bridge.

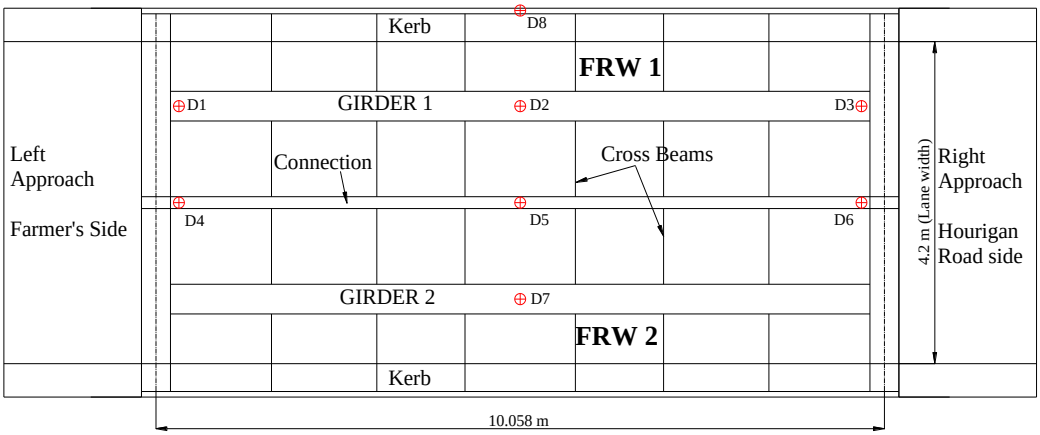

Figure 6.9 Displacement instrumentations layout

LVDTs were mounted at site on a framework of independent scaffold constructed with RHS section at the mid span of the bridge as shown in the Figure 6.10. Sufficient lateral and diagonal members were provided to each bay of the scaffold to ensure sufficient rigidity to avoid any accidental movements. Risk of potential vertical settlements of the scaffold framework was avoided by placing the scaffold posts on steel box bases positioned on leveled firm ground below the water level. The scaffolds near the bridge supports were designed like a tri-pod system with sufficient rigidity and were placed on rigid concrete platforms (Figure 6.11).

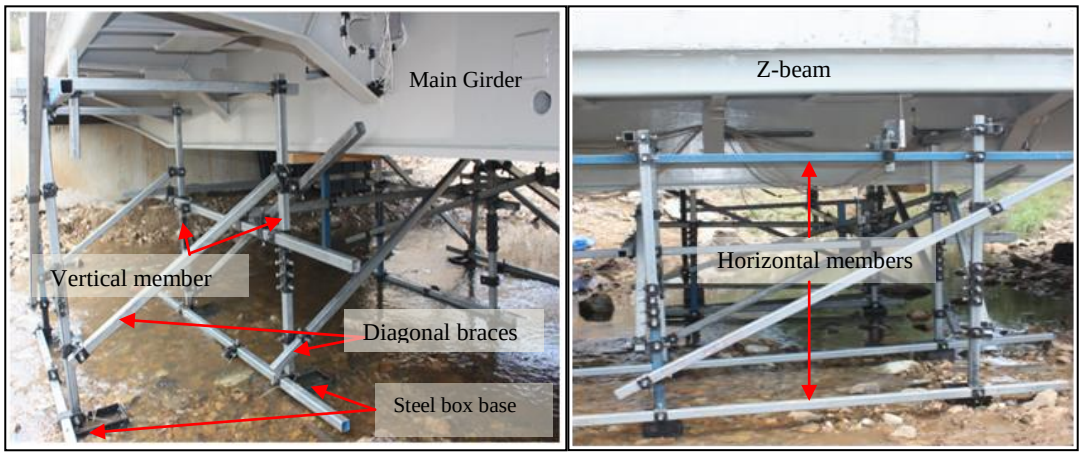

(a) Side view (b) Front view

Figure 6.10 RHS mounting frame for LVDTs

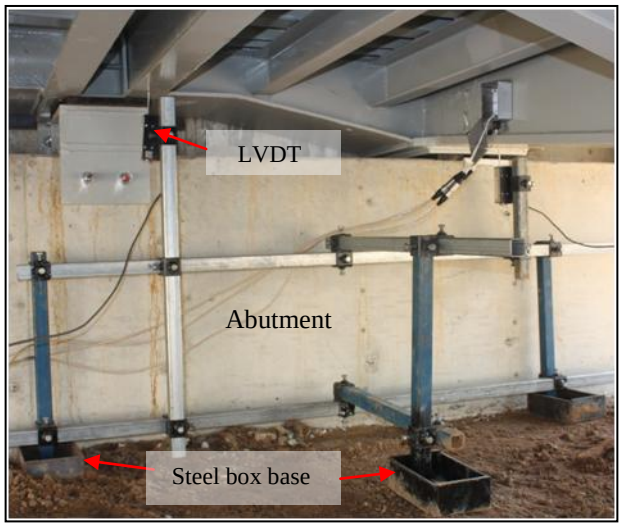

Figure 6.11 Tri-pod style mounting frame at support

6.3.2.2 Strain gauges

Linear and rosette strain gauges were placed at selected critical sections as shown in Figure 6.12. The locations correspond to maximum shear force or maximum bending moment; the strain gauge locations were the same as that of the full scale testing of FRW in the lab (Dhanaseker and Bayissa, 2011). Strain gauges were installed at both bottom and top flanges of the main box girder and on the web and flanges of in the cross girders. These gauges were installed at the steel fabrication yard after the minor modifications and anti-corrosion painting were completed on the FRW prior to transporting the wagons to the bridge site. The gauges were protected from accidental damage during transportation and concreting at site by using special adhesive sikaflex. The electrical wiring from the gauges was stored in an aluminum case mounted to the wagons. Timber battens were also glued to the main box girder bottom flange to protect the gauges underneath during transportation and installation of wagons to the abutment.

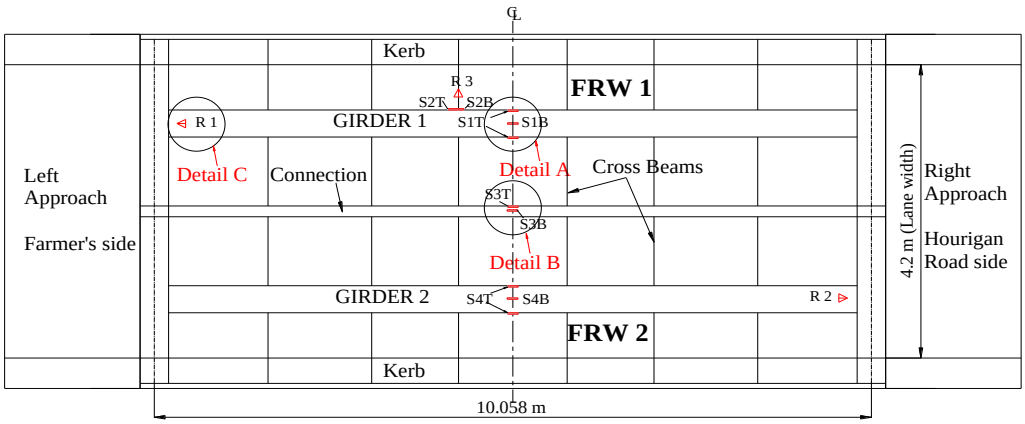

S = Uni-axial strain, R = Rosette, T = top, B= bottom

(a) Strain gauge layout (plan)

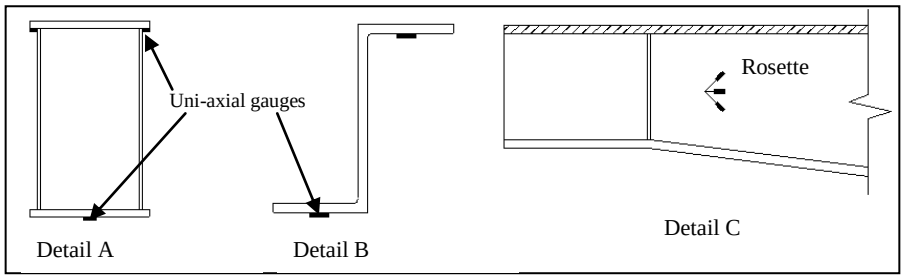

(b) Detail of strain gauges locations

Figure 6.12 Strain gauge instrumentations layout

The Figures 6.13 and 6.14 shows the rosette and uni-axial strain gauges attached to the members of FRW.

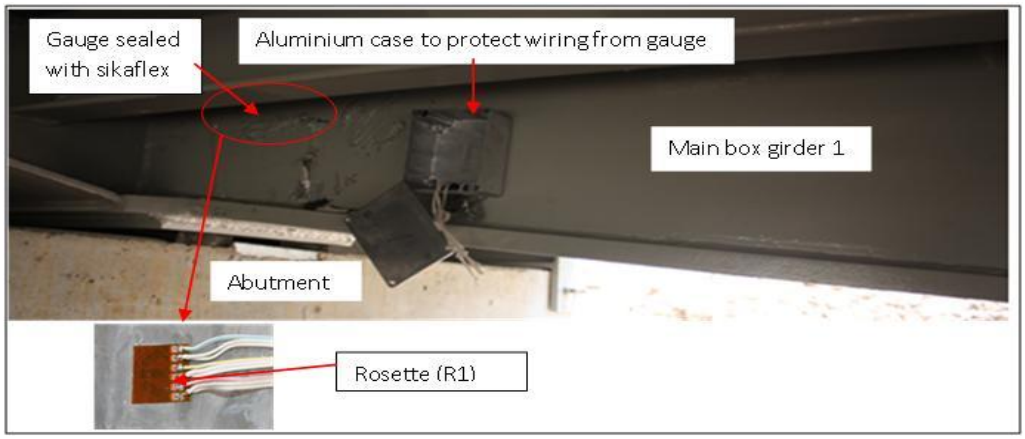

Figure 6.13 Rosette used for recording shear strain near the support (left abutment)

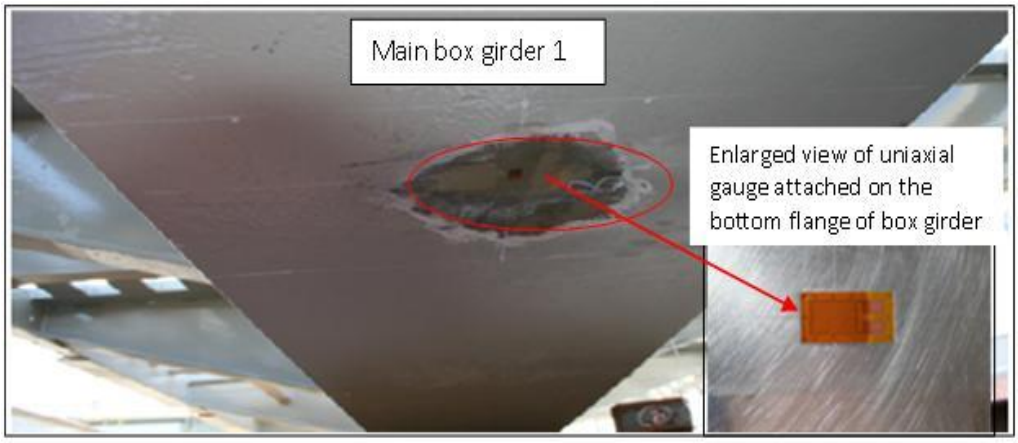

Figure 6.14 Uniaxial gauge underneath the main box girder at mid span (Girder 2)

6.3.2.3 High-speed camera

A high speed camera and the associated computer system (Figure 6.15) was used to video record the moving truck along the span of the bridge with a view to accurately capturing the wheel positions on the bridge for later analysis using a ProAnalyst commercial software package. Many load tests reported in the literature did not capture the load position well; this makes the sensor response difficult to interpret. Doornink et al. (2003) had used an auto clicker that worked well when there were no external electromagnetic disturbances at source. The wheel location was related to the sensor response; however, as the wheel circumference (approximately 1 m) was used to locate the wheel, the wheel position could only be located very coarsely. In this research thesis, the wheel positions was accurately captured using a high speed camera assisted by image analysis software; the load positions were thus easily correlated to the sensor responses using the time scale.

Figure 6.15 High-speed camera and computers set-up at site

The camera was set-up in the up-stream side of the river at a distance of 20m perpendicular to the longitudinal axis of the bridge. The camera was connected and time-synchronised with other sensors in the DAQ and both the DAQ and the camera were triggered simultaneously just prior to the truck enter the bridge. The recorded video of each test was immediately downloaded and stored in the external hard drive to create sufficient space for next recording. During the downloading process, the unwanted video recorded that was of no use i.e the truck far away from the bridge approaches were cut-off and only necessary video required for analysis at later stage was stored. This approach has expedited the testing sequence. Portable generator was engaged at the site to run the high speed camera and the associated computers for recording video data.

6.3.2.4 Data Acquisition System (DAQ)

An essential requirement of the testing procedure was the ability to monitor the measured data during the test. This was undertaken through the Data Acquisition (DAQ) system. DAQ was designed and developed by Center for Railway Engineering (CRE), Central Queensland University (CQU) and was capable of

recording 31channels. The DAQ employed for the load testing is shown in Figure 6.16 below.

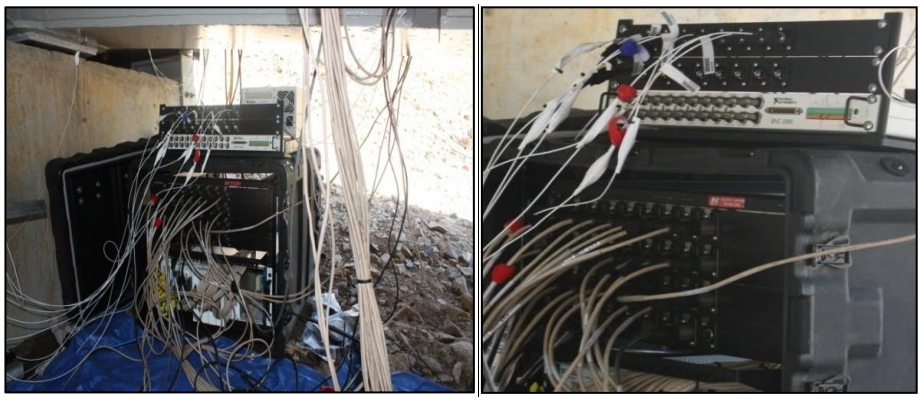

Figure 6.16 DAQ system set up at site

Prior to starting the load test, each channel was verified individually; the referenced numbers given were accurately matched as this verification was essential to avoid misrepresentation of sensors. Table 6.2 below outlines the sensor distribution and channel allocation for the performance test.

Table 6.2 Channel allocation in the field tests

Field load test	LVDT	Strain gauge
Centric loading	8	24
Eccentric loading	8	24

6.4 Field load test results

Field load test consisted of two different load tests; static load test and moving load test. The static tests were conducted by stopping the vehicle at the predetermined locations as shown in Figure 6.7 and the deformation responses of the bridge deck

were measured. Prior to starting the test, all channels were cross-checked and verified individually. Eight tests were conducted; two tests for maximum bending moment (BM) and two tests for maximum shear force (SF) – with one each on centric and eccentric load positions (Figure 6.5). Each test was repeated once to ensure repeatability of data and to investigate the behavior of the bridge. Moving tests were conducted under three speeds; crawl speed (approximately 5km/h), 20 km/h and 30km/h. Due to sudden dip and skew of the un-metalled approach roads on both side of the bridge (Figure 6.17), 30km/h was the highest speed possible (the experienced truck drivers insisted not to drive faster) and adopted for the test. The Figure 6.18 illustrates the test truck positioned at different locations during the tests.

Figure 6.17 Road alignments at the bridge site

(a) Truck positioned for max BM

(b) Truck positioned for max SF

(c) Back view of truck during crawl test

(d) Front view of truck during crawl test

Figure 6.18 Field load test Images

Two crawl tests were conducted; one centric and the other eccentric. The crawl tests took a long time; this has adversely affected downloading of the video from the camera into the computer and hence the crawl tests were not repeated. Eight moving load tests were conducted. The 20km/h and 30km/h tests were conducted through two repeats each through centric and eccentric lane drives respectively. In all a total of 18 tests were conducted including repeats as shown in Table 6.3. The tests took 28 hours over four days at site to complete.

Table 6.3 Summary of load tests undertaken in the field

Speed	Number of tests		Test designation
	Centric loading	Eccentric loading	
0 km/h	4	4	Static test
5km/h	1	1	Static test
20km/h	2	2	Moving test
30km/h	2	2	Moving test
Total	9	9	18 tests

Prior to starting each test, the LVDTs were checked for linearity and their calibration factors verified individually and their DAQ channel number correctly identified. The DAQ and the camera were commenced recording data well ahead of the truck entering the bridge and the recordings continued until the truck fully left the bridge for a distance of at least equal to its length (Carlsson, 2006). This approach has helped settling down any amplification that might have been induced due to the motion of the truck on the bridge deck and the adjacent section of road; no other external disturbances were permitted onto the bridge when the data were being recorded. Since the variation in the deflection and strain readings between the static and moving tests are minimal, with practically indistinct dynamic amplification due to short span of the bridge and stiff structure; the field test results are associated together and presented in deflection and strain responses in the section following.

6.4.1 Deflection response

Deflection was recorded at a rate of 128 Hz for all static tests and 1000Hz for all other tests. The deflection traces contained very limited noise and were in order and consistent with the expected behaviour of a simply supported deck system. Typical

traces for static and moving load tests are shown in Figures 6.19 and 6.20 respectively. These figures also show smoothed curves drawn using eyeball method to eliminate noises that are expected to be random. The smoothed curve thus drawn was used in the determination of the maximum values.

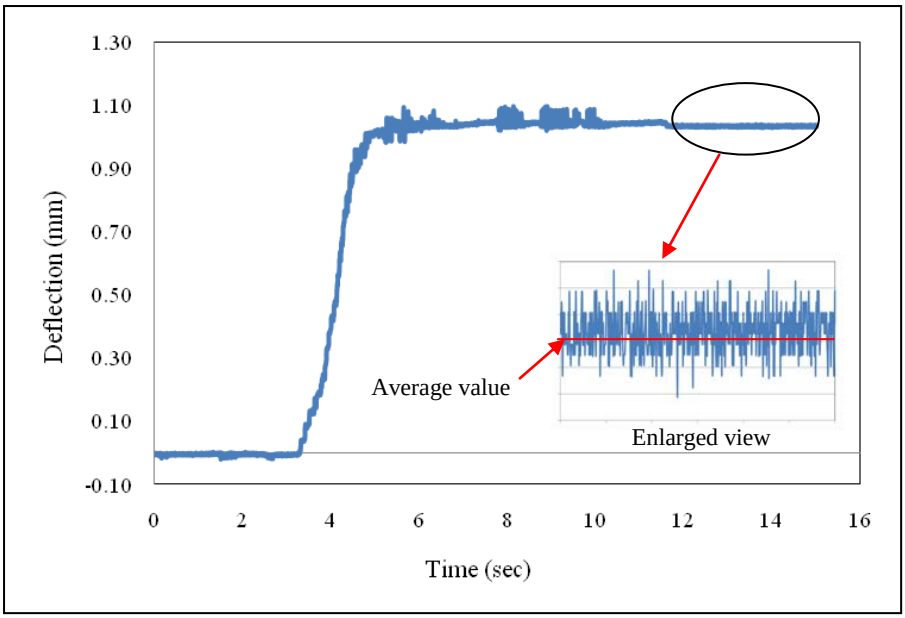

Figure 6.19 Typical traces observed in the measurement (static test)

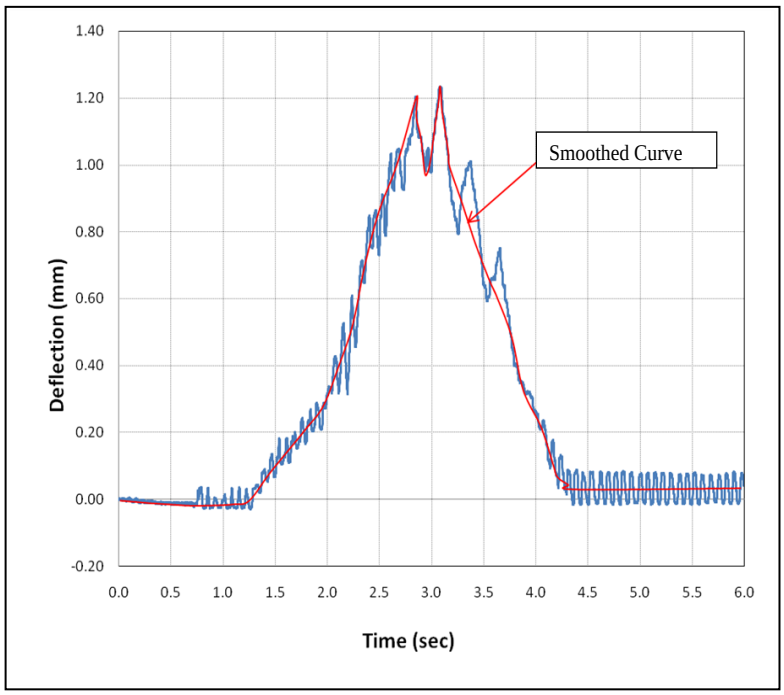

Figure 6.20 Typical traces observed in the measurement (moving test)

The deflections measured at mid span along the transverse direction for three different speeds (0km/h, 20km/h and 30km/h) during the live load tests are presented in Figures 6.21 to 6.22.

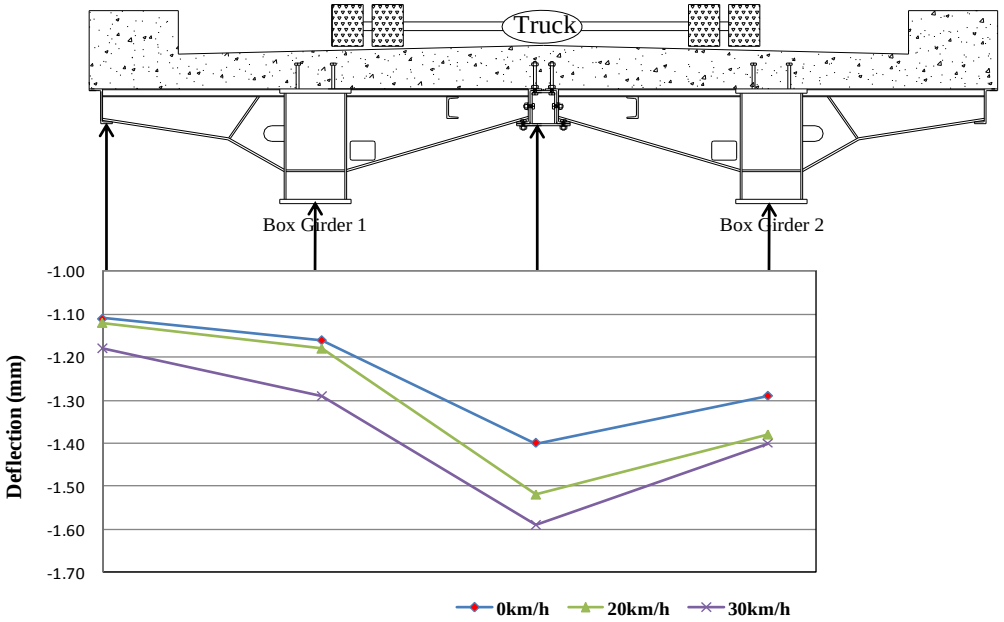

Figure 6.21 Mid-span deflections under centric loading

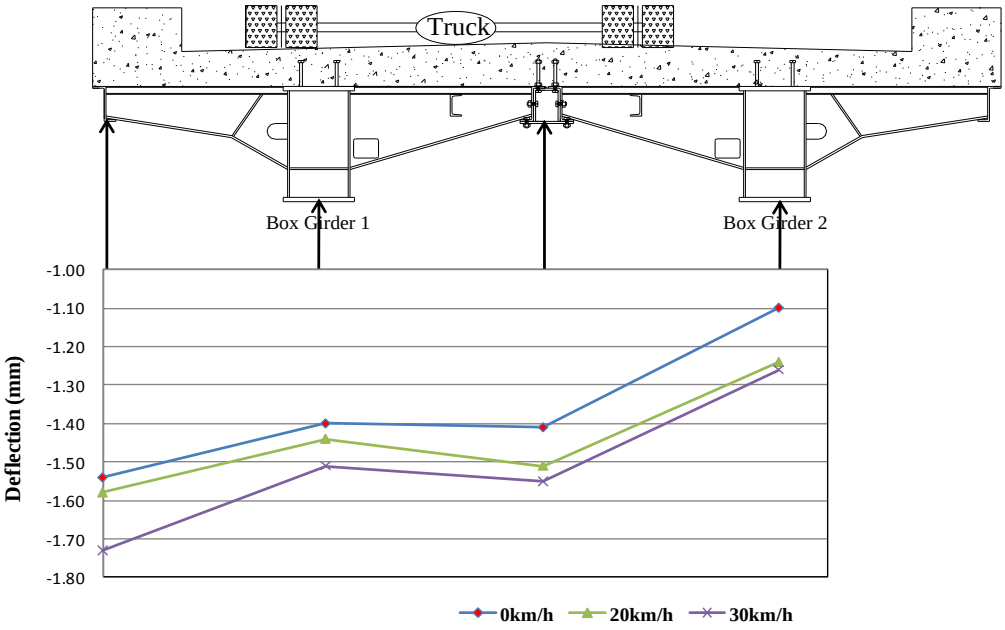

Figure 6.22 Mid-span deflections under eccentric loading

It can be seen from Figures 6.21 and 6.22 that there is small increased in deflection with increased speeds. The maximum deflection of 1.59 mm was recorded in the centre connection beam for centric loading, whilst 1.51 mm (larger than the centric loading, Figure 6.21) was measured in the girder 1 under 30km/h eccentric loading. Outer Z beam experienced larger deflection (1.73mm) when the truck was driven eccentrically. All the deflections measured were very small under the test truck load and such trucks are normally expected to ply on this low volume road. However, the deflections are linearly increased to M1600 load equivalent in the following sections in line with serviceability limit of AS 5100 (2004).

In the moving test, the sensors were time synchronised with high speed camera and triggered at the same time before the truck entered the bridge. The recorded video (1000 frames per second) was later analysed with ProAnalyst motion tool package for locating the truck wheel positions accurately on the bridge.

In the video analysis, both front and rear axle wheel reference points attached on the truck body (Figure 6.12) were used to track the wheel positions along the bridge span in relation to the synchronised time; a typical plot between the truck position and time at 30km/h speed is shown in Figure 6.23. Based on the front axle wheel position on the bridge length, a corresponding time can be read from the graph. The time is then, matched with the recorded data time in the deflection/strain time series. For example, to determine the max deflection corresponding to wheel position at location that is expected to generate maximum bending moment (front wheel at 8m), from Figure 6.23 the corresponding time (2.03 sec) was worked out and using Figure 6.24, the deflection corresponding to the time was read out (1.40 mm). Similarly the procedure can be repeated for various locations of the truck on the bridge. Similar

procedure was applied in determining the strain readings in relation to the load position.

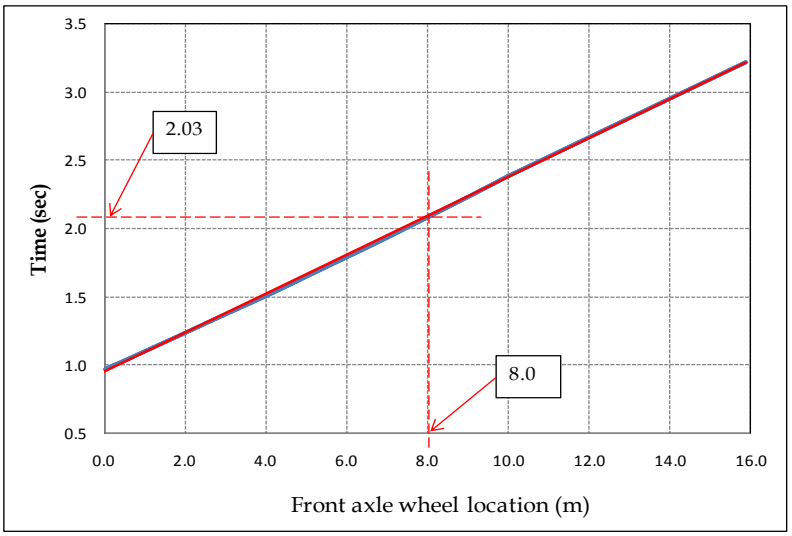

Figure 6.23 Typical plot of truck front axle over time (30km/h)

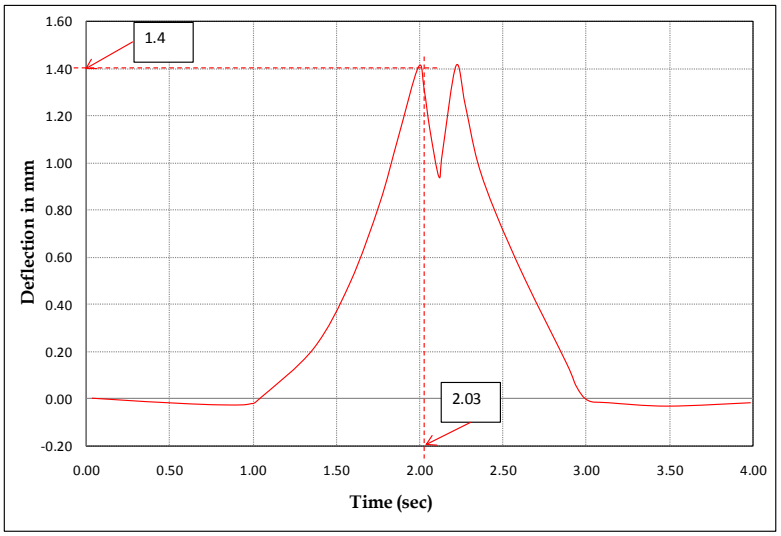

Figure 6.24 Typical deflection time series plot (Girder 2, 30km/h)

The measured maximum deflections at mid span at four different speeds are shown in Figures 6.25 and 6.26. The effect of speed to increased deflection is evident clearly in these figures and is consistent with the expectations of the principles of

engineering mechanics. Both the girders 1 and 2 have exhibited increased deflection with increased truck speed.

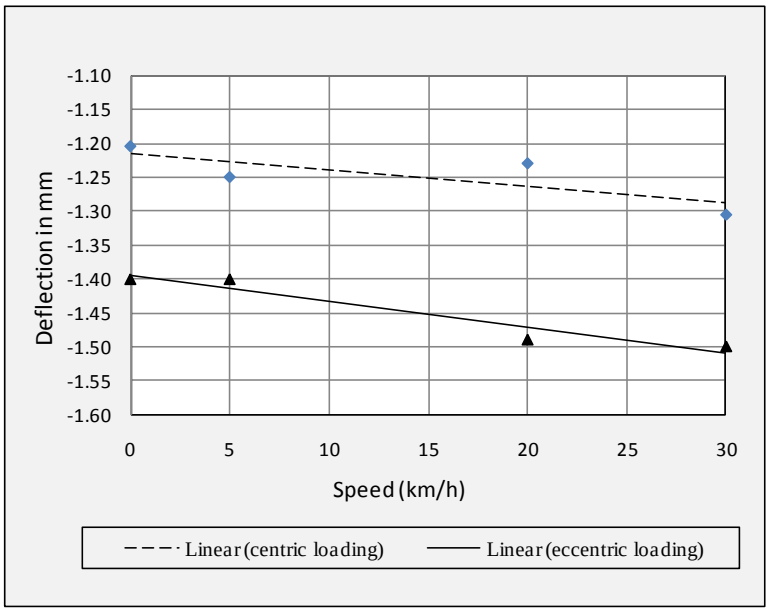

Figure 6.25 Maximum mid span deflection in Girder 1

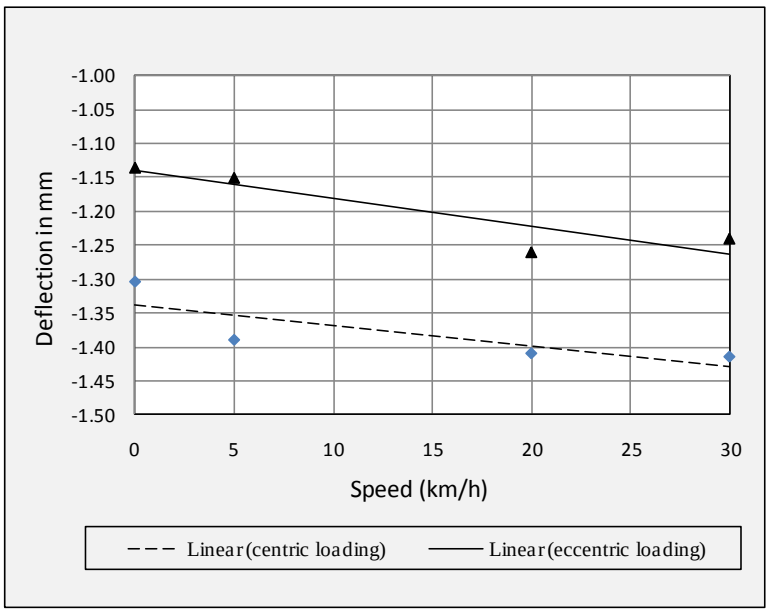

Figure 6.26 Maximum mid span deflection in Girder 2

6.4.2 Strain Response

Strains were also collected at the sampling rate of 128 Hz for static and 1000 Hz for all other tests. All the channels were individually checked, verified and set to zero reference before commencing the load tests. In all moving tests, the strain reading slowly peaked and reached maximum when the truck reached the mid span area and returned to zero when the truck was completely out off the bridge (Figure 6.27). Because of this, it can be deduced that the bridge was behaving linearly-elastically.

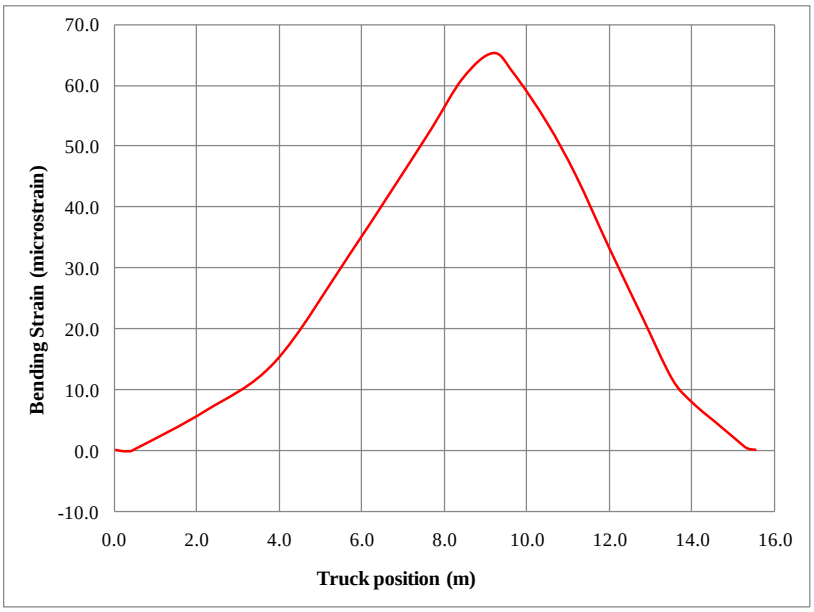

Figure 6.27 Typical bending strain plot under moving test (crawl speed)

As described in section 6.3.2.2 two types of strain gauges were used in the load test; uniaxial strain gauges and rectangular rosettes. The strain from the uniaxial gauge was directly read and compare with the limit state, while the strain from the rosettes were transformed from the well known Mohrs Circle methodology (Young & Budynas, 2002). The strains from all the tests were just over 80 microstrains while most tests yielded maximum strains between 50 – 75 microstrains. These low strains

can be attributed to the low weight of the test truck and or of stiff FRW Bridge. The live load tests were repeated in order to illustrate their reproducibility of data and as a standby data in the event of bad results being generated from one particular test. The Figure 6.28 illustrates that the two tests conducted on the same loading path behaved similarly for similar tests. The figure also indicates that the speed was not constant during the motion, which was one of the challenges faced during the load test. Although the driver made his best possible way to drive the truck at constant speed, due to sudden dip and skew on the approaches, small variations could not be eliminated completely. The maximum bending strains recorded under the truck load at the mid section in the transverse direction is presented in Figure 6.29.

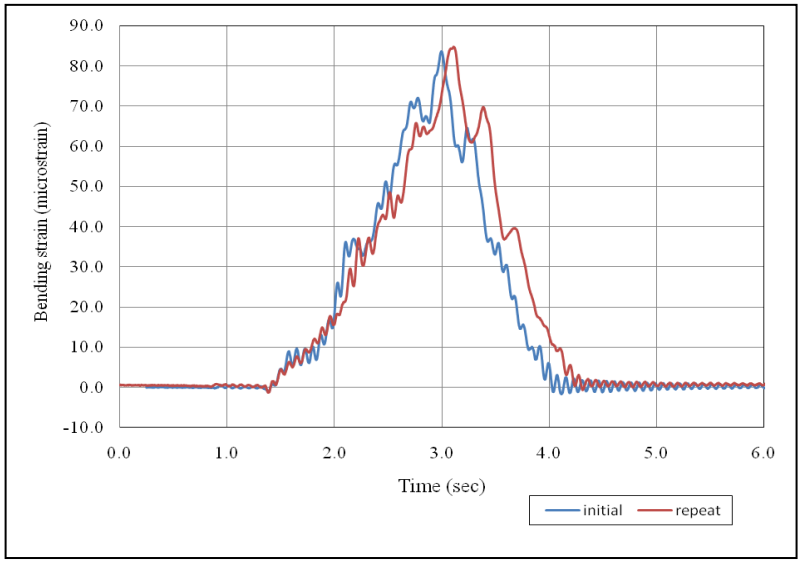

Figure 6.28 Comparison of strain measured at mid span in girder 2 under two tests on centric loading under 20km/h speed

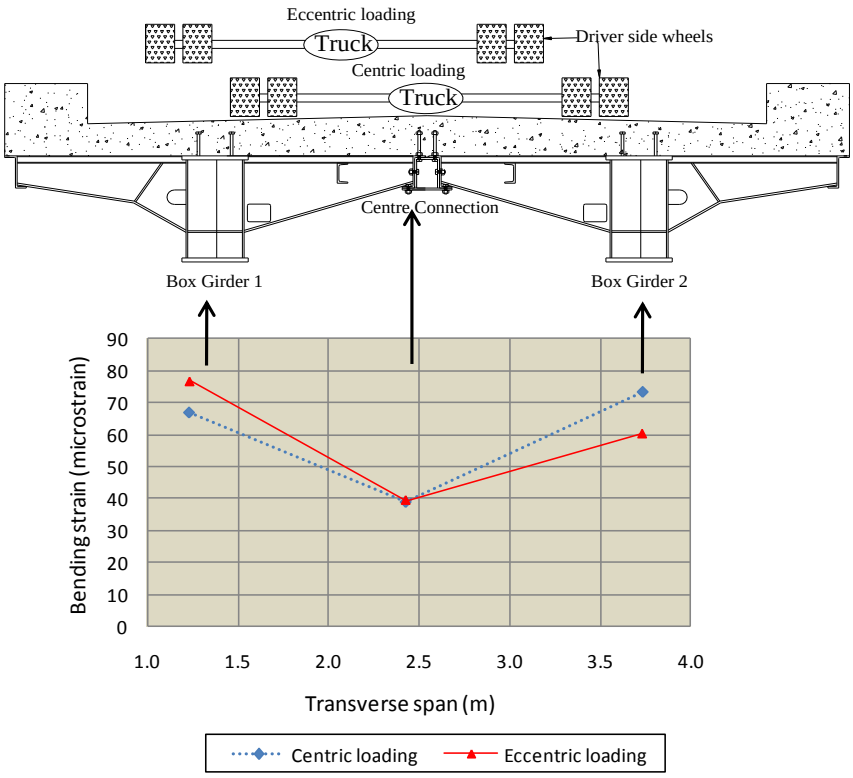

Figure 6.29 Maximum strain measured at mid span in the transverse direction

Consistent with the deflection, the girder 2 recorded higher bending strain under centric loading. Similar to the deflection plots, the measured maximum bending strains at mid span at four different speeds are plotted in Figures 6.30 and 6.31. The effect of speed to increased strain is evident clearly in these figures as well and is consistent with the expectations of the principles of engineering mechanics. Both the girders 1 and 2 have exhibited increased bending strain with increased truck speed.

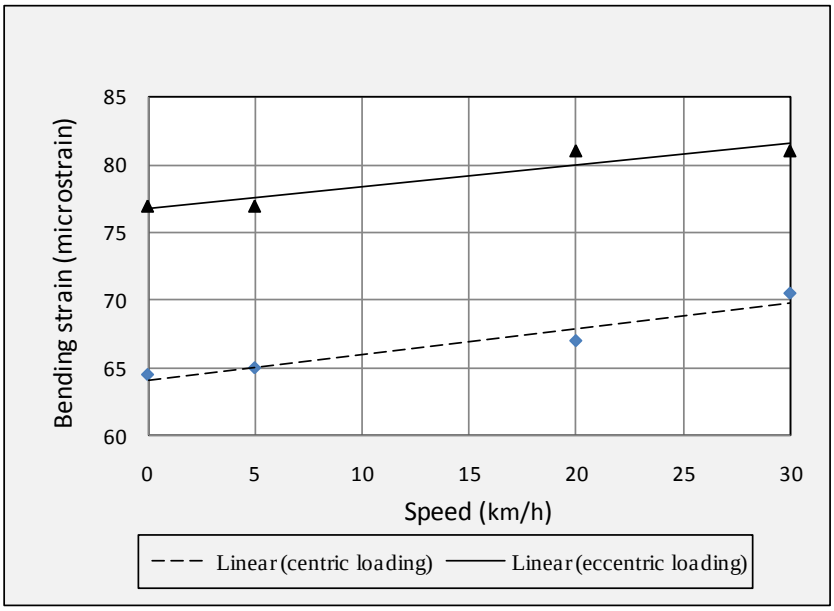

Figure 6.30 Maximum mid span bending strain in Girder 1

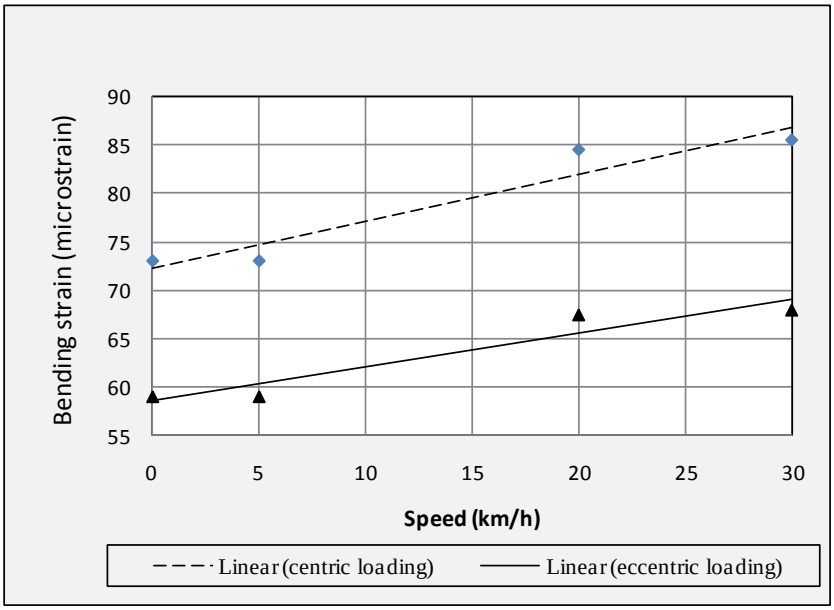

Figure 6.31 Maximum mid span bending strains in Girder 2

It can be seen from Figures 6.30 to 6.31 that the maximum bending strains increase linearly with the increase in the speed of moving truck. Consistent with the deflection response the bending strains were also linearly extrapolated to 70km/h and the highest value determined was 367με (in girder 2), occurring under eccentric loading.

It can be seen from Figure 6.31 that the girder 2 experienced higher bending strains than girder 1 under symmetrical loading (centric loading); this is because the wheels on the driver side were consistently loaded higher as described in Section 6.3.1 (Figure 6.3). However under eccentric loading, girder 2 recorded lower bending strain consistent with the shifting of the loaded wheels away from girder 2. Strain gauges were also placed on top and bottom of cross girder near the mid span to study their contributions in sharing the load. Eccentric loading was more critical for cross girder than the centric loading and the bending strains measured under this loading scheme were very small of 1 microstrain to 12 microstrain. This show that the cross girders are not really contributing in sharing the applied load and the design assumptions were correct. Shear strains were measured near the supports as described in Section 6.3.2.2 and the maximum average shear strain are presented in Table 6.4. Only two rosettes (R1 and R2 in Figure 6.12(a) were installed at the fabrication yard for the shear assuming similar behaviour of two FRWs as they were comprised of same design of the QRN wagon with similar configurations. The distance between the two rosettes is approximately 9.4 m apart.

Table 6.4 Maximum shear strains in girder 1 near the support

Speed (km/h)	Centric loading	Eccentric loading
0	43	74
5	98	104
20	97	107
30	104	109

Shear strain data from girder 2 were disregarded because the truck could not be located with maximum loads applied to the strain gauge rosettes in girder 2; this is because the trucks were driven in one direction only in all tests. The shear strain is

appeared to have been affected by the speed of the truck markedly; even a minor speed has elevated the shear strain but any further increase in speed has had minor effect only. This perhaps show the shear strain is more sensitive to the motion of the wheel as the wheel when entering the bridge can cause more 'disturbance' than when it has reached the mid span. It is interesting to note that all three moving load tests have produced consistent shear strains whilst the static shear strains were significantly lower.

6.5 Serviceability Limit State

For serviceability limit state deflection comparison, the clause 6.11 of AS 5100 (2004) stipulates the usage of M1600 moving traffic load. For span of 10.058 m bridge the M1600 gross load works out to be approximately 780kN including wheel loads and uniformly distributed load (UDL). Considering the gross weight of the tandem truck used in the test was 225.25kN, for serviceability limit comparison, the sensor responses measured at the test site were linearly increased by a *load factor* as follow:

$$Load\ \ factor = \frac{Gross\ weight\ of\ \ M1600}{Gross\ weight\ of\ \ test\ vehicle} = 3.46 \qquad 6.1$$

6.5.1 Deflection

The mid span deflection values under the test truck are linearly increased by load factor and deflection profile is plotted in Figure 6.32. The bridge satisfies the

serviceability deflection limit; the highest extrapolated deflection (5.8 mm) for 70km/h is well below the code limits 1/600th (16.70 mm) of the bridge span.

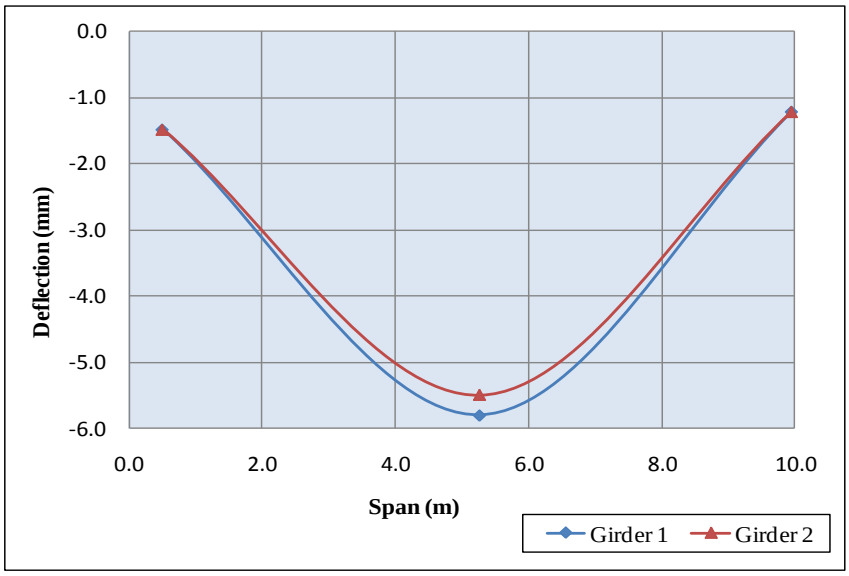

Figure 6.32 Extrapolated deflection profiles of the girders (eccentric loading)

6.5.2 Strain

Consistent with the displacement adjustment, the largest bending strain value from the field load test measurement were also linearly increased and plotted in Figure 6.33. The maximum M1600 equivalent bending strain is also well below the elastic limit (2000με).

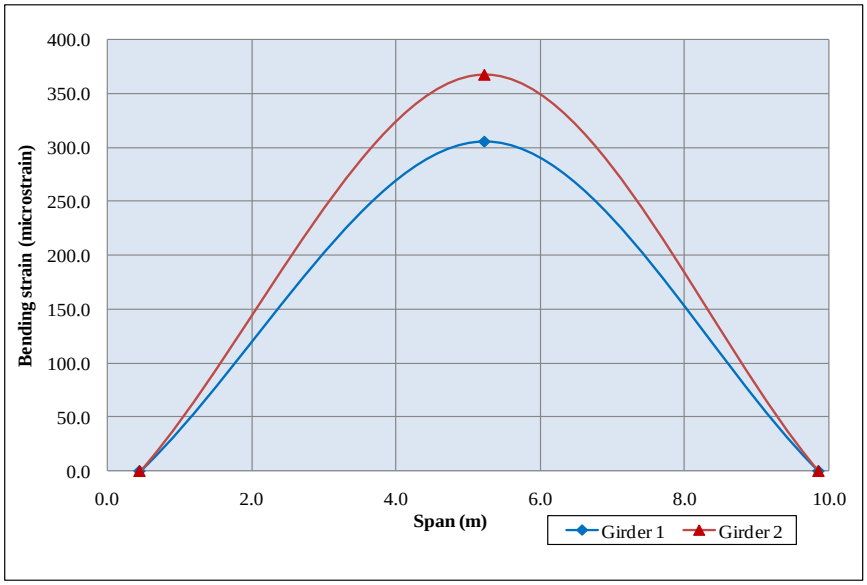

Figure 6.33 Extrapolated bending strain profiles along the girders (eccentric loading)

The linearly adjusted shear strains near the supports are shown in Table 6.5. The maximum linearly adjusted shear strains near the supports are below the shear yield limit (725 με).

Table 6.5 Maximum M1600 serviceability shear strain in girder 1 (70km/h)

Loading type	Left abutment (girder 1)
Centric loading	380 με
Eccentric loading	405 με

6.6 Composite Action

The main girders are connected with the RCS pavement through shear studs welded on their upper flange at 120 mm interval along the longitudinal direction; it is expected that this design will enforce composite action.

The strain measured under the upper and lower flanges of the box girder has indicated that there exists composite action between the concrete deck and steel girder, thus confirming the design assumption. Figure 6.34 shows that the upper flange strain is significantly lower than the lower flange strain, which is only possible due to composite interaction between the RCS pavement and the FRW as schematically illustrated in Figure 6.35.

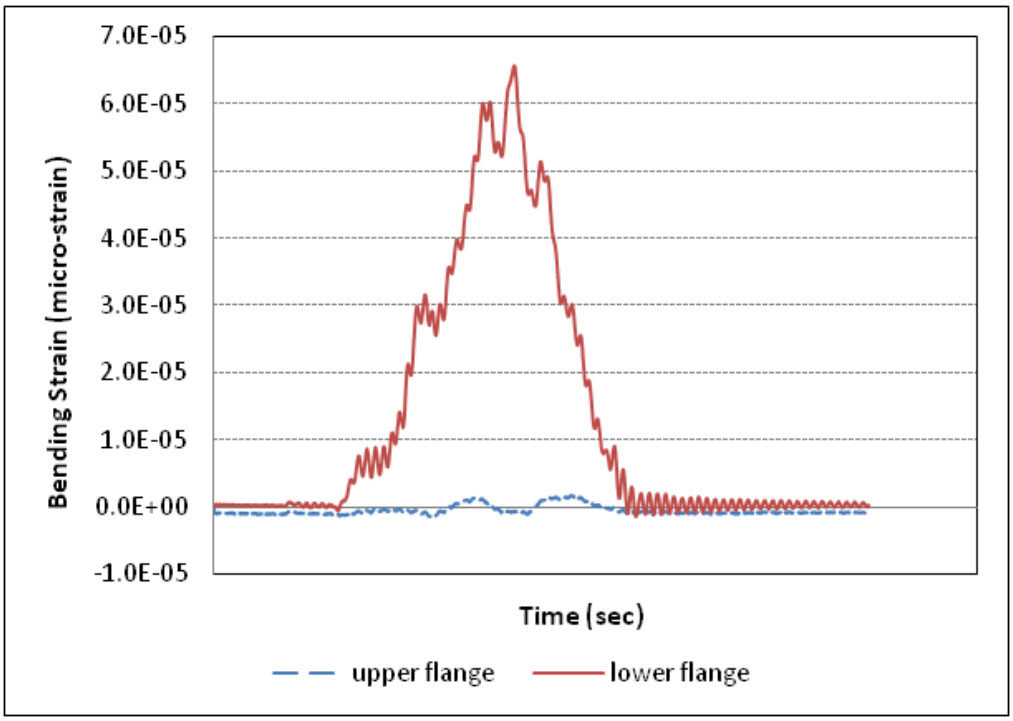

Figure 6.34 Typical bending strains measured at mid span (girder 1)

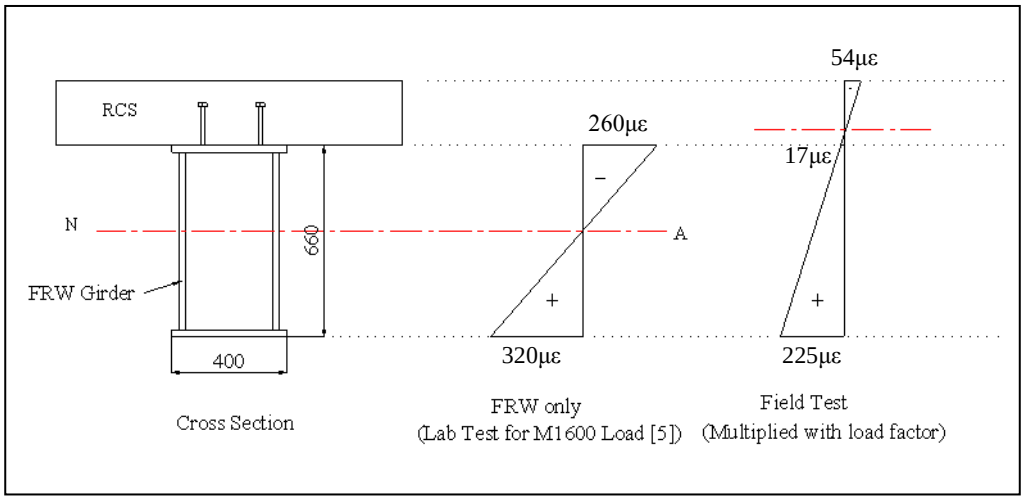

Figure 6.35 Flexural strains across the RCS pavement – FRW composite deck under static loading

Table 6.6 shows the comparison of deflection and bending strain values measured in the laboratory testing and the field test on the same FRW (FRW 1 in the Figure 6.12(a) under the same loading position. The measurements from the field test were linearly extrapolated by a load factor described in Section 6.5. The lab test consisted of bare FRW only with no RCS pavement – the testing and results are presented in (Dhanasekar & Bayissa, 2011).

Table 6.6 Mid-span deflection and bending strain values under two different tests

Girder No	Field test (static)		Lab test	
	Deflection (mm)	Strain at girder top (με)	Deflection (mm)	Strain at girder top (με)
Girder 1	5.2	+17	12.5	-260

It can be noted from Table 6.6 that the deflection and strain of the composite beam were reduced significantly; deflection was reduced by 58 % while 100 % reduction in the strain was observed.

Since the strains in the lower and upper flanges of the FRW are determined experimentally, it was easy to determine the maximum compressive strain at the top fiber of the RCS pavement using plane section remain plane assumption in pure bending. The calculated maximum strain was 15με. By extrapolating to 70km/h and multiplying with the load factor, this strain value worked out to be 85με, which is acceptable for a 32MPa concrete.

6.7 Summary

This chapter presented an overview of the in-service performance assessments of FRW Bridge deck containing RCS pavement. A full scale testing of the bridge was carried on the newly constructed completed bridge built in the rural area of Rockhampton Regional Council, Queensland, Australia.

A fully laden three axle truck of 225.25 kN gross load was driven along the bridge longitudinal direction at different safe speeds dictated by the approach roads; the strain and deflection responses at several critical locations were measured. The truck was also stationed at the predetermined positions along the bridge to record the largest bending and shear responses. The largest deflection and strain values measured at the mid span were linearly proportioned to obtain the serviceability limit state value of AS 5100 (2004). The extrapolated deflection were compared with the code provision and found to satisfy the serviceability limit; similarly the strains were also found to remain elastic well below the yield strength. The strain values measured at the upper flange of the FRW box girder have shown the existence of composite action between the reinforced concrete slab pavement and the FRW.

Since the FRW Bridge with concrete slab on top has shown adequate strength to resist high axle wheel loads of AS 5100, they can also be trailed on the highways. However due to high volume of average daily traffic (ADT) on the highway may pose a danger of fatigue failure of the structure as the fatigue study was beyond the scope of this thesis. Therefore, fatigue study is recommended.

Chapter 7: Structural adequacy of the FRW Bridge

7.1 Introduction

This chapter aims at determining the structural adequacy of the FRW bridge conforming to the provisions of the AS5100. For this, the bare frame of FRW grillage model described in chapter 4 was added with a RC slab using grillage idealisation of the slab. The FRW bridge model was then calibrated with field load test data (from Chapter 6). The final updated model was analysed for various combination of high axle wheel loads of the AS 5100 standard and the results are discussed and presented in relation to the serviceability and ultimate limit state limits prescribed in AS 5100 (2004).

7.2 Modelling of RC Slab

The grillage model presented in chapter 4 was first calibrated using the double FRW test data (SM1600 stationary load) as described in Section 4.3.3 of Chapter 4. The model was added with reinforced concrete slab (RCS) pavement on top as a grillage of beams as shown in Figure 7.1. The RCS was modeled using a grillage of beam elements in the X-Y plane, connected and restrained at their nodes to the FRW grillage. Each element posses a unique bending and torsional inertia to represent the portion of the deck which it represents. Recommendations given by Hambly (1991) and Bowles (1996, p. 562) were considered and incorporated in the formulation of grillage of 'beam' elements in modeling the RCS. Several assumptions were also

made to simplify the model without any loss in accuracy. The camber provided for drainage system was neglected, average thickness of 225mm was assumed, the steel placement through the deck remained constant, end kerbs are disregarded and the beam element line placed coinciding with the element line of main box girders and cross girders.

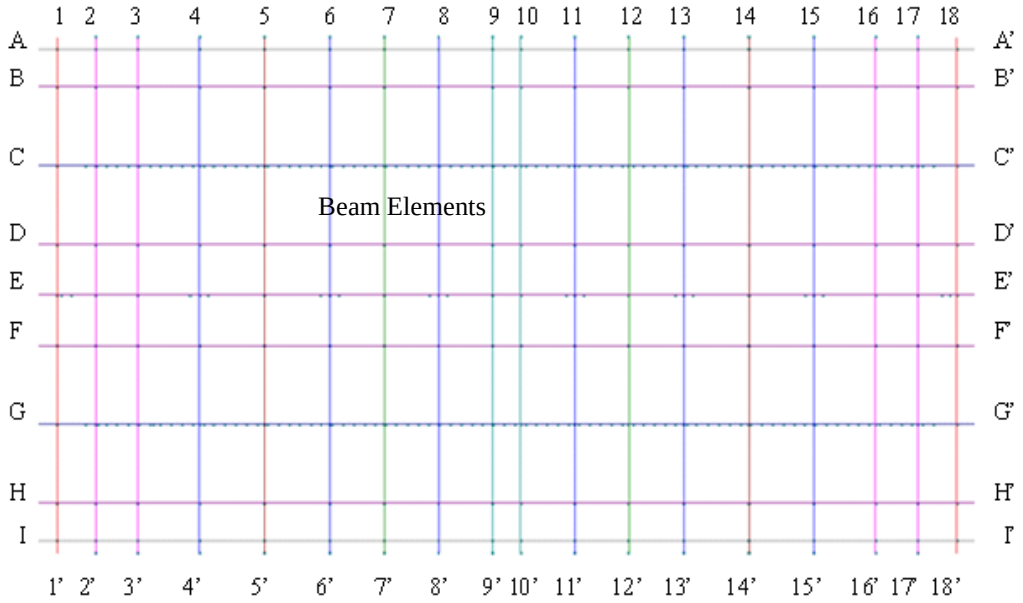

Figure 7.1 Grid line of beam element of RCS idealized in the model

In the idealisation of RCS, the longitudinal grid beam consist of nine elements and the transverse grid beams consist of eighteen elements in line with the spacing between the cross girders of the FRW (refer to Figure 7.1). The width of each beam element is shown in Table 7.1 and the depth of all beams is regarded as 225mm (corresponding to the average slab thickness). The ratio of spacing of transverse and longitudinal grid lines is maintained between 1 and 2 (1.57 ratio in the model) as recommended by Hambly (1991).The section properties of longitudinal and transverse grillage members are computed by considering each member as representing deck width to mid-way to

adjacent parallel members about the neutral axis of the deck. The sectional properties are computed as given in Equations 7.1 and 7.2 respectively.

$$I = \frac{bd^3}{12} \quad 7.1$$

$$J = \frac{bd^3}{6} \quad 7.2$$

Table 7.1 Details of beam element width idealised in the grillage model

Member	Element width (mm)
Longitudinal direction	
A-A' & I-I'	240
B-B', D-D',E-E', F-F'& H-H	500
C-C' & G-G'	1060
Transverse direction	
1-1'& 18-18'	400
2-2', 3-3', 16-16' & 17-17'	472.5
4-4', 6-6', 8-8', 11-11', 13-13' & 15-15'	900
5-5' & 14-14'	554
7-7' & 12-12'	318
9-9' & 10-10'	312

Despite a number of techniques available to model the composite action between the RCS and the girder, the technique of master-slave relationships between the element degrees of freedom without a physical connection employed by Harris (2007) has been adopted due to simplicity. This technique has ensured representation of the composite action between the steel main box girder and the RCS pavement available through the shear studs welded to the upper flange of the girder. Figure 7.2 illustrates the composite action achieved with imaginary link by employing master-slave constraint of the software program. Such imaginary links are provided along the length of the main girder at 120 mm spacing matching the spacing of the shear studs

attached to the main girder. The snapshots of the FRW bridge models are shown in Figures 7.3 through 7.5.

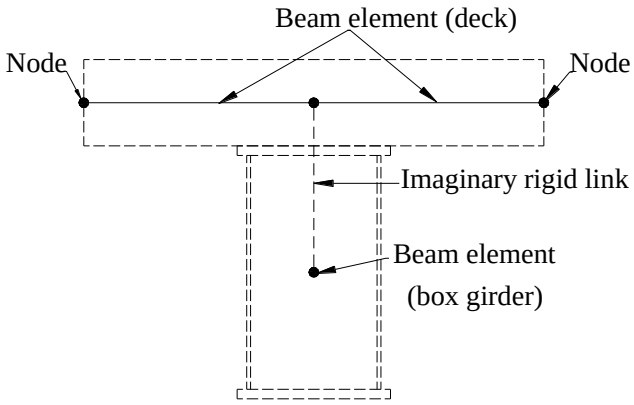

Figure 7.2 Deck and girder idealization in the model

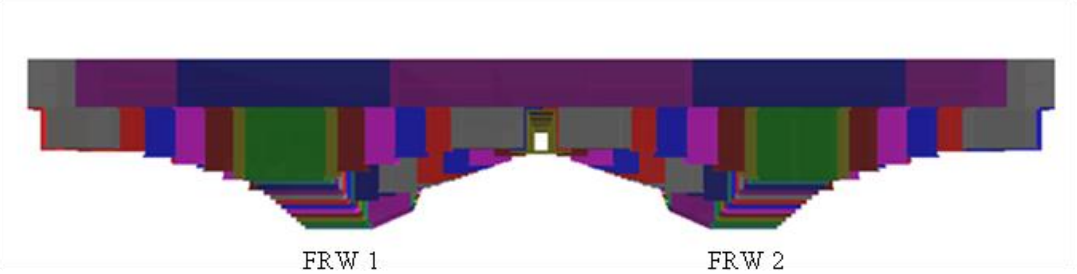

Figure 7.3 FRW bridge model (section view)

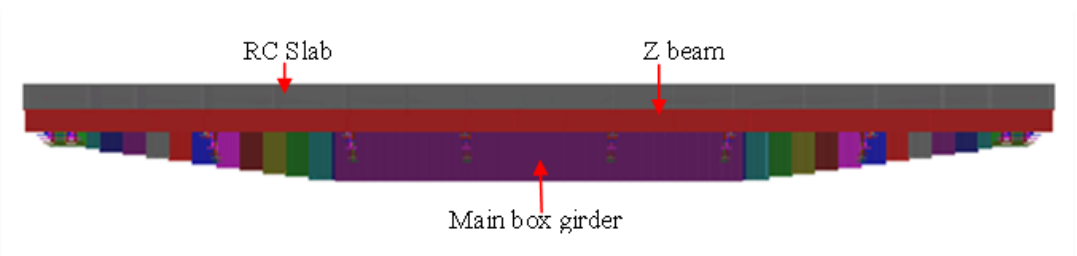

Figure 7.4 FRW bridge model (side view)

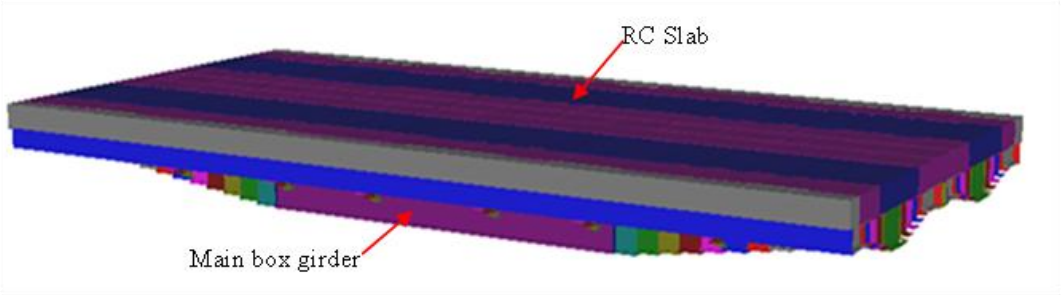

Figure 7.5 FRW bridge model (isometric view)

The model was further calibrated for the actual field support conditions. In the actual construction, the centre brackets connecting the two FRWs at the end of the bridge span were bolted to the abutment back wall which provided some partial rotational constraint, which was required to be calibrated. For this purpose the deflections measured close to the support (See Figure 6.9 – LVDTs D1, D3, D4, D6 of Chapter 6) were used. Spring constants (representing support) were adjusted until these deflections measured at site were matched with the prediction. .

The calibrated spring stiffness of each support using the updating method is presented in Table 7.2.

Table 7.2 Support spring stiffness adopted in the final model

Support Location	Spring stiffness (kN/mm)
Below main box girder	192.5
Below Edged Z-bam	200
Centre connection beam	100

7.3 Comparison of model and field test data

The updated grillage model was re-analysed with the test truck loading. The deflection measured along the bridge on the main box girder 1 between the model and the field load test is presented in Figures 7.6 and 7.7 under centric and eccentric loadings respectively. A good correlation between the updated grillage model and load test results is seen in Figures 7.6 and 7.7. The variation in the results is in between 2% to 2.5% only.

Girder 1 was selected for displacement comparison as this girder was installed with LVDTs at the mid span and near the supports, while only one LVDT was placed under

the girder 2 at mid span. The maximum mid span deflection in girder 2 between the model and test is presented in Table 7.3.

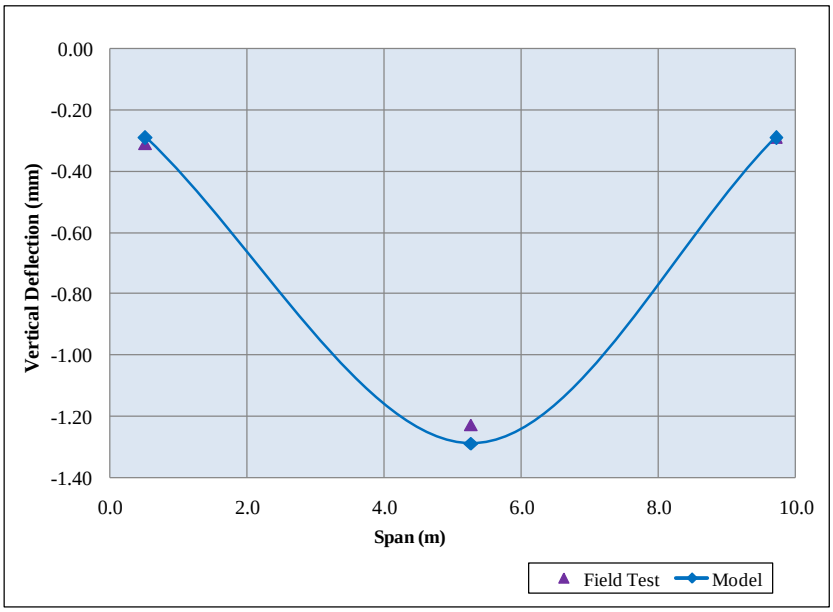

Figure 7.6 Deflection comparisons between the updated model and the test data along girder 1 (centric loading)

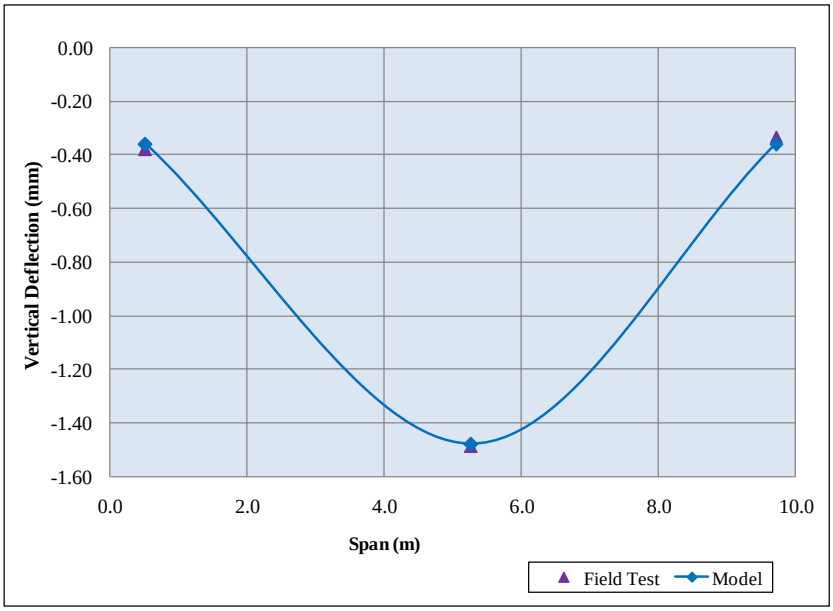

Figure 7.7 Deflection comparisons between the updated model and the test along the girder 1 (eccentric loading)

Table 7.3 Comparison of mid span deflection between field test and model in girder 2

Loading type	Test	Model
Centric loading	1.29	1.31
Eccentric loading	1.11	1.12

It can be seen from the Table 7.3 that the mid span deflections in the girder 2 between the field test and the updated model are very close to each other with variation of 1.5% maximum; thus demonstrating that the updated grillage model is capable to predict the bridge behaviour.

Further the displacements along the bridge transverse direction at the mid span are compared between the field test and the updated model for all LDVTs installed for all loading cases as shown in Figures 7.8 and 7.9.

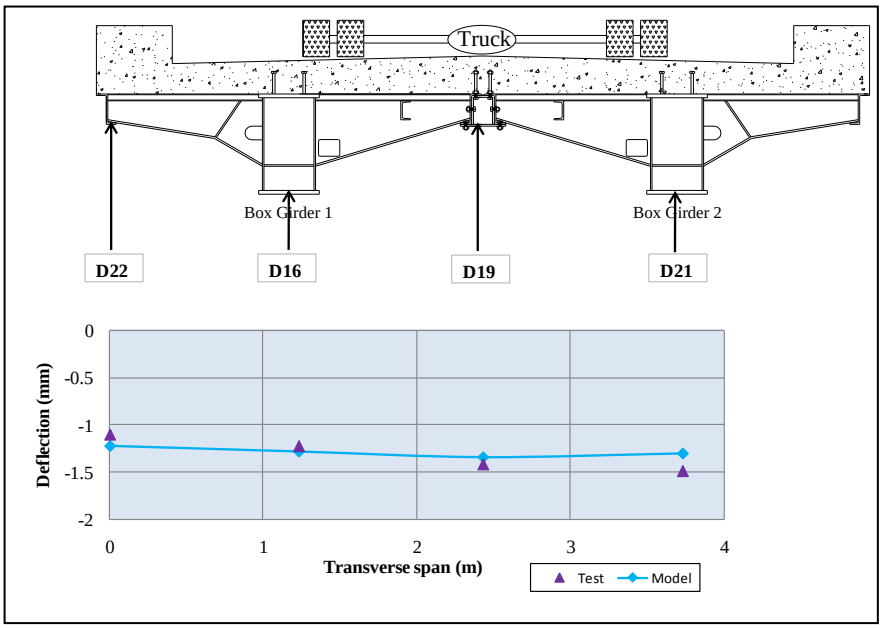

Figure 7.8 Deflection comparisons between model and the test at mid span along the bridge transverse direction (centric loading)

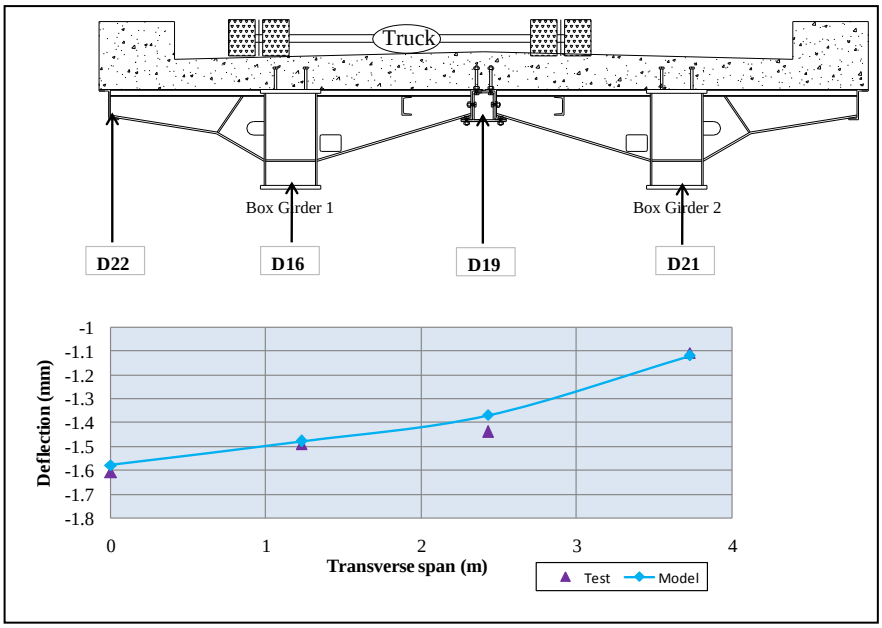

Figure 7.9 Deflection comparisons between model and the test at mid span along the bridge transverse direction (eccentric loading)

7.4 Serviceability Limit State

The updated grillage model of FRW bridge was further analysed for M1600 serviceability load.

7.4.1 Deflection

M1600 serviceability load defined in Chapter 4 was placed on the model at the critical locations (Figure 7.10 and Figure 7.11) and analysed. Eccentric loading was considered critical for main box girder. The vertical displacement profiles along the FRW box girder 1 and central connection beam are presented in Figures 7.12 and 7.13. For centric loading both girders 1 and 2 experienced same value of deflection along the span and hence only the displacement of girder 1 was plotted. However for eccentric loading the

displacement profiles for both girders 1 and 2 are plotted in Figure 7.14 and the displacement profile of the central connection beam under the eccentric loading is shown in Figure 7.15.

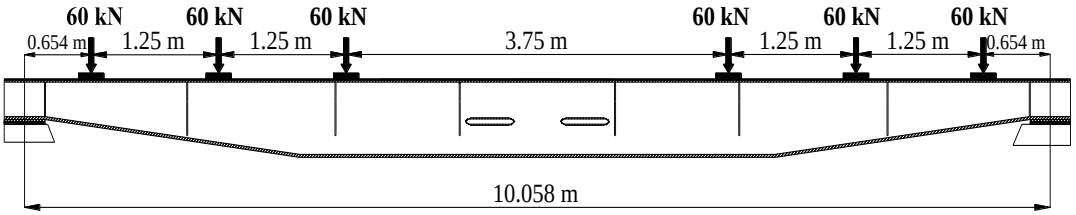

Figure 7.10 M1600 load configuration for maximum BM and deflection (Elevation)

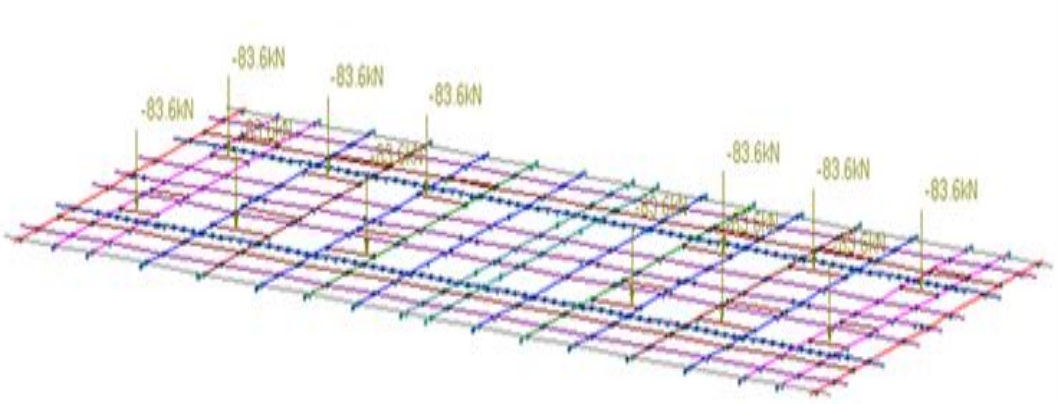

Figure 7.11 M1600 serviceability load applied on the grillage model (centric)

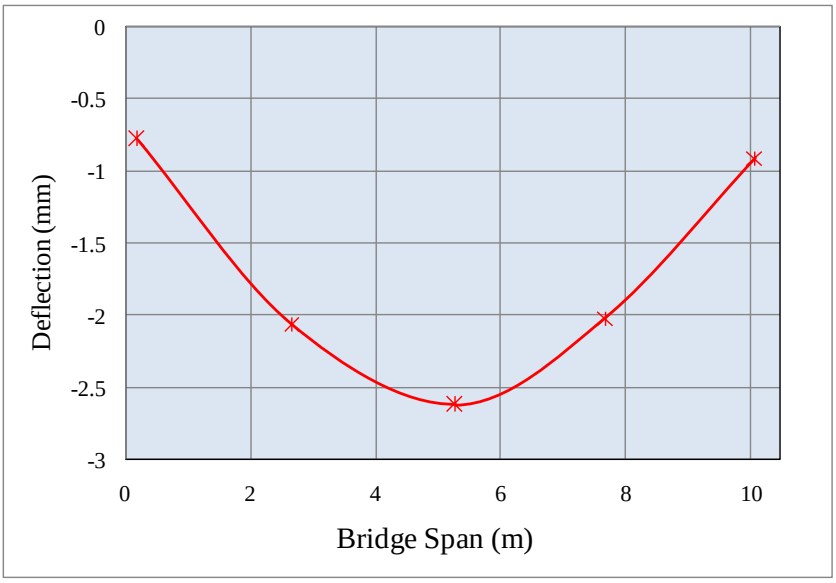

Figure 7.12 Vertical displacement profiles along the main box girder 1 (centric loading)

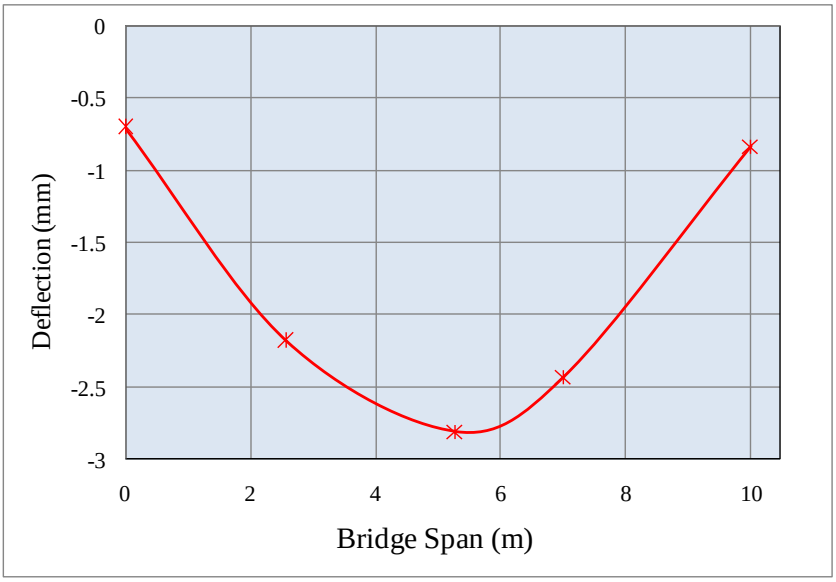

Figure 7.13 Vertical displacement profiles along the centre connection beam (centric loading)

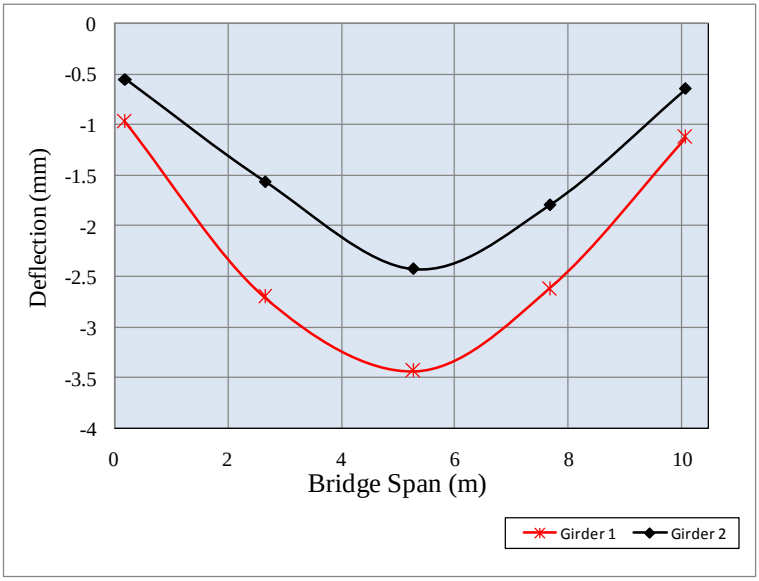

Figure 7.14 Vertical displacement profiles along the main box girders (eccentric loading)

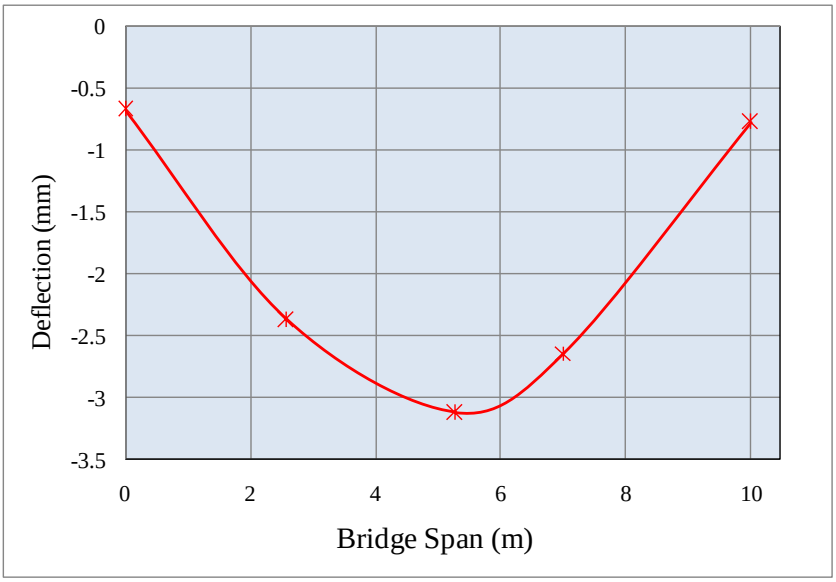

Figure 7.15 Vertical displacement profiles along the central connection beam (eccentric loading)

From Figures 7.12 through 7.15, it is seen that the maximum vertical deflections at the mid span under M1600 serviceability load are below the AS 5100 prescription (i.e maximum limit given is 1/600th of the span length, which is about 16.76 mm), thus satisfying the serviceability requirement. The vertical displacement along the edged Z-beam under M1600 loading at the extreme edge under eccentric loading is plotted in Figure 7.16 and found that it is also well below the code limit.

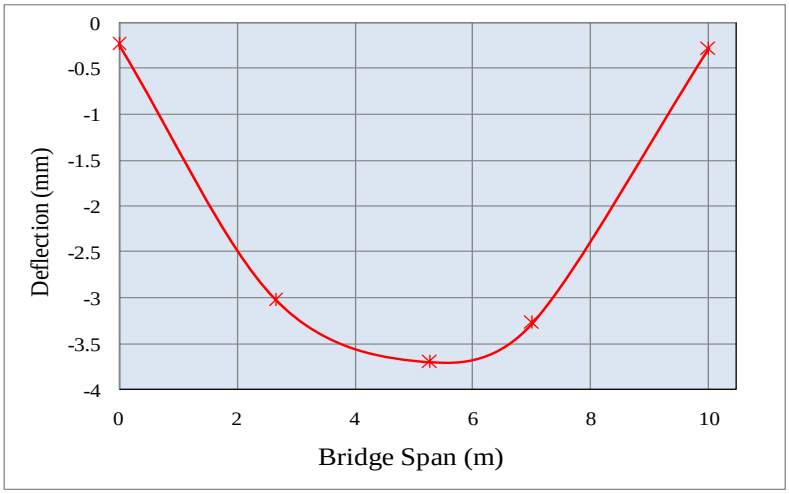

Figure 7.16 Vertical displacement profiles along the edge Z-beam (eccentric loading)

7.5 Ultimate limit state performance

The ultimate limit state performance was assessed by comparing the maximum bending moment output under the M1600 ultimate load applied in the FRW model at the critical locations defined in Section 7.4 with the member capacity determined in Chapter 3. The maximum shear force under the M1600 load obtained from the grillage analysis is compared with the member shear capacity calculated in Chapter 3.

7.5.1 Bending performance

The maximum bending moment profile generated under the M1600 ultimate load for the critical location (eccentric loading) in the model is plotted in Figure 7.17. In the same Figure 7.17, the bending capacity of the main box girder is also plotted for comparison.

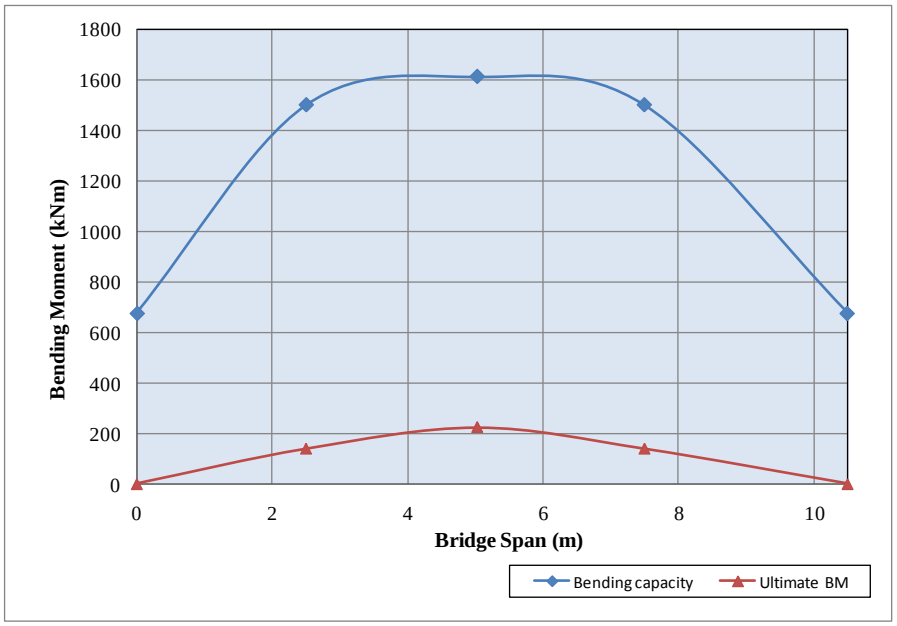

Figure 7.17 Bending moment profile due to M1600 ultimate load along the FRW main box girder vs bending capacity of box girder

It can be seen from the Figure 7.17 that the main box girder has sufficient bending capacity to resist the BM generated by the M1600 ultimate load applied on top of the slab. The max BM in the main box girder was only 227kNm; referring to Figure 4.17, the same M1600 load when applied directly on the bare FRW produced a maximum BM of 721kNm. The drastic reduction in the ultimate bending moment at the mid span of the main girder is attributed to the indeterminacy induced by the composite action between the grid members representing the RC slab and the FRW. The RCS grid members distributed the applied M1600 loading closer to the supports of the main box girder, thus reducing its BM (from 721kNm in bare frame to 227kNm in the composite deck).

The RCS was designed with a view to transferring the traffic load onto the main girders only without affecting the cross girders. The model was developed accordingly. To confirm the modelling methods, W80 ultimate load was applied on the RC slab at 650mm distance from the centre of the main box girder directly above the cross girder location and the maximum bending moment in the cross girder was found just 5kNm. Comparing this with the bare FRW BM (refer to Table 4.5), where the BM was 49kNm. Significant reduction in BM of cross girders due to the design of RCS is thus obvious.

7.5.2 Shear force

The shear force of the main box girders near the supports is of interest. Eccentrically applied M1600 loading generates maximum SF on a single girder and this SF is more critical than the SF due to concentrically applied loading. Therefore, only eccentric

loading was considered and the corresponding SF distribution is presented in Table 7.4. The table also shows the corresponding member shear capacities.

Table 7.4 Comparison of shear force against shear capacity of main box girder

Length from the bolster end (mm)	Girder depth (mm)	(ϕV_v) kN	V^* (kN)
0	341	707	474
300	380	802	358
600	418	894	312
900	456	986	272
1200	495	1081	275
1500	533	1174	275
1800	571	1266	212
2100	610	1361	195
2690	660	1482	134
5029	660	1482	3

It can be noted from Table 7.4 that the main girder of the FRW has sufficient shear capacity to resist high axle loads (M1600 ultimate load).

7.6 Summary

This chapter presented the comparison of displacements obtained from the 3D grillage model and the field test results. The grillage model was calibrated with field test results replicating near exact conditions of the supports provided at the bridge abutments. The calibrated model has accurately predicted the deformation response of the FRW bridge under both centric and eccentric loading.

The calibrated model was used for further analysis of the bridge subjected to M1600 serviceability and ultimate loads. The maximum displacements at the mid span of the main box girders, central connection beam and outer edge Z beam under the serviceability M1600 load was found to be well below the prescribed serviceability limit

in AS 5100 (2004). The maximum bending moment at the mid span and shear force near the supports under the ultimate load was found to be smaller than the member capacities, thus inferring the structural adequacy of FRW as the bridge superstructure. The one specific conclusion that can be drawn from this analysis is that the RCS pavement has enhanced the strength of FRW whilst significantly reducing the bending moment of the main girder.

Chapter 8: Conclusions

8.1 Conclusion

This research thesis has presented the in-service performance assessments of FRW Bridge deck containing RCS pavement. A full scale testing of the bridge was carried on the newly constructed demonstration bridge built in the rural area of the Rockhampton Regional Council, Queensland, Australia.

A fully laden three axle truck of 225.25 kN gross load was driven along the bridge longitudinal direction at different safe speeds dictated by the approach roads; the strain and deflection responses at several critical locations were measured. A high speed camera was used to capture the position of the wheels of the truck accurately. The load position thus determined has helped synchronising the data with the deformation / strain data and to draw useful conclusions on the behaviour of the bridge under loading.

The largest deflection and strain values measured at the mid span were linearly proportioned to obtain the serviceability limit state value of AS 5100 (2004). The linearly proportioned deflection were found to lie well below the serviceability limit state provisions in AS5100 (2004).The strains were also found to remain elastic well below the yield strength of the material of the FRW. The strain values measured at the upper flange of the FRW box girder have shown the existence of composite

action between the reinforced concrete slab pavement and the FRW, thus confirming the design assumptions.

3D grillage model of the FRW was developed in Spacegass, structural analysis software and experimental data were used to calibrate the model. Theoretical and experimental displacements and strains results were compared. The results of the numerical model compared well with the experimental data. The validated model was used in further analysis of the FRW bridge subject to SM 1600 loadings prescribed in AS 5100 (2004); the analyses the behavior of critical sections of the FRW when the load attained different speeds from 5km/h up to 100km/h, anticipating occasional over speeding in rural roads.

The following general conclusions have emerged from the study:

- The performance load testing using normal traffic load is suitable to investigate the structural behaviour of bridges containing innovative designs.
- Use of high speed camera to video record the test procedure has made it possible to accurately locate the wheel position and synchronise the wheel load data with the deformation and strain sensors. It also serves as a true record of the test for future references.
- Strain gauges are sensitive enough to predict the effect of speed of moving truck even in low speed range.
- Grillage method provides a workable, efficient and practical method of analysis of bridges containing innovative designs – however complex the geometry may have features such as taper and shapes of cross section.

The following conclusions are specific to the type of bridge superstructure employed in this research:

- FRW bridge is a viable solution to bridge replacement techniques in low volume road network in Queensland.
- The QRN FRW used in road bridge is capable to resist high axle loads envisioned in Australian standard AS 5100 (2004).
- The largest deflection measured under the truck load and linearly proportioned to match M1600 serviceability load (5.20 mm) remained well below the deflection limit (16.76mm).
- The largest bending and shear strains recorded and also linearly proportioned to the M1600 serviceability load has remained elastic well below the yield strains of steel.
- The largest deflections generated from the updated grillage model of all the longitudinal girders under M1600 serviceability load is well below the code limit (about 20 % of the code limit).
- The maximum BM at the mid span in the update grillage model containing RCS was significantly lower than the corresponding BM of the bare girder directly supporting M1600 loading.
- Reinforced concrete slab pavement has acted compositely with the FRW and has further enhanced the safety of the FRW to resist high axle loads (eg., SM1600). These slabs enhanced the capacities whilst reducing the maximum BM.
- Proper selection of rail wagons can be directly linked to the successful low cost bridge replacement technique in rural low volume road network.

- There is little, if any, dynamic amplification of an applied load on the bridge probably due to the short span and relatively large composite depths of the bridge; low speeds adopted in the field test could also have contributed to this observation.

In-service performance study concludes that the disused FRWs are competent to resist high axle loading prescribed in AS 5100 and are a viable alternate solution of bridge deck in context to low volume road network, where fatigue is of less prominence.

8.2 Contribution to scientific knowledge

The major contribution of this research study to the scientific knowledge is that the decommissioned FRWs that can be purchased at the scrap value of the metal, is a viable solution of ageing bridge replacement techniques in low volume, high axle roads network of the councils facing budget constraints. Current practices of recycling the disused FRWs through furnace process requiring large energy input can be improved through the technology advocated in this research as the direct re-use of the FRWs in road bridges contributes to significant energy saving.

In addition, despite many field load tests have been internationally conducted and sufficient literatures well established, only few handful of literatures were found in identifying the load positions accurately on the bridge structure. Use of high speed camera to record the moving load in this research has deduced that it is very

important to locate the load position on the structure to accurately correlate the sensor readings with the applied load.

8.3 Recommendation for future research

The main aim of this research was to evaluate the structural adequacy of FRW as the low cost bridge alternatives in low volume road network. This aim has been well realised both from theoretical modelling and from field load testing of the demonstration bridge. However, there are several improvements which need to be improved in future to make this solution more vibrant. The following issues are recognised as the possible future work:

- Although fatigue is less prominence in low volume road, however this phenomena is never to be ignored as most of the failure of steel structure through fatigue is abrupt. This is especially so for the FRWs as the wagons used for carrying rail freights over time might have undergone many cycles of loadings which are unrecorded. Coupons extracted from the FRWs can be examined for fatigue strength as well as true stress-strain behaviour.

- A two-lane demonstration bridge should be constructed and field load tested to cover various loading scenarios not covered in the single lane bridge. As single lane bridges are not encouraged from future perspective (inevitable growth in traffic even in rural settings), such a study would be very helpful.

- Multi span bridges should also be trailed in low volume roads to understand the dynamic load effects.

References

AASHTO. (2001). Standard specification for highway bridges, AASHTO, Washington, D.C.

Alampalli, S., & Kunin, J. (2002). Rehabilitation and field testing of an FRP bridge deck on a truss bridge. *Composite structures, 57*(1-4), 373-375.

Allison, B., & Woodward, R.J. (2005). Inspection, testing and monitoring of trunk road bridges in England. In 5th International Conference on Bridge Management – Conference Proceedings, ed G, Parke and P Disney, 171-178. Surrey: University of Surrey.

Australian Standards. 2004. AS 5100.1 – 2004 Bridge Design Part 1: Scope and general principles. Sydney: Standards Association of Australia.

Australian Standards. 2004. AS 5100.2 – 2004 Bridge Design Part 2: Design Loads. Sydney: Standards Association of Australia.

Australian Standards. 2004. AS 1580.0 – 2004 Bridge Design Part 2: Design Loads. Sydney: Standards Association of Australia.

Australian Standards. 2004. AS 5100.6 – 2004 Bridge Design Part 6: Steel and Composite construction. Sydney: Standards Association of Australia.

Australian Standards. 2004. AS 5100.7 – 2004 Bridge Design Part 7: Design Loads. Sydney: Standards Association of Australia.

Austroads. (2005). Roadfacts. An overview of Australian and New Zealand road systems, Austroads, Sydney.

Austroads. (1992). AustRoad Bridge Design Standard.

Barker, M. G. (1999). Steel girder bridge field test procedures. *Construction and Building Materials, 13*(4), 229-239.

Barker, R. M., & Puckett, J. A. (1997). *Design of highway bridges*: Wiley Online Library.

Bakht, B., & Jaeger, L. G. (1990). Bridge testing—a surprise every time. *Journal of Structural Engineering, 116*(5), 1370-1383.

Bakht, B. (1988). Testing of an Old Short Span Slab-on-girder Bridge: Research and Development Branch, Ministry of Transportation, Ontario.

Bakht, B., Jaeger, L., & Naik, T. (1981). Bridge Evaluation by Field Testing. *Proceedings of the International Symposium on Rehabilitation of Structures, Bombay, India*, December 1981, 2.57-2.64.

Bakht, B. & Jaeger, L. G. (1988) Bearing restraint in slab-on-girder bridges. *Journal of Structural Engineering*, 114**,** 2724-2740.

Battaglia, G. & Malerba, P. O. (2003) Bridge deck analysis through the use of grillage models. Taylor & Francis.

Beben, D. (2005). Static load tests of a road bridge with a flexible structure made from Super Cor type steel corrugated plates. *Journal of Bridge Engineering, 10,* 604.

BlueScope Steel. (2009). Steel girders support timber bridge maintenance. Retrieved April 10, 2009 from www.bluescopesteel.com/steeledge/issue31/march2009.

Boully, G., & Semple, B. (1997). Guildelines for bridge load capacity assessment in Bridging the Millennia, ed G.J.Chirgwin, *Proceedings of the AUSTROADS Bridge Conference*, December 3-5, Sydney, Vol 1, 35-50.

Bowles, Joseph. E. (1996). Foundation Analysis and Design (5th Edition). McGraw-Hill.

Carlsson, F. (2006). *Modelling of Traffic Loads on Bridges Based on Measurements of Real Traffic Loads in Sweden*. PhD Thesis, Lund Institute of Technology, Sweden.

Chajes, M. J., Shenton, H. W. & O'Shea, D. (2000) Bridge-condition assessment and load rating using non destructive evaluation methods. *Transportation Research Record: Journal of the Transportation Research Board,* 1696**,** 83-91.

Champion, C., Samali, B., Li, J., Crews, K., & Bakoss, S. (2002). *Assessing the load carrying capacity of timber bridges using dynamic methods*.

Cho, H. N., Choi, Y. M., & Sho, B. C. (1998). Field load testing and reliability-based integrity assessment of segmental PC box girder bridges before opening to traffic. *Engineering Structures*, *20*(11), 948-956.

Christopher. M. (2010). *An experiment investigation into disused Flat Bottom Rail Wagons as Bridges for low volume rural road*. Master thesis, Queensland University of Technology.

Crews, K., Samali, B., Li, J., Bakoss, S., & Champion, C. (2004). Testing and assessment procedures to facilitate the management of timber bridge assets.

Dhanasekar, M., & Bayissa, W. L. (2011). Structural adequacy assessment of a disused flat bottom rail wagon as road bridge deck. *Engineering Structures, 33*(5), 1838-1849.

Doornink JD, Wipf TJ, Klaiber FW. (2003). Use of railroad flatcar in cost-effective low-volume-road bridges. Transportation Research Record: *Journal of Transportation Research Board*, 1819:385-396.

Faber, M. H., Val, D. V., & Stewart, M. G. (2000). Proof load testing for bridge assessment and upgrading. *Engineering Structures*, *22*(12), 1677-1689.

Favre, R., Hassan, M., & Markey, I. (1992). Bridge Behaviour Drawn from Load Tests. 3rd. *International workshop on Bridge Rehabilitation*. Darmstadt, Germany: Ernst & Sohn Pub.

Ghosn, M., Moses, F., & Gobieski, J. (1986). Evaluation of steel bridges using in-service testing. *Transportation Research Record, 1072*, 71-78.

GangaRao, H. V. S., & Zelina, T. R. (1988). Development of Economical Low-Volume Road Bridges. *Journal of Structural Engineering, 114*(9), 1941-1961.

Giufre, A. (1997). Ultimate load testing of the Baranduda Bridge in Bridging the Millenia, ed G.J. Chirgwin, *Proceedings of the AUSTROADS bridge Conference*, December 3-5, Sydney, Vol 1, 167-184.

Hambly, E. C. (1991). *Bridge deck behaviour*: Taylor & Francis.

Harris, D. K., Cousins, T., Murray, T. M., & Sotelino, E. D. (2008). Field investigation of a sandwich plate system bridge deck. *Journal of Performance of Constructed Facilities*, 2008; 22(5), 305-315.

Harris, D. K. (2007). *Lateral Load Distribution and Deck Design Recommendations for the Sandwich Plate System (SPS) in Bridge Applications.* PhD thesis, Virginia Polytechnic Institute and State University.

HB 77.2 (1996). Australian Bridge Design Code – Design Loads.

Heywood, R. & McDonnell, A.(1996). Proof load testing and monitoring of the South Pine River Bridge, *Asia-Pacific Symposium on Bridge Loading and Fatigue*, Monash University, December.

Holcim. (2010). Bridge and platform solutions. Retrieved May 10, 2010 from www.humes.com.au/en/project-solutions/bridge-and-platform/modular-bridge-system.html.

Jaeger, L. G., & Bakht, B. (1982). The grillage analogy in bridge analysis. *Canadian Journal of Civil Engineering, 9*(Part 2), 224-235.

Jamtsho, L., Dhanasekar, M., Palliyaguru, N., & Bayissa, W. (2010). *Effects of opening in the cross girders of the flat bottom rail wagons to the load transferring mechanisms when used as road bridge deck.*

Ji, H. S., Son, B. J. & Chang, S. Y. (2007). Field testing and capacity-ratings of advanced composite materials short-span bridge superstructures. *Composite structures*, 78(2)**,** 299-307.

Keogh, D. L., & O'Brien, E. J. (1996). Recommendations on the use of a 3-D grillage model for bridge deck analysis. *Structural engineering review, 8*(4), 357-366.

Lamond, S. (2010). Bad bridge breaks farmers. Australian Broadcasting Corporation (ABC) August 2. Accessed March 30th 2011. http://www.abc.net.au/rural/content/2010/s2970990.htm

Liu, M., Frangopol, D. M., & Kim, S. (2009). Bridge safety evaluation based on monitored live load effects. *Journal of Bridge Engineering, 14*, 257.

Massa, J. J. (2008). *Field testing of multiple span railroad flatcar bridges on low volume roads*. Master thesis, Iowa State University.

Mehrkar-Asl, S & Brookes, C.L. (1997). Load testing in bridge assessment. In Structural Assessment: *The Role of Large and Full Scale Testing*, ed. K.S. Virdi, F/K. Garas, J.L. Clarke, and G.S. Armer, 45-52. London: E & FN Spon.

Moses, F., Lebet, J., & Bez, R. (1994). Application of Field Testing to Bridge Evaluation, *Journal of Structural Engineering*, 120(6), 1745-1762.

NAASRA. (1987). National Association of State Road Authorities - Bridge Design Code. 5th Ed.

Nowak, A. S., & Tharmabala, T. (1988). Bridge reliability evaluation using load tests. *Journal of Structural Engineering, 114*, 2268.

O'Brien, E. J., & Keogh, D. L. (1998). Upstand finite element analysis of slab bridges. *Computers & Structures, 69*(6), 671-683.

Palmer, K. S. (2005). *Field Testing of Railroad Flatcar Bridges*: Iowa State University.

Ryall, M. J. (2010). Load Testing. In *Bridge Management (Second Edition)* (pp. 177-203). Oxford: Butterworth-Heinemann.

Richard, B., Epaillard, S., Cremona, C., Elfgren, L., & Adelaide, L. (2010). Nonlinear finite element analysis of a 50 years old reinforced concrete trough bridge. *Engineering Structures*.

Ransom, A. L. (2000). *Assessment of bridges by proof load testing*. Master thesis, Queensland University of Technology.

Richard, B., Epaillard, S., Cremona, C., Elfgren, L., & Adelaide, L. Nonlinear finite element analysis of a 50 years old reinforced concrete trough bridge. *Journal of Engineering Structures* 2010; 32(12): 3899-3910.

Saraf, V., & Nowak, A. S. (1998). Proof load testing of deteriorated steel girder bridges. *Journal of Bridge Engineering, 3*, 82.

Schulz, J. L., Commander, B., Goble, G. G. & Frangopol, D. M. (1995). Efficient field testing and load rating of short-and medium-span bridges. *Structural Engineering Review,* 7**,** 181-194.

SPACE GASS version 10.82 (2011). Integrated Technical Software, Victoria, Australia.

Stallings, J. M., & Yoo, C. H. (1993). Tests and ratings of short-span steel bridges. *Journal of Structural Engineering, 119*(7), 2150-2168

Stone D, Nanni A, Meyers J. Field and laboratory performance of FRP bridge panels. In: Figueiras J, Juvandes L, Furia (Editors). *Proc. of Composites in Construction Conference*. Porto, Portugal; 2001, p. 701-706.

Stiller, W. B., Janos Gergely, P. E., & Rochelle, R. (2006). Testing, Analysis, and Evaluation of a GFRP Deck on Steel Girders. *Journal of Bridge Engineering, 11*, 394.

Surana, C. S., & Agrawal, R. (1998). *Grillage analogy in bridge deck analysis*: Narosa Pub House.

Taylor, R., Crews, K., & Carter, D. (1992). Bridge Testing and the Instrumentation System, *R.J.Taylor Consulting Report for Roads* and Traffic Authority of NSW.

West, R. (1973). C&CA/CIRIA-Recommendation on the use of grillage analysis for slab and pseudo-slab bridge decks.

Wipf, T.J., F.W. Klaiber, and T.L. Threadgold. (1999). Use of Railroad Flat Cars for Low Volume Road Bridges. Iowa: Iowa Department of Transport.

Wipf, T. J., Iowa. Dept. of Transportation. Project Development, D., & Iowa. Highway Research, B. (1999). *Use of Railroad Flat Cars for Low-Volume Road Bridges*: Dept. of Civil and Construction Engineering, Iowa State University.

Wipf, T. J., Iowa. Highway, D., Iowa. Highway Research, B., Iowa State University. Dept. of, C., & Construction, E. (2003). *Demonstration Project Using Railroad Flatcars for Low-Volume Road Bridges*: Dept. of Civil & Construction Engineering, Iowa State University.

Young, W. C., & Budynas, R. G. (2002). Roark's formulas for stress and strain. NewYork; McGraw Hill.

Appendices

Appendix A: Ultrasonic test results of FRW

PROJECT:	The Ultrasonic Flaw Detection and Thickness Examination on Two (2) Flat Top Rail Wagons. The examination was carried out at CQU's Rockhampton Campus
IDENTIFICATION:	Wagon 1 & 2
DATE OF TEST:	8/03/2010 & 09/03/2010
TECHNICAL DATA	
Manufacturing Specification:	Not Specified
Evaluation Specification:	AS2207 Level 2
Material:	Carbon Steel Not Further Specified
DETAILS OF ULTRASONIC EXAMINATION (Thickness Testing)	
Test Procedure:	2452.3
Test Method:	Single Spot
Scanning Locations:	As Per Results
Equipment:	Panametrics DL37 Plus
Probes:	5MHz Twin Crystal 0˚
Couplant:	Cellulose Pastel
Surface Finish:	Ground
Temperature:	Ambient
Accuracy:	± 0.2mm
DETAILS OF ULTRASONIC EXAMINATION (Flaw Detection)	
Test Procedure:	AS2207
Test Method:	UMB2
Ultrasonic Instrument:	Panametrics Epoch LT S/N 050048109
Probes:	5MHz D790 0° 4MHz KK MWB 70°
Couplant:	Cellulose Paste
Scanning Location:	1, 2, & 4
Surface Condition:	As Welded & in Accordance with Section 3.3.1

RESULTS OF THICKNESS TESTING

WAGON No 1

SIDE 2

Location F

Location	1	2	3	4	5	6	7	8	9	10
Thickness	9.4	9.4	8	9.4	9.3	9.4	9.9	9.8	9.7	9.7
Location	11	12	13	14	15	16	17	18	19	20
Thickness	9.8	9.7	10	10	9.8	10	10	10	9.9	9.9
Location	21	22	23	24						

Thickness	9.8	9.8	10	10						
Location G										
Location	1	2	3	4	5	6	7	8	9	10
Thickness	5.2	4.8	4.9	10	10.2	10	9.9	9.9	9.8	12.6
Location	11	12	13	14	15					
Thickness	12.8	12.6	12.8	12.8	12.8					
Location H										
Location	1	2	3	4	5	6	7	8	9	10
Thickness	4.8	4.9	4.9	10.5	10.6	9.9	10	9.9	12.7	12.7
Location	11	12	13	14	15					
Thickness	12.8	12.8	12.8	12.9	12.8					
Location I										
Location	1	2	3	4	5	6	7	8	9	10
Thickness	5	4.8	49	9.9	9.9	9.9	9.9	10	9.9	18.9
Location	11	12	13	14	15					
Thickness	18.9	19.3	19.3	19.2	19.4					
Location J										
Location	1	2	3	4	5	6	7	8	9	10
Thickness	5.2	4.9	4.8	9.9	10.1	9.9	9.8	9.8	9.8	12.7
Location	11	12	13	14	15					
Thickness	12.8	12.8	12.8	13	12.9					
Location K										
Location	1	2	3	4	5	6	7	8	9	10
Thickness	9.4	9.3	9.3	9.3	9.5	9.4	9.8	9.8	9.9	9.9
Location	11	12	13	14	15	16	17	18	19	20
Thickness	9.9	10.1	10	9.9	9.9	10	9.9	9.8	10.1	10
Location	21	22	23	24						
Thickness	10.1	10.1	10	10						
Location L										
Location	1	2	3	4	4A	5	6	7	8	8A
Thickness	9.6	9.8	9.6	9.7	12.8	9.8	9.6	9.6	9.7	12.6
Location	9	10	11	12	12A					
Thickness	9.8	9.8	9.7	9.8	12.8					
Location M										
Location	1	2	3	4	4A	5	6	7	8	9
Thickness	9.6	9.8	9.8	9.7	12.6	9.7	9.8	9.7	9.8	9.8
Location	10	11	12							
Thickness	9.7	9.8	9.8							
Location N										
Location	1	2	3	4	5	6	7	8	9	10
Thickness	9.8	9.8	9.7	9.8	10	9.8	9.9	9.8	9.8	10
Location	11	12								
Thickness	9.9	10								
Location O										
Location	1	2	3	4	5	6	7	8	9	10
Thickness	10	9.9	10	10	9.9	9.8	10	10	9.9	9.8
Location	11	12								

Thickness	10	9.9								
Location P										
Location	1	2	3	4	4A	5	6	7	8	8A
Thickness	9.8	9.9	9.7	9.9	12.6	9.9	10	9.8	9.9	12.6
Location	9	10	11	12						
Thickness	9.7	9.8	9.9	9.8						
Location Q										
Location	1	2	3	4	4A	5	6	7	8	8A
Thickness	10	9.8	10	10	12.7	10	10	9.9	10	12.6
Location	9	10	11	12	12A					
Thickness	9.8	9.9	9.9	10	12.7					

Wagon No 2

Side 2

Visual examination highlighted localised corrosion on side 2 at location D. Ultrasonic thickness testing confirmed the plate thickness as 9.5mm with no internal corrosion. The pitting was measured with a calibrated digital pit depth gauge and remaining material thickness was minimum 7.6mm and average 8mm. The thickness examination also identified localised thinning on the underside of the exposed edges on section F & K. The thickness recorded is of the thinned location. There is also localised corrosion along the top edge of sections G, H, I and J for approximately 25mm, but is inaccessible to accurately confirm the depth. The examination identified no loss of thickness in any box section checked.

Location F										
Location	1	2	3	4	5	6	7	8	9	10
Thickness	7.8	7.3	7.6	8.7	8.8	7.9	7.4	6.7	9.5	9.6
Location	11	12	13	14	15	16	17	18	19	20
Thickness	9.6	9.6	9.6	9.6	9.2	9.5	9.5	9.7	9.7	9.5
Location	21	22	23	24						
Thickness	7.4	8.9	8.2	8						
Location G										
Location	1	2	3	4	5	6	7	8	9	10
Thickness	5	5.1	5	9.6	9.6	9.5	9.5	9.5	9.5	11.5
Location	11	12	13	14	15					
Thickness	12.7	11.8	12	11.8	10.7					
Location H										
Location	1	2	3	4	5	6	7	8	9	10
Thickness	4.8	5.7	4.5	9.9	9.9	9.9	9.9	9.9	9.9	18.2
Location	11	12	13	14	15					
Thickness	18.2	18.1	18.1	16.7	16.7					
Location I										
Location	1	2	3	4	5	6	7	8	9	10
Thickness	4.5	5.7	3.9	10	10	10	10	10	10	10.7
Location	11	12	13	14	15					
Thickness	10.7	10.8	10.9	10.8	10.7					

Location J

Location	1	2	3	4	5	6	7	8	9	10
Thickness	4.5	5.4	5.6	9.6	9.6	8.4	9.6	9.6	9.6	10.9
Location	11	12	13	14	15					
Thickness	10.8	12.6	12.6	11.4	11.6					

Location K

Location	1	2	3	4	5	6	7	8	9	10
Thickness	8.6	8	9.8	9.8	9.6	9.9	9.3	8	9.7	9.7
Location	11	12	13	14	15	16	17	18	19	20
Thickness	9.7	9.7	9.6	9.6	9.7	9.7	9.7	9.5	9.5	9.5
Location	21	22	23	24						
Thickness	8.6	8.4	7.8	9.1						

Location L

Location	1	2	3	4	4A	5	6	7	8	8A
Thickness	7.4	7.9	8.8	7.9	12	8.7	9.6	9	9.3	12.7
Location	9	10	11	12	12A					
Thickness	9.4	9.6	8.9	8.8	12.7					

Location M

Location	1	2	3	4	4A	5	6	7	8	9
Thickness	9	9.6	8.8	8.8	12.6	8.5	9.2	7.3	8	8
Location	10	11	12							
Thickness	8.2	7.9	8							

Location N

Location	1	2	3	4	5	6	7	8	9	10
Thickness	7	9.3	7.9	8	7.4	8.3	8	6.6	7.6	8.2
Location	11	12								
Thickness	7.6	7.1								

Location O

Location	1	2	3	4	5	6	7	8	9	10
Thickness	7.7	8	8.6	7	8.4	9.4	9.4	8.1	8	9.5
Location	11	12								
Thickness	7.9	8.8								

Location P

Location	1	2	3	4	5	6	7	8	9	10
Thickness	8.4	9.4	9.4	7.4	8.5	9.4	9.4	9.5	9.4	9.6
Location	11	12								
Thickness	9.5	9.4								

Location Q

Location	1	2	3	4	4A	5	6	7	8	8A
Thickness	9.9	9.9	8.3	8.7	12.7	8.5	9.4	9.4	8.1	12.7
Location	9	10	11	12	12A					
Thickness	7.7	7.7	8.9	9.4	12.6					

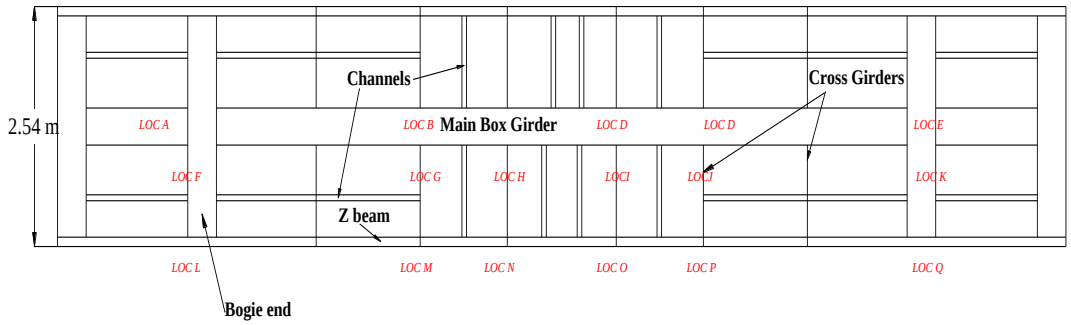

LOCATION F & K

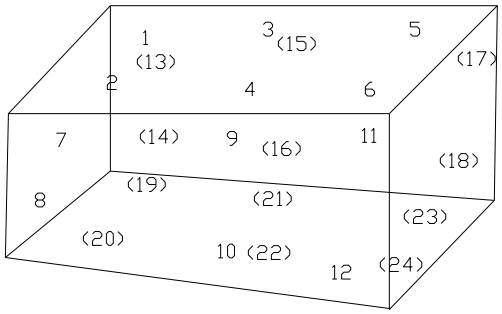

LOCATION G, H, I & J

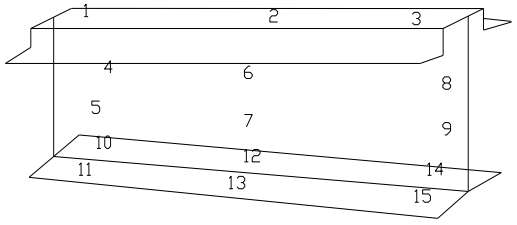

LOCATION L, M, N, O, P & Q

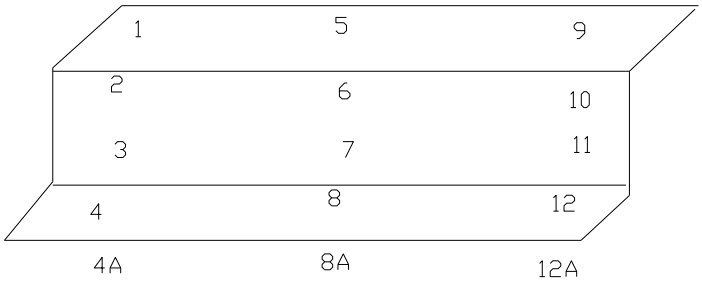

RESULTS OF FLAW DETECTION

Wagon No 1

Centre Girder

Side 1

Weld 1	Lack of penetration (1-1.5mm full length)
Weld 2	Lack of Penetration (1-1.5mm full length)
Weld 3	Lack of Penetration (1-1.5mm full length)
Weld 4	Lack of Penetration (1-1.5mm full length)

Side 2

Weld 1	Lack of penetration (1-1.5mm full length)
Weld 2	Lack of Penetration (1-1.5mm full length)
Weld 3	Lack of Penetration (1-1.5mm full length)
Weld 4	Lack of Penetration (2-2.5mm full length)

Top

Weld 1	Lack of penetration (1-1.5mm full length)
Weld 2	Lack of Penetration (1-1.5mm full length)
Weld 3	Lack of Penetration (1-1.5mm full length)
Weld 4	Lack of Penetration (1-1.5mm full length)

Bottom

Weld 1	Lack of penetration (1.5-2mm full length)
Weld 2	Lack of Penetration (1mm from 370mm to 410mm)

Cross Beams to Centre Girder

Side 1

Location 1 (thickness location F to A)

Side Plate to Girder	5mm to 6mm fillet weld only
Side Plate to Girder	5mm to 6mm fillet weld only
Bottom Plate to Girder weld	4mm to 7mm fillet weld only with external sealing

Location 2 (thickness location G to B)

Web	5mm fillet weld only
Bottom Flange	6mm fillet weld only

Location 3 (thickness location H to C)

Web	5mm fillet weld only
Bottom Flange	6mm fillet weld only

Location 4 (thickness location I to C)

Web	6mm fillet weld only
Bottom Flange	8mm fillet weld only
Location 5 (thickness location J to D)	
Web	5mm fillet weld only
Bottom Flange	3mm fillet weld plus 4mm penetration
Location 6 (thickness location K to E)	
Side Plate to Girder	5mm to 6mm fillet weld only
Side Plate to Girder	5mm to 6mm fillet weld only
Bottom Plate to Girder weld	4mm to 6mm fillet weld only with external sealing

Cross Beams to Centre Girder

Side 2

Location 1 (thickness location F to A)	
Side Plate to Girder	5mm to 6mm fillet weld only
Side Plate to Girder	5mm to 6mm fillet weld only
Bottom Plate to Girder weld	4mm to 7mm fillet weld only with external sealing
Location 2 (thickness location G to B)	
Web	6mm fillet weld only
Bottom Flange	6mm fillet weld only
Location 3 (thickness location H to C)	
Web	6 to 7mm fillet weld only
Bottom Flange	6mm fillet weld only
Location 4 (thickness location I to C)	
Web	6mm fillet weld only
Bottom Flange	5mm fillet weld plus 10mm Penetration Less 2mm Undercut.
Location 5 (thickness location J to D)	
Web	5 to 6mm fillet weld only
Bottom Flange	3mm fillet weld plus 3mm penetration
Location 6 (thickness location K to E)	
Side Plate to Girder	5mm to 6mm fillet weld only
Side Plate to Girder	6mm fillet weld only
Bottom Plate to Girder weld	4mm to 7mm fillet weld only with external sealing

Wagon No 2

Centre Girder

Side 1

Weld 1	Lack of penetration (1.5-2mm full length)
Weld 2	Lack of Penetration (1.5-2mm full length)
Weld 3	Lack of Penetration (1.5-2mm full length)
Weld 4	Lack of Penetration (2-3mm full length)

Side 2

Weld 1	Lack of penetration (1.5-2mm full length)
Weld 2	Lack of Penetration (2-3mm full length)
Weld 3	Lack of Penetration (1.5-2mm full length)
Weld 4	Lack of Penetration (2-3mm full length)

Top

Weld 1	Lack of penetration (1-1.5mm 0 to 60mm & 280mm to 400mm)
Weld 2	Lack of Penetration (3mm 0 to 60mm 1.5mm 60mm to 400mm)
Weld 3	Lack of Penetration (1-1.5mm full length)
Weld 4	Lack of Penetration (1-1.5mm full length)

Bottom

Weld 1	Lack of penetration (1.5-2mm full length)
Weld 2	Lack of Penetration (1.5-2mm full length)

Cross Beams to Centre Girder

Side 1

Location 1 (thickness location F to A)

Side Plate to Girder	5mm to 6mm fillet weld only
Side Plate to Girder	5mm to 6mm fillet weld only
Bottom Plate to Girder	6mm to 7mm fillet weld only with external sealing weld

Location 2 (thickness location G to B)

Web	6mm fillet weld only
Bottom Flange	7mm fillet weld only

Location 3 (thickness location H to C)

Web	6mm fillet weld only
Bottom Flange	6mm fillet weld only

Location 4 (thickness location I to C)

Web	5 to 6mm fillet weld only
Bottom Flange	8mm fillet weld only

Location 5 (thickness location J to D)

Web	6mm fillet weld only
Bottom Flange	8mm fillet weld only

Location 6 (thickness location K to E)

Side Plate to Girder	5mm to 6mm fillet weld only
Side Plate to Girder	6mm fillet weld only
Bottom Plate to Girder	7mm fillet weld only with external sealing weld

Cross Beams to Centre Girder

Side 2

Location 1 (thickness location F to A)
Side Plate to Girder 5mm to 6mm fillet weld only
Side Plate to Girder 5mm to 6mm fillet weld only
Bottom Plate to Girder 6mm fillet weld only with external sealing weld
Location 2 (thickness location G to B)
Web 5 to 6mm fillet weld only
Bottom Flange 6mm fillet weld only
Location 3 (thickness location H to C)
Web 5 to 6mm fillet weld only
Bottom Flange 4mm fillet weld with 14mm penetration
Location 4 (thickness location I to C)
Web 5 to 6mm fillet weld only
Bottom Flange 9mm fillet weld with 6mm Penetration
Location 5 (thickness location J to D)
Web 6mm fillet weld only
Bottom Flange 7mm fillet weld only
Location 6 (thickness location K to E)
Side Plate to Girder 6mm fillet weld only
Side Plate to Girder 6mm fillet weld only
Bottom Plate to Girder 6mm fillet weld only with external sealing weld

COMMENTS ON WELD INSPECTION

The size of internal fillet welds on the box sections at location 1 and 6 could not be confirmed. The lack of penetration detected is consistent with weld preparations designed for full penetration, but the root area not back gouged or ground when welding has been completed from the 2nd side and a slag line is left unfused.
The ultrasonic examination or visual inspections did not identify any suspected areas of cracking.

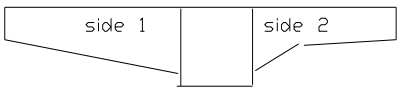

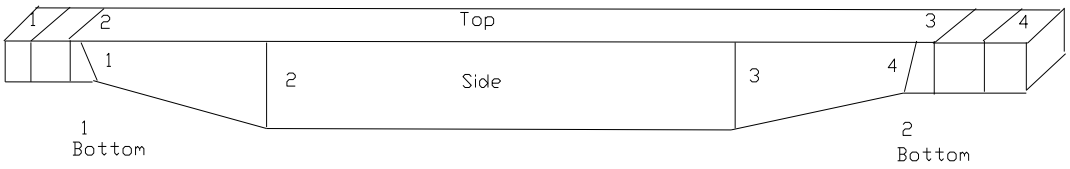

Typical weld 1 & 4 side of centre girder

Typical welds on girder top plate

Appendix B: QRN Drawings

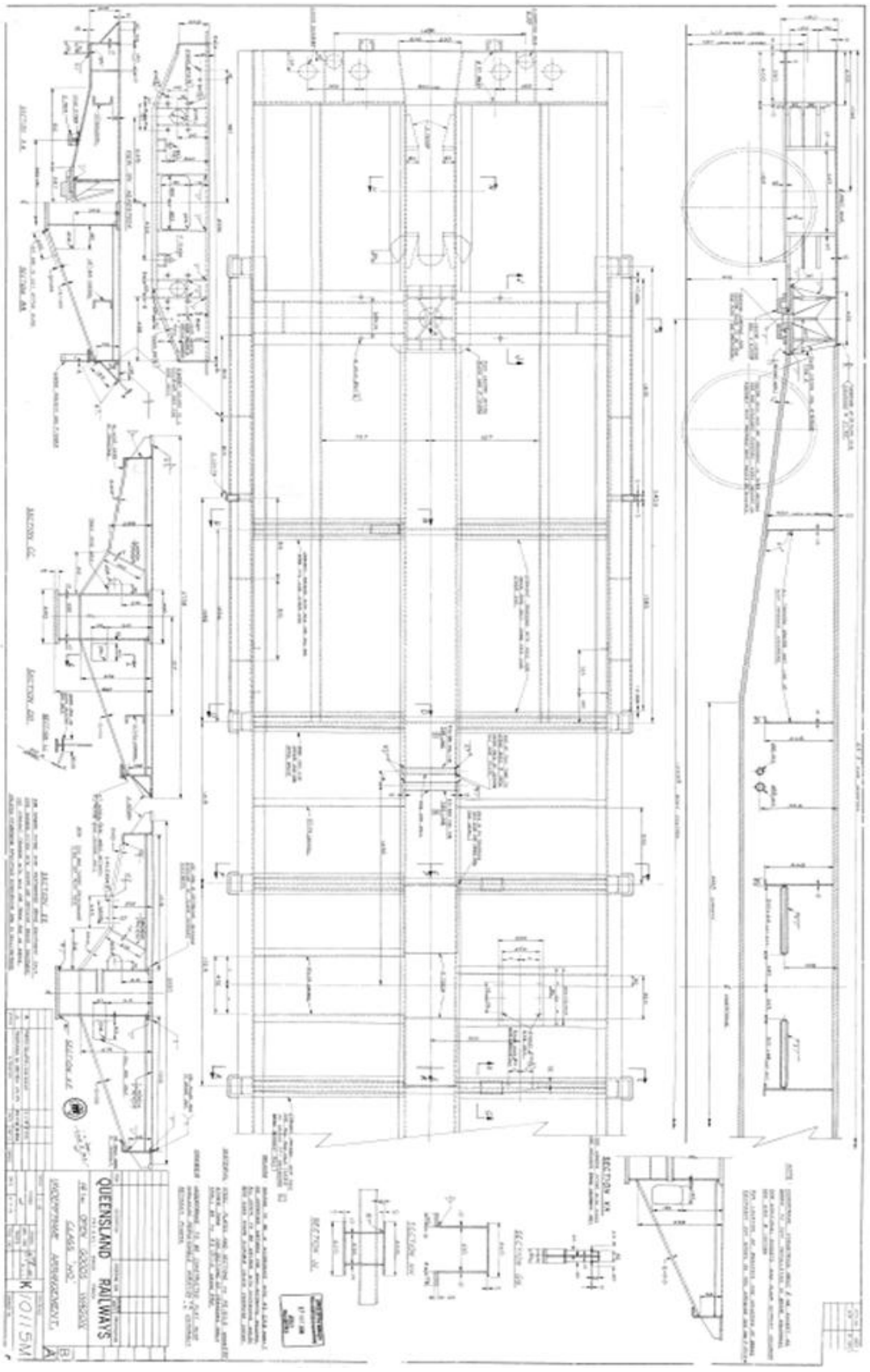

Appendix C: FRW bridge construction drawings

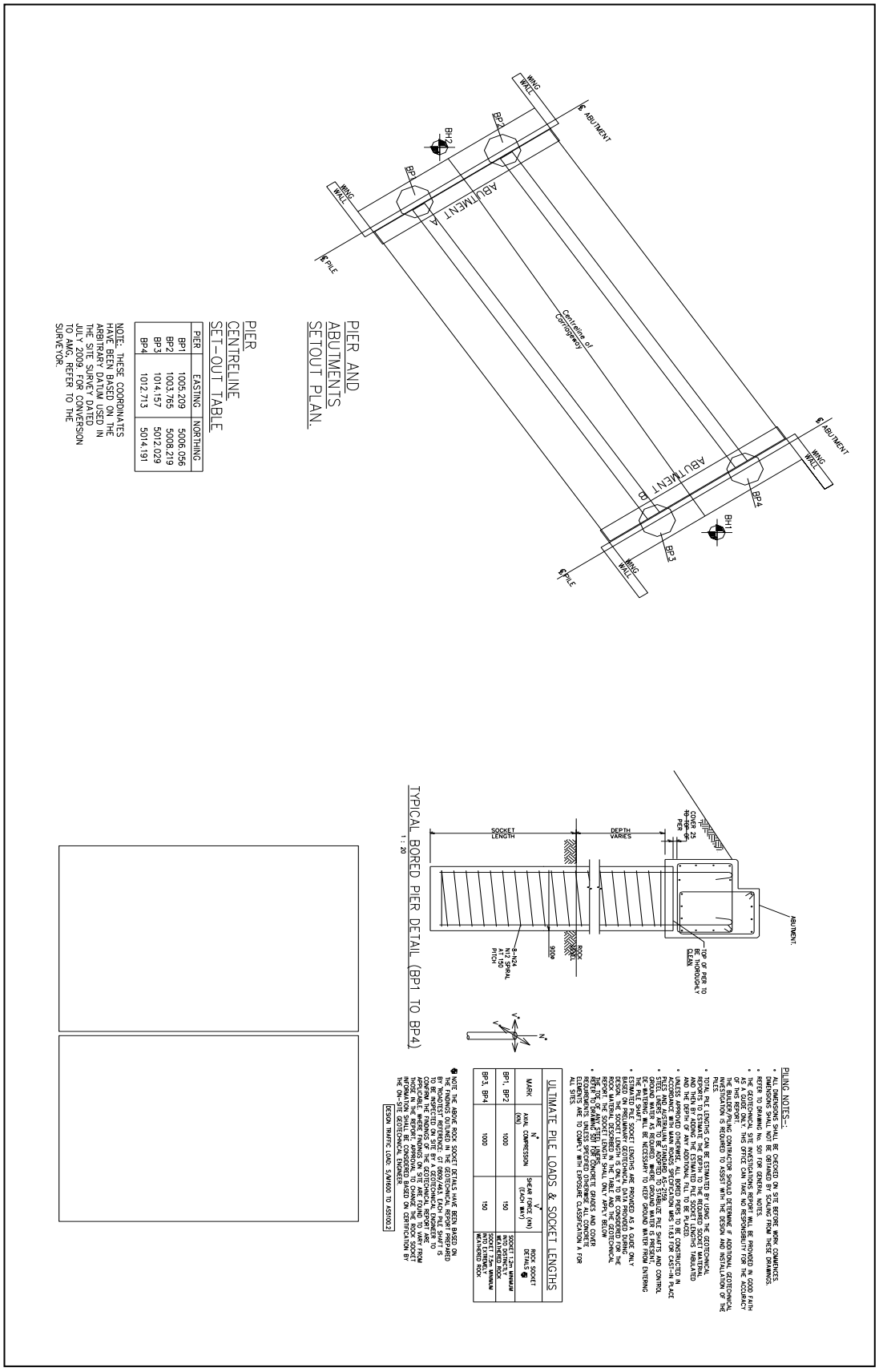

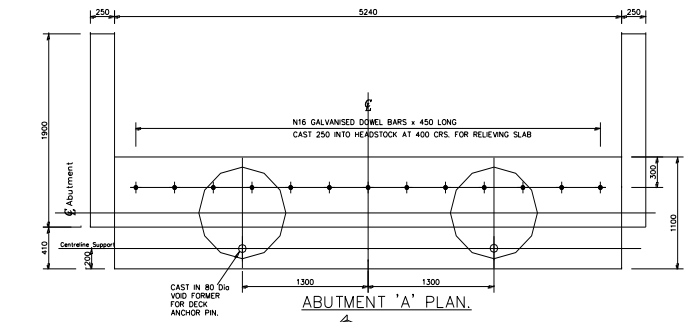

ABUTMENT 'A' PLAN.

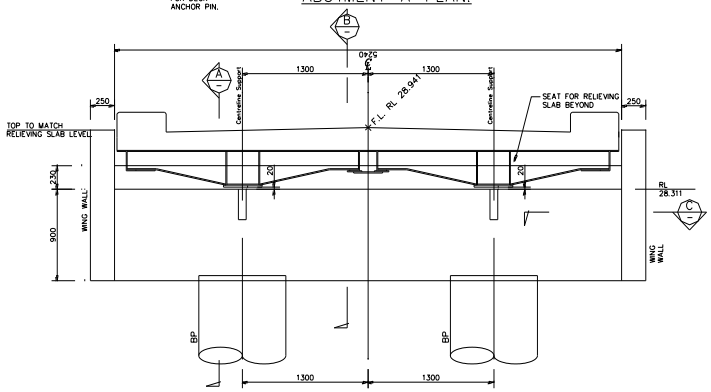

ABUTMENT 'A' ELEVATION.

ABUTMENT 'B' SIMILAR OPPOSITE HAND

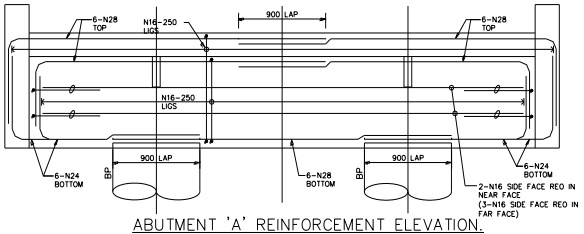

ABUTMENT 'A' REINFORCEMENT ELEVATION.

ABUTMENT 'B' SIMILAR OPPOSITE HAND

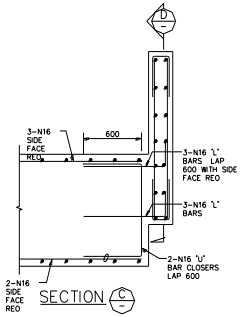

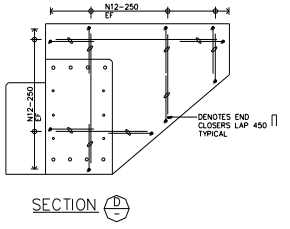

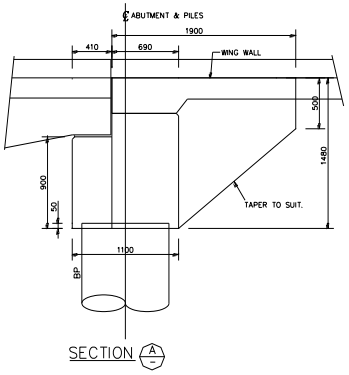

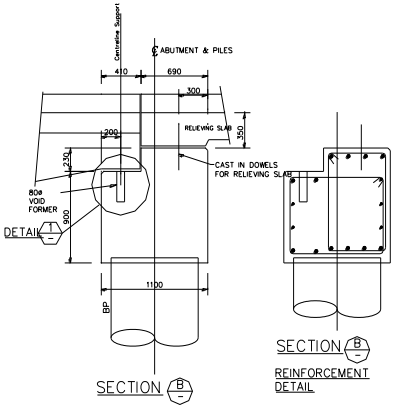

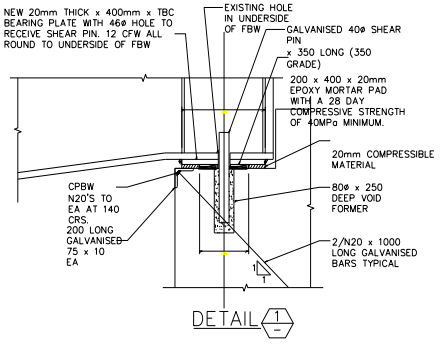

DETAIL 1

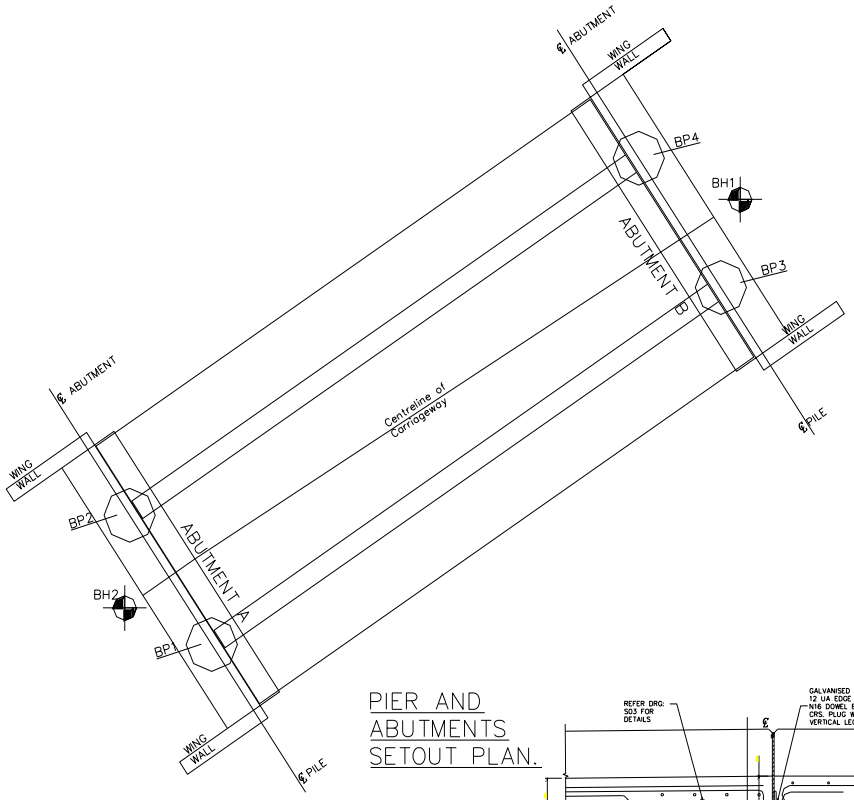

PIER AND ABUTMENTS SETOUT PLAN.

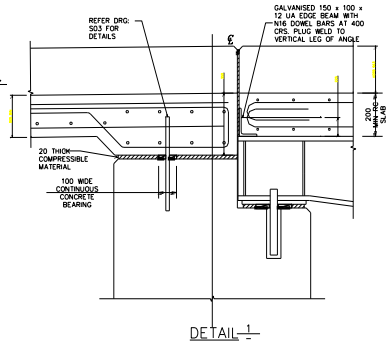

DETAIL 1

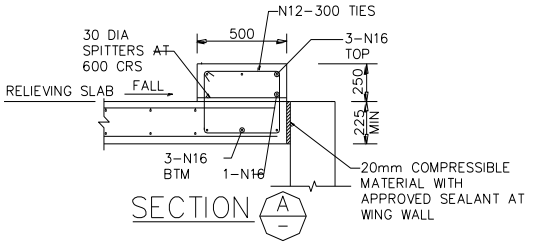

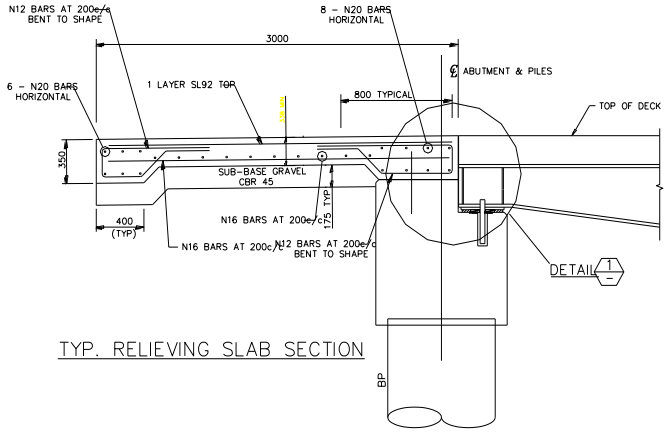

TYP. RELIEVING SLAB SECTION

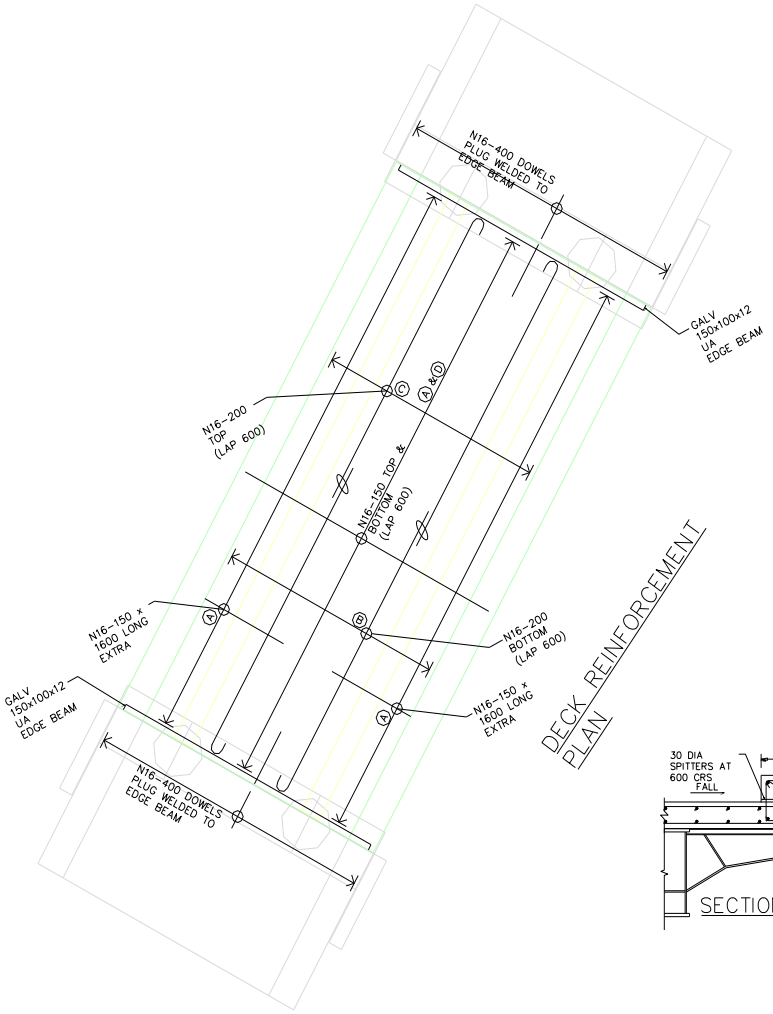

DECK REINFORCEMENT PLAN

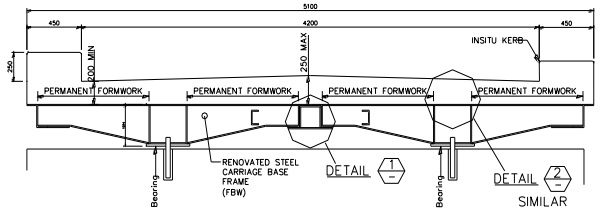

DECK SECTION (AT SUPPORT)

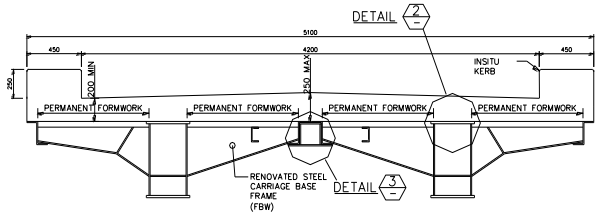

DECK SECTION (AT INTERMEDIATE TRANSOMS)

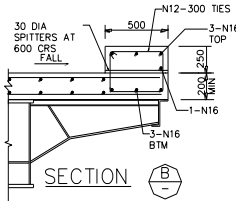

SECTION B

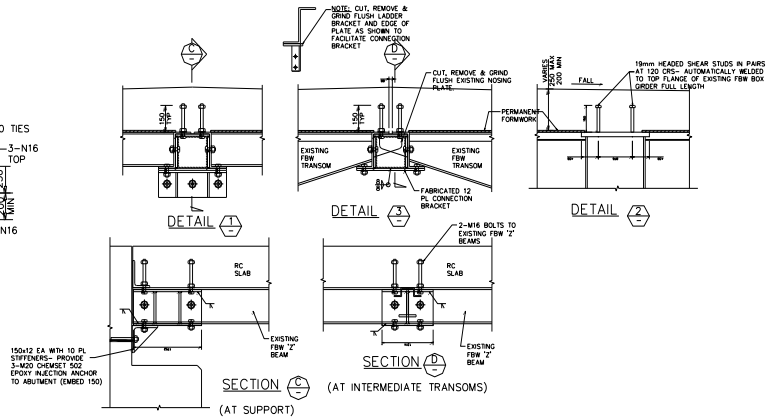

SECTION C (AT SUPPORT)

SECTION D (AT INTERMEDIATE TRANSOMS)